Search for long-lived particles using displaced jets in proton-proton collisions at $\sqrt{s} = 13$ TeV

A. M. Sirunyan *et al.*[*]
CMS Collaboration

(Received 2 December 2020; accepted 14 June 2021; published 30 July 2021)

An inclusive search is presented for long-lived particles using displaced jets. The search uses a data sample collected with the CMS detector at the CERN LHC in 2017 and 2018, from proton-proton collisions at a center-of-mass energy of 13 TeV. The results of this search are combined with those of a previous search using a data sample collected with the CMS detector in 2016, yielding a total integrated luminosity of 132 fb^{-1}. The analysis searches for the distinctive topology of displaced tracks and displaced vertices associated with a dijet system. For a simplified model, where pair-produced long-lived neutral particles decay into quark-antiquark pairs, pair production cross sections larger than 0.07 fb are excluded at 95% confidence level (C.L.) for long-lived particle masses larger than 500 GeV and mean proper decay lengths between 2 and 250 mm. For a model where the standard model-like Higgs boson decays to two long-lived scalar particles that each decays to a quark-antiquark pair, branching fractions larger than 1% are excluded at 95% C.L. for mean proper decay lengths between 1 mm and 340 mm. A group of supersymmetric models with pair-produced long-lived gluinos or top squarks decaying into various final-state topologies containing displaced jets is also tested. Gluino masses up to 2500 GeV and top squark masses up to 1600 GeV are excluded at 95% C.L. for mean proper decay lengths between 3 and 300 mm. The highest lower bounds on mass reach 2600 GeV for long-lived gluinos and 1800 GeV for long-lived top squarks. These are the most stringent limits to date on these models.

DOI: 10.1103/PhysRevD.104.012015

I. INTRODUCTION

The existence of long-lived particles (LLPs) that have macroscopic decay lengths is a common feature in both the standard model (SM) and beyond-the-SM (BSM) scenarios. There are numerous alternative BSM physics cases for the production of LLPs at the CERN LHC. Examples include, but are not limited to: split supersymmetry (SUSY) [1–7], where the gluino decays are suppressed by heavy scalars; SUSY with weak R-parity violation (RPV) [8–12], where the decays of the lightest supersymmetric particle are suppressed by small RPV couplings; SUSY with gauge-mediated SUSY breaking (GMSB) [13–15], where the decays of the next-to-lightest supersymmetric particle are suppressed by a large SUSY breaking scale; "stealth SUSY" [16,17]; "hidden valley" models [18–20]; dark matter models [21–28]; models with heavy neutral leptons that have small mixing parameters [29–32]; and models incorporating neutral naturalness [33–38]. In the examples listed above, it is very common for the LLPs to further decay into final states containing jets, giving rise to displaced-jets signatures.

Given the large variety of the BSM scenarios that lead to displaced-jets signatures, it is important to make the displaced-jets search as model independent as possible. In this paper, we present an inclusive search for LLPs decaying into jets, with at least one LLP having a decay vertex within the tracker acceptance, but which is displaced from the production vertex by up to 550 mm in the plane transverse to the beam direction. The search looks for a pair of jets known as dijets, where the jets are clustered from energy deposits in the calorimeters. For jets arising from the decay of an LLP, the associated tracks are usually displaced from the primary vertices (PVs), and the decay vertex can be reconstructed from the displaced tracks. The properties of the tracks and the decay vertex can provide discrimination power to distinguish long-lived signals from SM backgrounds. As mentioned above, a large number of models predict LLPs decaying into displaced jets. Our tests for some of these will be discussed in detail in Sec. III.

Events used in this analysis were collected with the CMS detector [39] at the LHC from proton-proton (pp) collisions at a center-of-mass energy of 13 TeV in 2017 and 2018, corresponding to an integrated luminosity of 95.9 fb^{-1}. The results are combined with those of a

[*]Full author list given at the end of the article.

Published by the American Physical Society under the terms of the Creative Commons Attribution 4.0 International license. Further distribution of this work must maintain attribution to the author(s) and the published article's title, journal citation, and DOI. Funded by SCOAP[3].

 © 2021 CERN, for the CMS Collaboration

previous displaced-jets search using the events collected in 2016 [40], yielding a total integrated luminosity of 132 fb^{-1}. For the models that were not studied in the 2016 displaced-jets search, additional simulated signal samples have been produced following the 2016 run condition of the CMS detector. These additional samples are then processed with the reconstruction and selection procedures described in Ref. [40] to compute the additional signal yields and systematic uncertainties for the 2016 data that are used in the combination.

Compared to the 2016 displaced-jets search, a set of new techniques that significantly improves the sensitivity to long-lived signatures is implemented in this analysis. The new techniques include one additional dedicated trigger aimed at selecting events containing displaced jets to recover efficiencies for high-mass LLPs, an auxiliary nuclear interactions (NIs) veto map to improve background rejection, a dedicated variable based on the sum of signed impact parameters of the tracks assigned to the displaced vertex, and the use of machine learning techniques to improve signal-to-background discrimination. With these new techniques, compared to the 2016 search, we have reduced the background rate by approximately a factor of three, while significantly increasing the signal efficiencies for almost all signal points in different LLP models. Results of searches for similar LLP signatures with hadronic decays at $\sqrt{s} = 13$ TeV have also been reported by ATLAS [41–45] and CMS [46–48].

The paper is organized as follows. A brief description of the CMS detector is introduced in Sec. II. The data and the simulated samples are described in Sec. III. Section IV details the event reconstruction and the preselection criteria. Section V describes the event selections and the background estimation methods. The systematic uncertainties are summarized in Sec. VI. The observation and the interpretation of the results are described in Sec. VII. The paper is summarized in Sec. VIII.

II. THE CMS DETECTOR

The central feature of the CMS apparatus is a superconducting solenoid of 6 m internal diameter, providing a magnetic field of 3.8 T. Within the solenoid volume are a silicon pixel and strip tracker, a lead tungstate crystal electromagnetic calorimeter (ECAL), and a brass and scintillator hadron calorimeter (HCAL), each composed of a barrel and two endcap detectors. Muons are detected in gas-ionization chambers embedded in the steel flux-return yoke outside the solenoid.

The silicon tracker measures charged particles within the pseudorapidity range $|\eta| < 2.5$. During the LHC run in 2017 and 2018, the silicon tracker consisted of 1856 silicon pixel and 15 148 silicon strip detector modules, and it occupies a cylindrical volume around the interaction point with a length of 5.8 m and a diameter of 2.6 m. For nonisolated particles with $1 < p_{\text{T}} < 10$ GeV and $|\eta| < 1.4$, the track resolutions are typically 1.5% in p_{T}, and 25–75 μm in the transverse impact parameter [49].

In the region $|\eta| < 1.74$, the HCAL cells have widths of $\Delta\eta = 0.087$ in pseudorapidity and $\Delta\phi = 0.087$ in azimuth. In the η-ϕ plane, and for $|\eta| < 1.48$, the HCAL cells map on to 5×5 arrays of ECAL crystals to form calorimeter towers projecting radially outward from the nominal interaction point. For $|\eta| > 1.74$, the coverage of the towers increases progressively to a maximum of 0.174 in $\Delta\eta$ and $\Delta\phi$. Within each tower, the energy deposits in ECAL and HCAL cells are summed to define the calorimeter tower energies, and are subsequently used to provide the energies and directions of hadronic jets.

Events of interest are selected using a two-tiered trigger system [50]. The first level, composed of custom hardware processors, uses information from the calorimeters and muon detectors to select events at a rate of around 100 kHz within a time interval of less than 4 μs. The second level, known as the high-level trigger (HLT), consists of a farm of processors running a version of the full event reconstruction software optimized for fast processing, and reduces the event rate to around 1 kHz before data storage.

A more detailed description of the CMS detector, together with a definition of the coordinate system used and the relevant kinematic variables, can be found in Ref. [39].

III. DATASETS AND SIMULATED SAMPLES

Data were collected with two dedicated triggers aimed at selecting events containing displaced jets. At the HLT, jets are reconstructed from the energy deposits in the calorimeter towers, clustered using the anti-k_{T} algorithm [51,52] with a distance parameter of 0.4. In this process, the contribution from each calorimeter tower is assigned a momentum, the magnitude and the direction of which are given by the energy measured in the tower and the coordinates of the tower. The raw jet energy is obtained from the sum of the tower energies, and the raw jet momentum from the vector sum of the tower momenta, which results in a nonzero jet mass. The raw jet energies are then corrected [53] to establish a uniform relative response of the calorimeter in η and a calibrated absolute response in transverse momentum p_{T}.

Identification of the PV is a prerequisite for the selection of displaced jets at the HLT. Events may contain multiple PVs, corresponding to multiple pp collisions occurring in the same bunch crossing. The candidate vertex with the largest value of summed physics-object p_{T}^2 is taken to be the primary pp interaction vertex. The physics objects are the jets, clustered using the jet finding algorithm [51,52] with the tracks assigned to candidate vertices as inputs, and the associated missing transverse momentum, taken as the negative vector sum of the p_{T} of those jets. More details are given in Sec. 9.4.1 of Ref. [54].

The first trigger, referred to as the "displaced" trigger, requires $H_{\text{T}} > 430$ GeV, where H_{T} is the scalar sum of the

jet p_T for all jets that have $p_T > 40$ GeV and $|\eta| < 2.5$ in the event. The trigger also requires the presence of at least two jets, with the following requirements satisfied for each jet:

(i) $p_T > 40$ GeV and $|\eta| < 2.0$;
(ii) at most two associated prompt tracks with $p_T > 1$ GeV, where prompt tracks are those having a transverse impact parameter (IP_{2D}) with respect to the leading PV smaller than 1.0 mm; and
(iii) at least one associated displaced track with $p_T > 1$ GeV, where a displaced track is a track having an IP_{2D} larger than 0.5 mm and an impact parameter significance ($Sig[IP_{2D}]$) larger than 5.0. The significance is defined as the ratio between the impact parameter and its uncertainty.

The second trigger, referred to as the "inclusive" trigger, requires $H_T > 650$ GeV and the presence of at least two jets, each of them satisfying:

(i) $p_T > 60$ GeV and $|\eta| < 2.0$; and
(ii) at most two associated prompt tracks with $p_T > 1$ GeV.

The displaced trigger is more efficient for low-mass LLPs, while the inclusive trigger is designed to recover the trigger efficiency for high-mass LLPs with small ($\lesssim$3 mm) or large ($\gtrsim$300 mm) mean proper decay lengths ($c\tau_0$).

The background sources in this search include NIs between outgoing particles and detector material, long-lived SM hadrons, and misreconstructed displaced vertices formed by accidentally crossing tracks. The background events mainly arise from SM events containing jets produced through the strong interaction, referred to as quantum chromodynamics (QCD) multijet events. The QCD multijet Monte Carlo (MC) sample is simulated at leading order with MADGRAPH5_aMC@NLO 2.4.2 [55]. Parton showering and hadronization are simulated with PYTHIA8.226 [56]. The matching of jets from the matrix element calculations and parton shower jets is achieved using the MLM algorithm [57]. The PYTHIA parameters for the underlying event modeling are set to be the CP5 tune [58]. The set of parton distribution functions (PDFs) used for the production is the NNPDF3.1 NNLO PDF set [59]. The QCD multijet MC sample is mainly used to inspire the analysis strategy and to estimate systematic uncertainties, while the background estimation for this search is purely determined from data.

Feynman diagrams for the benchmark models studied in this paper are summarized in Fig. 1. One of the benchmark signal models is a simplified model, where long-lived scalar neutral particles X are pair produced through a scattering process mediated by an off-shell Z boson. In this model, each X particle decays to a quark-antiquark pair, assuming equal branching fractions to u, d, s, c, and b quark pairs. The decays to top quark pairs are excluded to provide a simple final-state topology for this model, but it was important that the analysis strategy would still be sensitive to a variety of other models. We checked the impact on the signal efficiencies of excluding decays to top quark pairs, and found it to be small, where the relative changes of the signal efficiencies are generally at the order of a few percents. This model is referred to as the jet-jet model. The samples are produced with different resonance masses ranging from 50 to 1500 GeV, and with different proper decay lengths ranging from 1 to 10^4 mm.

Another signature we consider is the case where LLPs arise from exotic decays of an SM-like Higgs boson, which can happen in many BSM scenarios (a review can be found in the Sec. IV. 6. 6 of Ref. [60]), including "hidden valley" models [18,19], twin Higgs models [36], and the folded SUSY model [61]. For the simulation, we use POWHEG 2.0 [62–65] to generate events containing a 125 GeV Higgs boson produced through gluon-gluon fusion. The 125 GeV Higgs boson then decays to two long-lived scalar particles S, and each scalar particle then decays to a quark-antiquark pair. Two scenarios are considered; in the first scenario the scalar particle has a branching fraction of 100% to decay to a down quark-antiquark pair, while in the second one the scalar particle has a branching fraction of 100% to decay to a bottom quark-antiquark pair. The samples are produced with the scalar particle mass m_S set to be 15, 40, or 55 GeV, while the $c\tau_0$ of S varies from 1 to 3000 mm.

We also consider a group of SUSY models with different final-state topologies. The first one is a GMSB SUSY model [66] in the general gauge mediation scenario [14,15], where gluinos are pair produced and the gravitino is the lightest SUSY particle, while the gluino is the next-to-lightest supersymmetric particle. After the gluino is produced, it decays to a gluon and a gravitino, producing a single displaced jet and missing transverse momentum. This decay is suppressed by the SUSY-breaking scale, and therefore the gluino is long lived. The model in which this process occurs is referred to as the $\tilde{g} \to g\tilde{G}$ model. The samples are produced with gluino masses from 800 to 2500 GeV, and with the $c\tau_0$ of the gluino varying from 1 to 10^4 mm.

The second SUSY model we consider is a mini-split SUSY model [6,7], referred to as the $\tilde{g} \to q\bar{q}\tilde{\chi}_1^0$ model. In this model the gluino decays to a quark-antiquark pair and the lightest neutralino ($\tilde{\chi}_1^0$), with equal branching fractions to u, d, s, and c quark pairs. This decay is mediated by a squark, which is much heavier than the gluino. The squark's large mass suppresses the gluino decay, making it long lived. The mass of the neutralino is assumed to be 100 GeV, the samples are produced with gluino masses from 1400 to 3000 GeV, and the $c\tau_0$ of the gluino varies from 1 to 10^4 mm.

The third SUSY model is an RPV SUSY model [67] with minimal flavor violation, where gluinos are pair produced and long lived. Each long-lived gluino decays to top, bottom, and strange antiquarks through the RPV coupling λ''_{323} and the mediation of a virtual top squark [12],

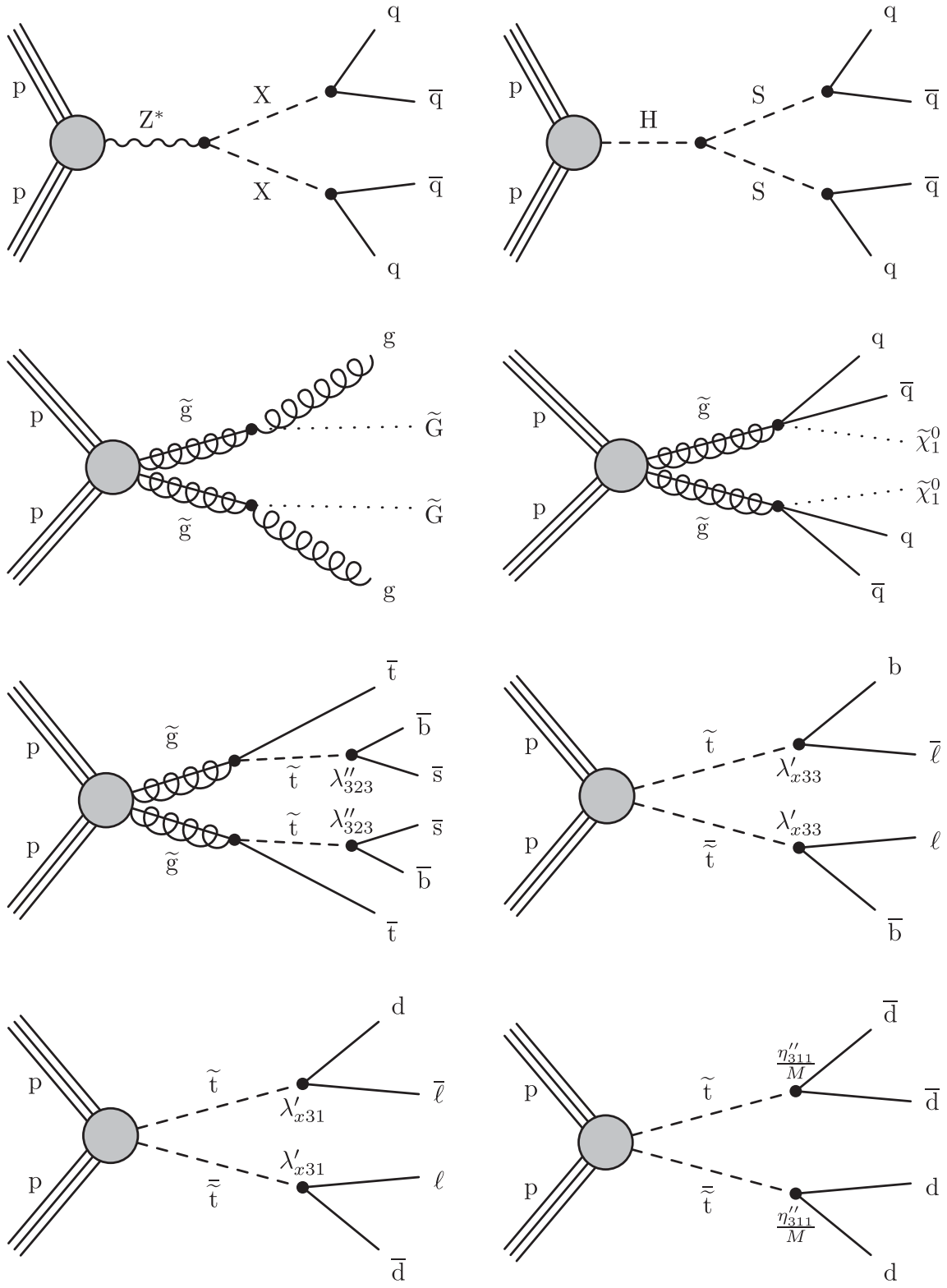


FIG. 1. The Feynman diagrams for the different long-lived models considered, including the jet-jet model (upper left), models with an exotic decay of the SM-like Higgs boson (upper right), general gauge mediation models with $\tilde{g} \to g\tilde{G}$ decay (second row, left), mini-split SUSY with $\tilde{g} \to q\bar{q}\tilde{\chi}_1^0$ decay (second row, right), RPV SUSY with $\tilde{g} \to tbs$ decay (third row, left), RPV SUSY with $\tilde{t} \to b\ell$ decay (third row, right), RPV SUSY with $\tilde{t} \to d\ell$ decay (lower left), and dRPV SUSY with $\tilde{t} \to \bar{d}\,\bar{d}$ decay (lower right).

leading to a multijet final-state topology. This model is referred to as the $\tilde{g} \to tbs$ model. The samples are produced with gluino masses from 1200 to 3000 GeV, and a $c\tau_0$ varying from 1 to 10^4 mm.

We also consider two other RPV SUSY models [68] with semileptonic decays, in which long-lived top squarks are pair produced, and each top squark decays to a bottom quark (down quark) and a charged lepton via RPV couplings λ'_{133}, λ'_{233}, and λ'_{333} (λ'_{131}, λ'_{231}, and λ'_{331}) [12]. The decay rate to each of the three lepton flavors is assumed to be equal. The two models are referred to as the $\tilde{t} \to b\ell$ ($\tilde{t} \to d\ell$) models. The samples are produced with different top squark masses from 600 to 2000 GeV, and a $c\tau_0$ varying from 1 to 10^4 mm.

Finally, we consider another SUSY model, referred to as the $\tilde{t} \to \bar{d}\bar{d}$ model, motivated by dynamical RPV (dRPV) [69,70], where long-lived top squarks are pair produced, and each top squark decays to two down antiquarks via a nonholomorphic RPV coupling η''_{311} [71]. The nonholomorphic RPV coupling is suppressed by some large scale M, thus giving rise to long lifetimes. The samples are produced with different top squark masses from 800 to 1800 GeV, and a $c\tau_0$ varying from 1 to 10^4 mm.

PYTHIA8.226 is used for the production of the signal samples, and the PDF set used for the production is NNPDF3.1 LO. For SUSY-particle production, the PYTHIA8.226 simulation is cross checked with MADGRAPH5_aMC@NLO 2.4.2 for representative signal points, where the MADGRAPH5_aMC@NLO simulation is performed at LO with up to two additional outgoing partons. The resulting signal efficiencies are found to be consistent within the statistical uncertainties. The PYTHIA parameters for the underlying event modeling are set to be the CP2 tune [58]. In the SUSY models, a long-lived gluino or top squark can form a hadronic state through strong interactions, an R-hadron [9,72,73], which is simulated with PYTHIA. The interactions of the R-hadron with matter were studied following the simulation described in Ref. [74,75], and were found to have negligible impact on this analysis, since they have very little influence on the vertex reconstruction.

The simulated background and signal events are processed with a GEANT4-based [76] simulation for the detailed CMS detector response. To take into account the effects of additional pp interactions within the same or nearby bunch crossings ("pileup"), additional minimum-bias events are overlaid on the simulated events to match the pileup distribution observed in the data.

IV. EVENT RECONSTRUCTION AND PRESELECTION

This search examines dijet candidates in a given event. The algorithms for the offline jet reconstruction and PV selection are the same as those applied at the HLT (as described in Sec. III), except that the full offline information is used. To make sure that the online H_T and jet p_T requirements in the displaced-jet triggers reach full efficiency, we apply selections on the offline H_T of the event as well as on the p_T and η of each jet. After the trigger selection, if an event passes the displaced trigger, we require the event to have offline $H_T > 500$ GeV, and dijet candidates are formed from all possible pairs of jets in the event, with the jets satisfying $p_T > 50$ GeV and $|\eta| < 2.0$. On the other hand, if an event only passes the inclusive trigger, it is required to have offline $H_T > 700$ GeV, and the dijet candidates are formed from all possible pairs of jets in the event, with the jets satisfying $p_T > 80$ GeV and $|\eta| < 2.0$.

In this search, the track candidates are required to have $p_T > 1$ GeV and to be high-purity tracks. The high-purity selection is based on track information (such as the normalized χ^2 of the track fit, the impact parameters, and the number of hits in different tracker layers) to reduce the fraction of misreconstructed tracks, and the selection is optimized separately for each iteration of the tracking [49], so that it is efficient for selecting tracks with different displacements. More details of the high-purity selection can be found in Ref. [49]. The η and ϕ of a given track are determined by the direction of its momentum vector at the closest approach point to the leading PV. For a given dijet candidate, we associate track candidates with each jet by requiring that $\Delta R < 0.5$, where $\Delta R = \sqrt{(\Delta\eta)^2 + (\Delta\phi)^2}$ is the angular distance between the jet axis and the track direction. When a track satisfies $\Delta R < 0.5$ for both jets, it is associated with the jet giving the smaller ΔR.

After associating track candidates with each jet, the next step is to reconstruct a secondary vertex (SV) for each dijet candidate. From all the tracks associated with a dijet candidate, we select displaced tracks that satisfy $\mathrm{IP_{2D}} > 0.5$ mm and $\mathrm{Sig[IP_{2D}]} > 5.0$. We then attempt to reconstruct an SV from these displaced tracks using an adaptive vertex fitter algorithm [77]. The reconstructed SV is not required to have associated tracks from both jets, so that the search can be sensitive to the models where the LLP decays to a single displaced jet. To improve the signal-to-background discrimination, we implement a set of preselection criteria on the dijet/SV candidates, which are described in the rest of this section.

To ensure the quality of the vertex reconstruction, the SV is selected only if it is reconstructed with a χ^2 per degree of freedom ($\chi^2/\mathrm{n_{dof}}$) of less than 5.0. In order to suppress long-lived SM mesons and baryons, the invariant mass of the vertex is required to be larger than 4 GeV, and the transverse momentum of the vertex is required to be larger than 8 GeV, where the four-momentum of the vertex is calculated assuming the charged pion mass for all assigned tracks.

We only consider dijet candidates that have a reconstructed SV satisfying the above requirements. Furthermore, SVs in background events tend to have only one track with a high value for $\mathrm{IP_{2D}}$, corresponding to the tail of the impact parameter distribution. We therefore consider the track with

the second-highest $\mathrm{Sig}[\mathrm{IP}_{2D}]$ among the tracks that are assigned to the SV, since this provides a more sensitive discriminant for identifying displaced jets. We require the second-highest $\mathrm{Sig}[\mathrm{IP}_{2D}]$ to be larger than 15.

We also compute another quantity ϵ, which is the ratio between the sum of energy for all the tracks assigned to the SV and the sum of the energy for all the tracks associated with the two jets:

$$\epsilon = \frac{\sum_{\mathrm{track}\in\mathrm{SV}} E_{\mathrm{track}}}{\sum_{\mathrm{track}\in\mathrm{dijet}} E_{\mathrm{track}}}. \quad (1)$$

Since ϵ is expected to be large for displaced-jet signatures, dijet candidates with ϵ smaller than 0.15 are rejected.

An additional variable, ζ, is defined to characterize the contribution of prompt activity to the jets. For each track associated with a jet, we identify the PV (including the leading PV and the pileup vertices) with the minimum three-dimensional (3D) impact parameter significance to the track. If this minimum value is smaller than 5, we assign the track to this PV. Then for each jet, we compute the track energy contribution from each PV, and the PV with the largest track energy contribution to the jet is chosen. Finally, we define ζ as

$$\zeta = \frac{\sum_{\mathrm{track}\in\mathrm{PV}_1} E_{\mathrm{track}}^{\mathrm{Jet}_1} + \sum_{\mathrm{track}\in\mathrm{PV}_2} E_{\mathrm{track}}^{\mathrm{Jet}_2}}{E_{\mathrm{Jet}_1} + E_{\mathrm{Jet}_2}}, \quad (2)$$

where $\sum_{\mathrm{track}\in\mathrm{PV}_i} E_{\mathrm{track}}^{\mathrm{Jet}_i}$ is the sum of the track energy coming from the most compatible PV for a given jet, while E_{Jet_i} is the energy of a given jet, thus ζ is the charged energy fraction of the dijet associated with the most compatible PVs. For displaced-jet signatures, ζ tends to be small since the jets are not compatible with PVs. Dijet candidates with ζ larger than 0.2 are rejected.

To suppress the background events arising from NIs in the tracker material, we compare the positions of the SVs with a map of the distribution of material in the inner tracker. The map was obtained from the distribution of NI candidate vertices, which are reconstructed using the adaptive vertex fitter on a sample of events collected with isolated single-muon triggers. The NI candidates are required to satisfy the following criteria:

(i) The tracks are required to be associated with dijet candidates, which are formed from the jets having $p_{\mathrm{T}} > 10$ GeV and $|\eta| < 2.0$;
(ii) The associated tracks must have $p_{\mathrm{T}} > 0.2$ GeV, high purity, $\mathrm{IP}_{2D} > 0.5$ mm, and $\mathrm{Sig}[\mathrm{IP}_{2D}] > 5.0$;
(iii) vertex track multiplicity is larger than 3;
(iv) the ratio ϵ of the energy sum for SV tracks to that for all tracks is less than 0.15 for the dijet candidate;
(v) vertex L_{xy} significance is larger than 200, where the transverse decay length L_{xy} is the distance between the SV and the leading PV; and
(vi) vertex $\chi^2/\mathrm{n}_{\mathrm{dof}}$ is smaller than 3.0.

After these selections, the distribution of the NI vertex candidates is transferred to an NI-veto map in the transverse plane, with $|x|$ and $|y| < 25$ cm, as shown in Fig. 2. To suppress misreconstructed vertices and the displaced vertices produced by decaying long-lived SM mesons and baryons, we only select the region where the NI vertex density is above a threshold that varies for different layers of the pixel detector. In the NI-veto map, we can clearly see the structures of the beam pipe (at $r = \sqrt{x^2+y^2} \approx 23$ mm),

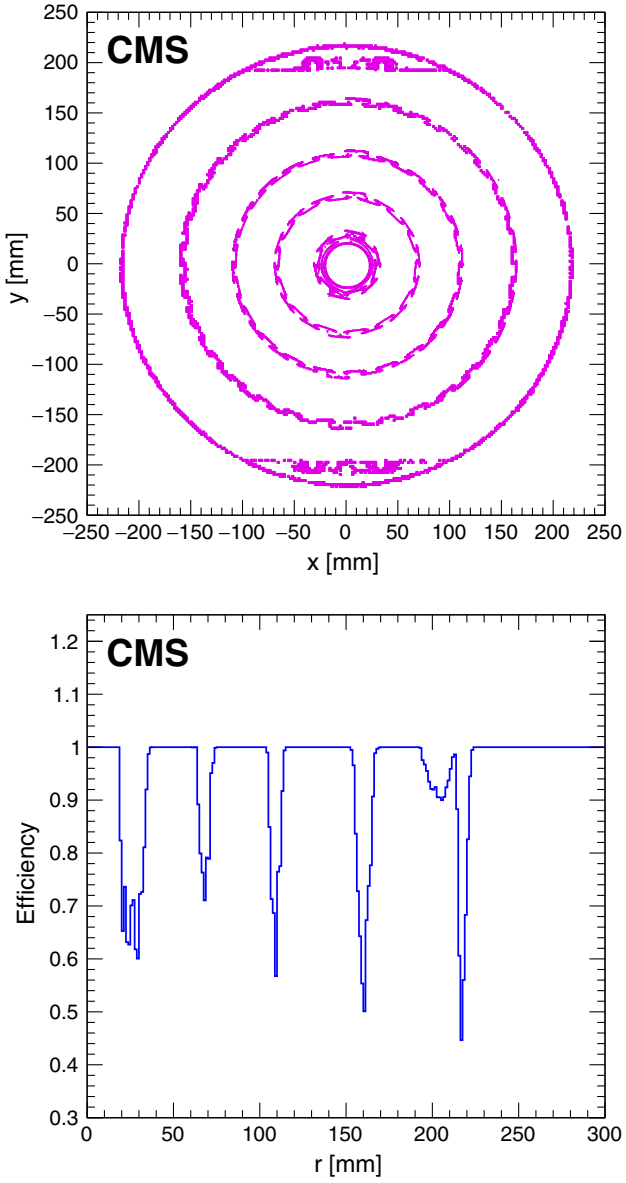


FIG. 2. Upper: the NI-veto map based on the NI vertex reconstruction in the 2017 and 2018 data collected by the CMS detector, the map corresponds to the geometry of the CMS pixel detector used in 2017–2018 data taking [79]. The structures of the different pixel layers can be clearly seen. Lower: the efficiency for a given vertex candidate to pass the NI-veto as a function of radius r.

TABLE I. Summary of the preselection criteria.

SV/dijet variable	Requirement
Vertex χ^2/n_{dof}	<5.0
Vertex invariant mass	>4 GeV
Vertex transverse momentum	>8 GeV
Second largest IP_{2D} significance	>15
ϵ (SV track energy fraction in the dijet)	>0.15
ζ (energy fraction from compatible PVs)	<0.20
Vertex position in the x-y plane	No overlap with the NI-veto map

the four pixel layers (at $r \approx 29$, ≈68, ≈109, and ≈160 mm), and the support rails (at $r \approx 200$ mm). In our search, any SV candidate that overlaps with the NI-veto map is rejected. The loss of the fiducial volume within $r <$ 300 mm due to the veto is around 4%, and the efficiencies for signal events to pass this selection are generally well above 90%. In the veto no requirement is placed on the z coordinates of the SVs, but the impact of restricting the veto to the barrel region of the pixel detector ($|z| < 27$ cm) is negligible on the signal efficiencies. A similar study on the structure of the CMS inner tracking system using a more sophisticated NI reconstruction technique with 2016 data has been reported in Ref. [78].

The preselection criteria for this search, summarized in Table I, are efficient for a wide range of long-lived models with different final-state topologies.

V. EVENT SELECTION AND BACKGROUND PREDICTION

After reconstructing the SV using the adaptive vertex fitter, we employ an auxiliary algorithm to check the consistency between the SV system and the dijet system. For each displaced track (having $IP_{2D} > 0.5$ mm, $Sig[IP_{2D}] > 5.0$) associated with the dijet, we determine an expected decay point consistent with the displaced dijet hypothesis by finding the crossing point of the track helix and the dijet direction in the transverse (x-y) plane. The dijet direction is the space direction of the four-momentum-sum of the two jets, for which the production vertex of the two jets is taken to be the SV. For each crossing point, an expected transverse decay length (L_{xy}^{exp}) is computed with respect to the leading PV. The L_{xy}^{exp} is positive if the crossing point is at the same side of the dijet direction, otherwise it is negative. The associated displaced tracks are then clustered based on their L_{xy}^{exp}, using a hierarchical clustering algorithm [80]. During the clustering, two clusters are merged when the smallest L_{xy}^{exp} difference between the two clusters is smaller than 15% of the L_{xy} of the SV. After the clustering procedure is finished, if more than one cluster is formed, the one closest to the SV is selected. The cluster root-mean-square (RMS), taken to be the relative RMS of individual tracks L_{xy}^{exp} with respect to the SV L_{xy}, is computed to provide signal-to-background discrimination:

$$\mathrm{RMS}_{\mathrm{cluster}} = \sqrt{\frac{1}{N_{\mathrm{tracks}}} \sum_{i=1}^{N_{\mathrm{tracks}}} \frac{(L_{xy}^{\mathrm{exp}}(i) - L_{xy})^2}{L_{xy}^2}}, \quad (3)$$

where N_{tracks} is the number of tracks in the selected cluster.

For each track assigned to the SV, a sign is given to the IP_{2D} and $Sig[IP_{2D}]$ based on the angle between the dijet direction and the impact parameter vector that points from the leading PV to the closest approach point (with respect to the leading PV) of the track in the transverse plane. The sign is positive if this angle is smaller than $\pi/2$; otherwise the sign is negative. A new variable, κ, is then introduced as the signed $Sig[IP_{2D}]$ sum of the six leading tracks from the SV (where the tracks are ordered by the absolute values of their $Sig[IP_{2D}]$):

$$\kappa = \sum_{i=1}^{6} \mathrm{Sig}[\mathrm{IP}_{2\mathrm{D}}(\mathrm{track}_i)]. \quad (4)$$

If the track multiplicity is smaller than six, the sum is taken over all the tracks from the SV. For background processes, since the tracks assigned to the SV are uncorrelated with the dijet direction, the signed $Sig[IP_{2D}]$ of different tracks tend to cancel each other, therefore κ peaks sharply around zero. On the other hand, for displaced jets that originate from the SV, the directions of the tracks will be highly correlated with the dijet direction, therefore κ is significantly different from zero and $|\kappa|$ tends to be large.

To improve signal-to-background discrimination and to define a region with signal events enriched, we proceed to construct a multivariate discriminant based on the following variables for the vertex/dijet candidates:

(i) Vertex track multiplicity;
(ii) Vertex L_{xy} significance;
(iii) Cluster RMS;
(iv) The magnitude of the signed $Sig[IP_{2D}]$ sum of the six leading tracks $|\kappa|$.

The distributions of the four variables are shown in Fig. 3, with displaced-jet triggers, offline H_T, and offline jet kinematic variables selections (described in Section IV) applied. For the multivariate discriminant we utilize the gradient boosted decision tree (GBDT) algorithm [81–83], with cross entropy as the loss function. The GBDT algorithm is implemented using the TMVA (toolkit for multivariate data analysis) package [84] interfaced with Scikit-learn [85]. Given the large cross section of the QCD multijet process and the relatively low H_T threshold of our displaced-jet triggers, the event count of the simulated QCD multijet sample (after preselections) is insufficient for the GBDT training, since it is much smaller than the number of expected QCD multijet events in the analyzed

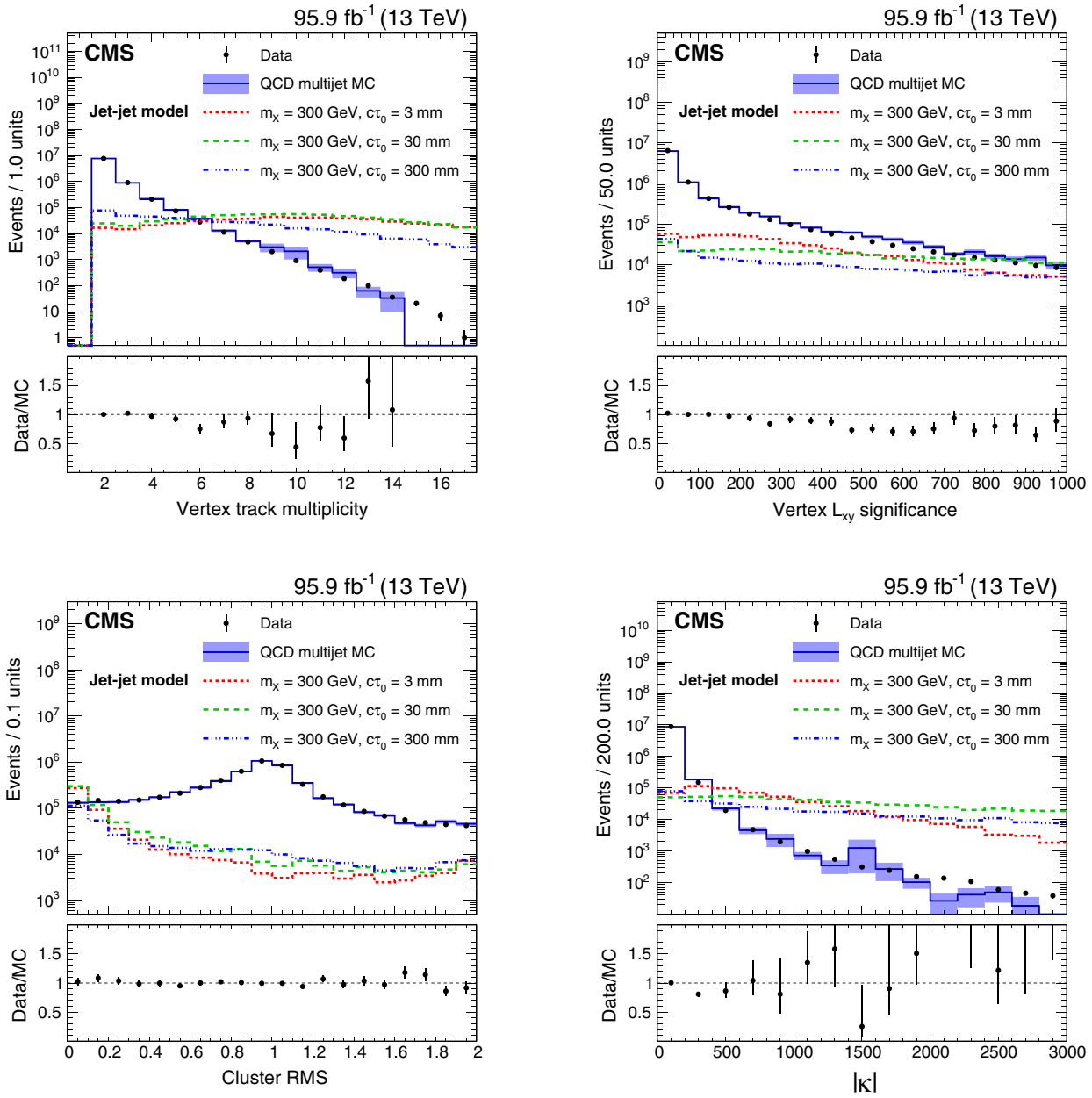


FIG. 3. The distributions of the vertex track multiplicity (upper left), vertex L_{xy} significance (upper right), cluster RMS (lower left), and the magnitude of the signed Sig[IP_{2D}] sum $|\kappa|$ (lower right), for data, simulated QCD multijet events, and simulated signal events. Data and simulated events are selected with the displaced-jet triggers and with the offline H_T, jets p_T, and η selections applied. For a given event, if there is more than one SV candidate being reconstructed, the one with the largest vertex track multiplicity is chosen. If the track multiplicities are the same, the one with the smallest χ^2/n_{dof} is chosen. The lower panels show the ratios between the data and the simulated QCD multijet events. The blue shaded error bands and vertical bars represent the statistical uncertainties. Three benchmark signal distributions are shown (dashed lines) for the jet-jet model with $m_X = 300$ GeV and varying $c\tau_0$. For visualization purposes, each signal process is given a cross section that yields 10^6 events produced in the analyzed data sample.

data sample. Therefore, for the background sample in the GBDT training, we use the data in the following region:

(i) events are selected by the displaced-jet triggers, and pass the offline H_T and jet kinematic variables selections;

(ii) $\epsilon < 0.12$ for the dijet candidate, making this region orthogonal to the signal region;

(iii) the veto using the NI-veto map is not applied;

(iv) all the other preselection criteria are satisfied.

For the signal sample in the GBDT training, simulated jet-jet model events that pass the preselection criteria are used, with $m_X = 100$, 300, and 1000 GeV, and with $c\tau_0 = 1$, 10, 100, 1000 mm. If there is more than one dijet/SV candidate passing the selection criteria in a given event, the one with

the largest track multiplicity is chosen for the training. If the track multiplicities are the same, the one with the smallest SV $\chi^2/\mathrm{n_{dof}}$ is chosen. An event weight is assigned separately to each signal point with a given m_{X} and $c\tau_0$ such that the sum of weights is identical for each point, thus each signal point has the same priority in the training. Twenty percent of the events in the signal and background samples are randomly selected to validate the performance of the GBDT and to make sure it is not overtrained.

The GBDT output values or scores for data, simulated QCD multijet events, and simulated signal events are shown in Fig. 4. The signal efficiencies for this search are measured with simulated signal events produced separately. The background prediction is purely based on some other control samples in data, which are different from the one used for the GBDT training. Although only the jet-jet model is used as the signal sample in the GBDT training, the GBDT is highly efficient in selecting signatures of other LLP models with different final-state topologies, since we have explicitly chosen the input variables to make the GBDT as model-independent as possible.

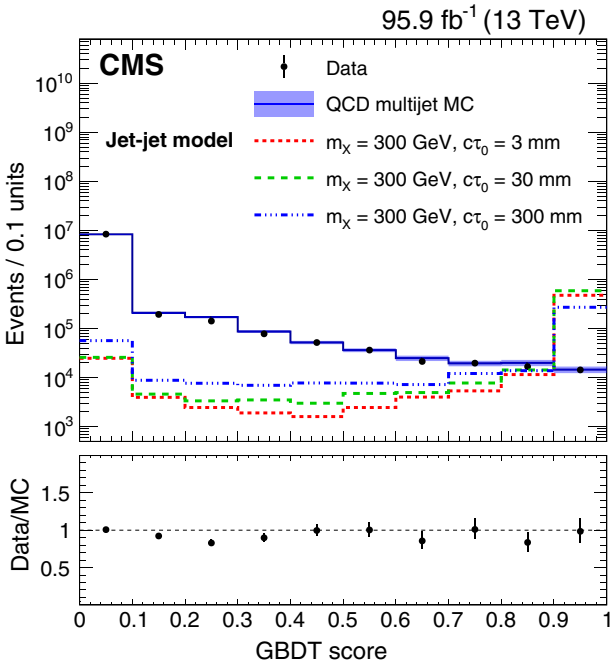


FIG. 4. The distributions of the GBDT output score for data, simulated QCD multijet events, and simulated signal events. Data and simulated events are selected with the displaced-jet triggers and with the offline H_{T}, jets p_{T}, and η selections applied. For a given event, if there is more than one SV candidate being reconstructed, the one with the largest vertex track multiplicity is chosen. If the track multiplicities are the same, the one with the smallest $\chi^2/\mathrm{n_{dof}}$ is chosen. The lower panel shows the ratio between the data and the simulated QCD multijet events. The blue shaded error bands and vertical bars represent the statistical uncertainties. Three benchmark signal distributions are shown (dashed lines) for the jet-jet model with $m_{\mathrm{X}} = 300$ GeV and varying $c\tau_0$. For visualization purposes, each signal process is given a cross section corresponding to 10^6 events produced in the analyzed data sample. The signal events shown in this plot are not used in the GBDT training.

In addition to the GBDT score g, we use another variable $N^{\mathrm{3D}}_{\mathrm{tracks}}$ in the final event selection, which is the number of 3D prompt tracks in a single jet, where the 3D prompt tracks are the tracks that have 3D impact parameters with respect to the leading PV smaller than 0.3 mm.

If more than one dijet candidate passes the preselection criteria described in Sec. IV, the one with the largest GBDT score is selected. If the GBDT scores are the same, the one with the smallest SV $\chi^2/\mathrm{n_{dof}}$ is selected. In the final signal region, the candidate is further required to pass three final selection criteria, which are

(i) Selection 1: for the leading jet in p_{T}, $N^{\mathrm{3D}}_{\mathrm{tracks}}$ is smaller than 3;
(ii) Selection 2: for the subleading jet, $N^{\mathrm{3D}}_{\mathrm{tracks}}$ is smaller than 3; and
(iii) Selection 3: the GBDT score g is larger than 0.988.

The numerical values for the selection criteria are chosen by optimizing the discovery potential of 5 standard deviations based on the Punzi significance [86] for the jet-jet model and the $\tilde{g} \to g\tilde{G}$ model across different LLP masses and lifetimes. The chosen models encompass the displaced-dijet and displaced-single-jet signatures, with $m_{\mathrm{X}} = 100$, 300, and 1000 GeV for the jet-jet model, and with $m_{\tilde{g}} = 600$, 1000, and 1600 GeV for the $\tilde{g} \to g\tilde{G}$ model, while $c\tau_0$ is taken to be 1, 10, 100, and 1000 mm. Thus there are 24 signal points considered in total for the selection optimization.

Based on the three selection criteria, we can define eight nonoverlapping regions A–H, which include the final signal region. The event counts in different regions are $N_{fff}, N_{pff}, \cdots$, and N_{ppp}, for regions $\mathrm{A}, \mathrm{B}, \cdots$, and H, respectively, as shown in Table II. The region H is the region where the events pass all the three selection criteria, and thus is the final signal region. Events in the remaining regions (A–G) fail one or more of the three selection criteria. Since the three selection criteria have little correlation between them for the background events, a property

TABLE II. The definitions of the different regions used in the background estimation.

Region	Selection 1	Selection 2	Selection 3	Event count
A	Fail	Fail	Fail	N_{fff}
B	Pass	Fail	Fail	N_{pff}
C	Fail	Pass	Fail	N_{fpf}
D	Fail	Fail	Pass	N_{ffp}
E	Fail	Pass	Pass	N_{fpp}
F	Pass	Fail	Pass	N_{pfp}
G	Pass	Pass	Fail	N_{ppf}
H	Pass	Pass	Pass	N_{ppp}

that has been verified with simulated QCD multijet events, the background yield in the signal region H can be estimated by different ratios of event counts in regions A–G, where the ratio $b_{\text{nominal}} = N_{ppf}(N_{ffp} + N_{fpp} + N_{pfp})/(N_{fff} + N_{pff} + N_{fpf})$ uses the fraction of events passing to those failing the GBDT selection (Selection 3) and is taken as the central value of the predicted background yields. Three additional ratios are computed using the events failing either one of the first two selections:

(i) Cross-check 1: $N_{ppf}(N_{ffp} + N_{fpp})/(N_{fff} + N_{fpf})$;
(ii) Cross-check 2: $N_{ppf}(N_{ffp} + N_{pfp})/(N_{fff} + N_{pff})$;
(iii) Cross-check 3: $N_{ppf}(N_{fpp} + N_{pfp})/(N_{fpf} + N_{pff})$.

These cross-checks provide an important test of the robustness of the background prediction and the assumption that the three selection criteria are minimally correlated. Differences between the predictions obtained with the nominal ratio b_{nominal} and the cross-checks are used to estimate the systematic uncertainties in the background prediction.

The method described above can be generalized to predict the background yield in arbitrary intervals of the GBDT score g, where the first two selections are also satisfied. In this way we can verify our background prediction method in the different bins of GBDT score g. The background prediction method is first tested with simulated QCD multijet events and simulated signal events, and is found to be robust both with and without signal contaminations. We then test the background prediction in data, for which we define a control region by inverting the selection on ϵ, requiring ϵ to be smaller than 0.15. In order to improve the statistical precision, we remove the selection requirement that uses the NI-veto map, although the background prediction method is still robust with the presence of the NI-veto map. The predicted background yields and observed events in the control region are shown in Fig. 5, which shows a good agreement between the predicted and observed yields. The predicted background yields in the different bins of GBDT score are correlated, since the events that are used for background predictions in lower bins are also used in the background predictions in higher bins.

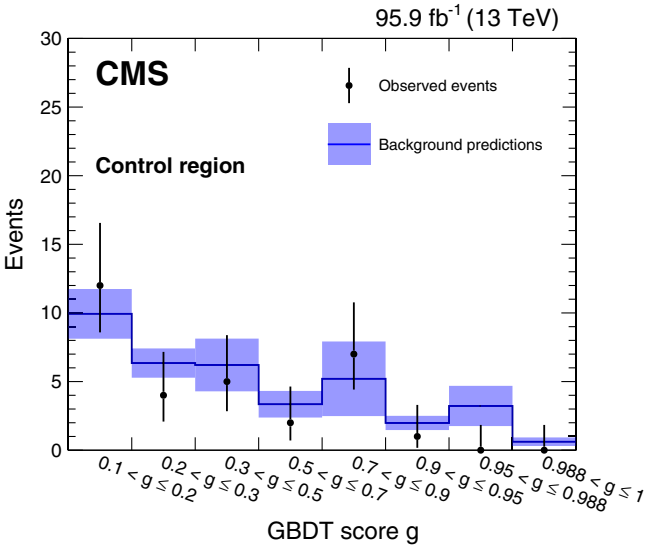


FIG. 5. The predicted background yields and the numbers of observed events in the control region, for different bins of the GBDT scores. The background predictions in different bins are correlated, since the events that are used for background predictions in lower bins are also used in the background predictions in higher bins. The error bands for the predictions represent statistical uncertainties and systematic uncertainties added in quadrature. The error bars for the observed events represent statistical uncertainties, assuming Poisson statistics.

VI. SYSTEMATIC UNCERTAINTIES

The systematic uncertainty in the background prediction is taken to be the largest deviation of the three cross checks from the nominal prediction b_{nominal}, and is found to be 52% in the final signal region where the GBDT score g is larger than 0.988.

The systematic uncertainties in the integrated luminosity for 13 TeV pp collision data are 2.3% and 2.5% for the 2017 and 2018 [87,88] data taking periods, respectively, and are modeled as uncorrelated nuisance parameters between the years.

The systematic uncertainty in the signal yields arising from the pileup modeling is estimated by varying the inelastic pp cross section [89] used in the pileup distribution determination by 4.6%. The resulting variations of the signal yields are generally smaller than 1% and are well within the statistical fluctuations, therefore the impact of the pileup modeling is negligible and no corresponding systematic uncertainty is assigned.

The systematic uncertainty in the signal yields due to the online H_{T} requirements of the displaced-jet triggers is estimated by comparing the efficiency of the online H_{T} requirements measured in data with the one measured in the QCD multijet MC sample. The efficiencies are measured using the events collected with an isolated single-muon trigger. The discrepancies between the measurements in data and MC simulation are parameterized as functions of offline H_{T}, and corresponding corrections are applied to the simulated signal events. The signal yields are then recalculated for different masses and mean proper decay lengths. The largest correction in the signal yield for a given model is taken as the corresponding systematic uncertainty, and is found to be smaller than 2%.

The systematic uncertainty in the signal yields due to the online jet p_{T} requirements of the displaced-jet triggers is estimated by measuring the per-jet efficiencies of the online jet p_{T} requirements in data and in the QCD multijet MC

sample, using events collected with a prescaled H_T trigger that requires $H_T > 425$ GeV. Corrections for the discrepancies between the measurements in data and MC simulation are applied to the simulated signal events, and the signal yields are recalculated. The correction is more significant for low-mass LLPs (with $m \sim 50$ GeV), and is smaller than 8%, which is taken as the corresponding systematic uncertainty.

To estimate the systematic uncertainty due to the online tracking requirements of the displaced-jet triggers, we measure the per-jet efficiencies of the online tracking requirements as functions of the number of prompt tracks and displaced tracks, using events collected with the prescaled H_T trigger. The efficiencies obtained in data are found to be consistent with the efficiencies obtained in MC simulations. Therefore no corresponding systematic uncertainty is assigned.

To estimate the impact of the possible mismodeling of the GBDT score in MC simulation on the signal yields, we compare the distribution of the GBDT score in simulated QCD multijet events with the distribution measured in data, using events collected with the prescaled H_T trigger. The discrepancies between data and MC simulation are taken into account by varying the GBDT scores in the simulated samples by the same magnitude. The largest variation in the signal efficiency for a given model is taken as the corresponding systematic uncertainty in signal yields, and is found to be in the range of 4%–15%.

Similarly, the uncertainty in the signal yields due to impact parameter modeling is estimated by comparing the distribution of the impact parameters in simulated QCD multijet events with the distribution measured in data, also using events collected with the prescaled H_T trigger. The impact parameters in simulated QCD multijet events are varied until the discrepancies between data and MC simulation are covered by the variation. The impact parameters in the simulated signal samples are then varied by the same magnitude. The largest variation in the signal efficiency for a given model is taken as the corresponding systematic uncertainty, and is found to be in the range of 8%–18%.

The impact of the jet energy scale uncertainty on the signal yields is estimated by varying the jet energy and p_T by one standard deviation of the jet energy scale uncertainty [53]. The variations of the signal efficiencies are smaller than 3%, which is taken as the corresponding systematic uncertainty.

The impact of the PDF uncertainty on the signal acceptance is estimated by reweighting the simulated signal events with NNPDF, CT14 [90] and MMHT14 [91] PDF sets, and their associated uncertainty sets [92,93], following the PDF4LHC recommendation [92]. The uncertainty in signal efficiency for a given signal model is quantified by comparing the efficiencies calculated with alternative PDF sets and the ones with the nominal NNPDF set, and is found to be in the range of 4–6%.

TABLE III. Summary of the systematic uncertainties in the signal yields.

Source	Uncertainties (%)
Integrated luminosity	2.3–2.5
Online H_T requirement	0–2
Online jet p_T requirement	0–8
Offline vertexing	4–15
Track impact parameter modeling	8–18
Jet energy scale	0–3
PDF	4–6
Primary vertex selection	8–15
Total	17–25

The uncertainty in the signal yields due to the selection of the PV is estimated by replacing the leading PV with the subleading PV when calculating impact parameters and vertex displacement. The largest variation of the signal efficiency for a given signal model is taken as the corresponding systematic uncertainty, and is found to be in the range of 8–15%.

The various systematic uncertainties in the signal yields are summarized in Table III.

VII. RESULTS

A. Data in the signal region

The predicted background yields and the numbers of observed events in different GBDT ranges, after all the preselection criteria are applied, are shown in Fig. 6, with N^{3D}_{tracks} smaller than 3 for both jets. The final signal region is defined by a GBDT score larger than 0.988, and the predicted background yield is $0.75 \pm 0.44(\text{stat}) \pm 0.39(\text{syst})$ events in the data samples collected in 2017 and 2018. After all the preselection criteria are applied, the efficiencies for signal events to have at least one SV/dijet candidate satisfying GBDT > 0.988 are generally above 80–90% for the different LLP models considered with $m_{\text{LLP}} \gtrsim 300$ GeV and $1 \lesssim c\tau_0 \lesssim 1000$ mm, while the background rate has been reduced by a factor of around 3×10^3 by the GBDT selection.

Event yields in data after different selection requirements have been applied are shown in Table IV. We observe one event in the final signal region, which is consistent with the predicted background yield. The observed event has an offline H_T of 570 GeV, and an SV candidate with an L_{xy} of ≈26 cm and 8 associated tracks. The position of the SV is close to one of the silicon strip layers, and was likely produced by NIs with the silicon strip detector.

B. Interpretation of the results

The signal yields in the final signal region are used to set limits on a variety of models. The signal efficiencies for representative signal points in different models can be found in Tables V–XIII and Fig. 15 of Appendix. The

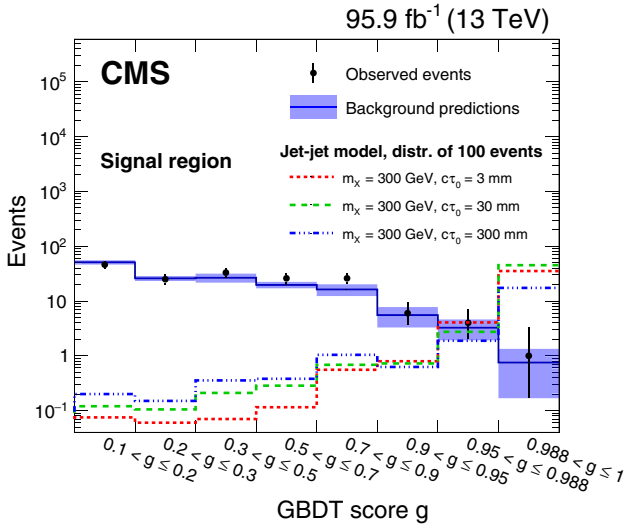


FIG. 6. The predicted background yields and the number of observed events for the data in the signal region, with N^{3D}_{tracks} smaller than 3 for both jets, shown for different bins of the GBDT scores. The background predictions in different bins are correlated, since the events that are used for background predictions in lower bins are also used in the background predictions in higher bins. For comparison, three benchmark signal points are also shown (dashed lines) for the jet-jet model with $m_X = 300$ GeV and different lifetimes. For visualization purposes, each signal process is given a cross section that yields 100 events produced in the analyzed data sample.

results obtained with the 2017–2018 analysis are further combined in this paper with the results from the displaced-jets search using the pp collision data collected with the CMS experiment in 2016 [40], for which the systematic uncertainties arising from the same source are taken to be fully correlated, while the other systematic uncertainties and the statistical uncertainties in signal yields or expected background yields are taken to be uncorrelated. The total integrated luminosity is 132 fb^{-1}. For the models that were not studied in the 2016 displaced-jets search, we have produced additional signal MC samples following the 2016 run condition of the CMS detector. We then process these samples with the reconstruction and selection procedures implemented in the 2016 search to compute the additional signal yields and systematic uncertainties for the 2016 data that are used in the combination.

Upper limits on the cross section for a given model are presented with different masses and lifetimes by computing the 95% confidence level (C.L.) associated with each signal point using the CL_s prescription [94–97], for which an LHC-style profile likelihood ratio [96,97] is taken as the test statistic. Systematic uncertainties are incorporated through the use of nuisance parameters treated according to the frequentist paradigm. The asymptotic approximation [96] is used for the calculation of the CL_s values, which have been verified with full-frequentist results for representative signal points. Since the background yields of this search are small, the impact of the associated statistical or systematic uncertainties on the upper limits are also small.

The expected and observed upper limits on the pair production cross section for the jet-jet model at different values of $c\tau_0$ and LLP mass m_X are shown in Fig. 7, where a branching fraction of 100% for X to decay into a quark-antiquark pair is assumed. For a fixed LLP mass m_X, the limits are most restrictive for $c\tau_0$ between 3 and 300 mm. For smaller $c\tau_0$, the limits become less stringent, because we only select displaced tracks to reconstruct SVs and we veto dijet candidates with a large number of prompt tracks. The limits also become less restrictive for larger $c\tau_0$ ($c\tau_0 > 300$ mm), because the tracking efficiency becomes worse with large displacement of the SV. For high-mass

TABLE IV. Event yields after different selection requirements have been applied for data collected in 2017 and 2018. Signal efficiencies for the jet-jet model with $m_X = 1000$ GeV and different $c\tau_0$ are also shown for comparison. Selection requirements are cumulative from the first row to the last.

		Signal efficiency (%) $m_X = 1000$ GeV $c\tau_0$		
Selections	Observed events	3 mm	30 mm	300 mm
Displaced-jet triggers, offline H_T selections	17758640	69.4	91.2	80.5
Offline jet p_T and η selections, vertex $\chi^2/n_{dof} < 5.0$	8387775	68.9	90.7	73.5
Vertex $p_T > 8$ GeV	3794960	68.2	90.3	69.4
Vertex invariant mass > 4 GeV	1129531	66.5	89.3	61.6
Second largest Sig[IP_{2D}] > 15	422449	66.0	89.0	60.9
Charged energy fraction from the SV $\epsilon > 0.15$	93873	64.3	87.6	58.4
Energy fraction from the PVs $\zeta < 0.20$	15891	63.6	86.9	57.9
Veto using the NI-veto map	13721	63.6	84.9	55.4
$N^{3D}_{tracks} < 3$ for each jet	2753	54.6	76.4	48.4
GBDT > 0.988	1	51.5	73.5	42.5

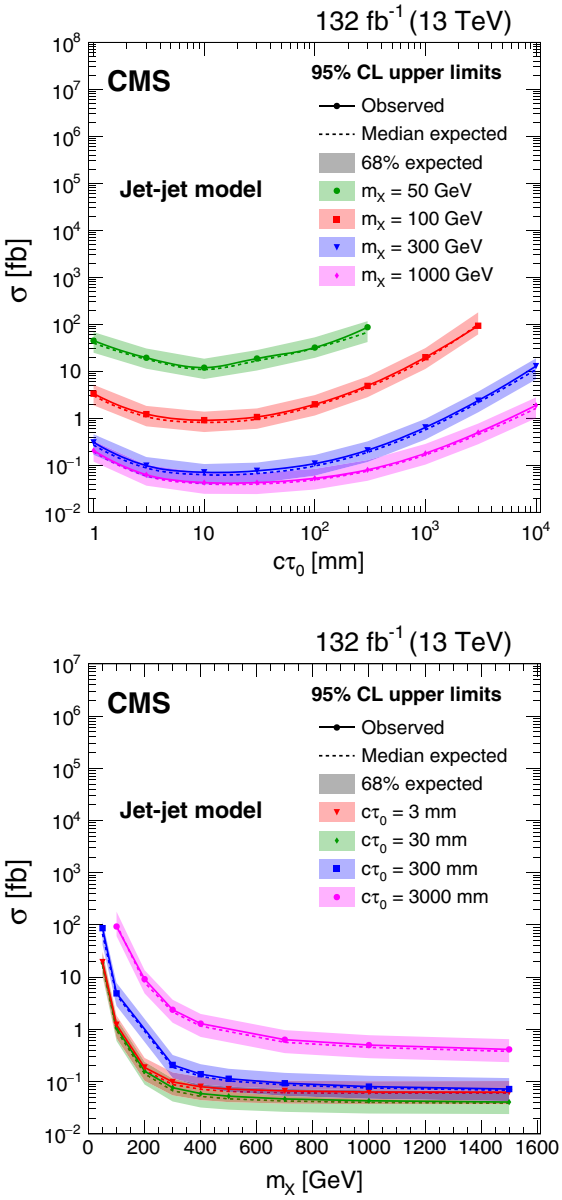


FIG. 7. The 95% C.L. upper limits on the pair production cross section of the LLP X, where a 100% branching fraction for X to decay to a quark-antiquark pair is assumed. Upper: the upper limits as functions of $c\tau_0$ for different masses. Lower: the upper limits as functions of the particle mass for different $c\tau_0$. The solid (dashed) curves show the observed (median expected) limits. The shaded bands indicate the regions containing 68% of the distributions of the limits expected under the background-only hypothesis.

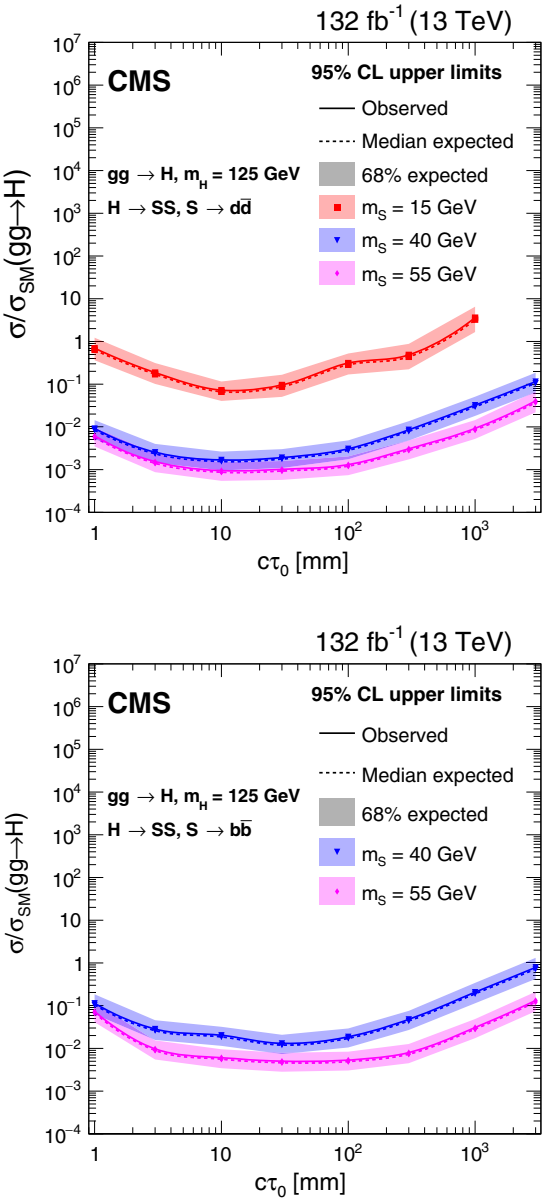


FIG. 8. The expected and observed 95% C.L. upper limits on the branching fraction of the SM-like Higgs boson to decay to two long-lived scalar particles, assuming the gluon-gluon fusion Higgs boson production cross section of 49 pb at 13 TeV with $m_H = 125$ GeV, shown at different masses and $c\tau_0$ for the scalar particle S. Upper: the upper limits when each scalar particle decays to a down quark-antiquark pair. Lower: the upper limits when each scalar particle decays to a bottom quark-antiquark pair. The solid (dashed) curves represent the observed (median expected) limits. The shaded bands represent the regions containing 68% of the distributions of the expected limits under the background-only hypothesis.

LLPs ($m_X > 500$ GeV), pair production cross sections larger than 0.07 fb are excluded for $c\tau_0$ between 2 and 250 mm. The lowest pair production cross section excluded is 0.04 fb, at $c\tau_0 = 30$ mm and $m_X > 1000$ GeV.

Figure 8 presents the expected and observed upper limits on the branching fraction of the SM-like Higgs boson to decay to two long-lived scalar particles S, each of which decays 100% of times to a quark-antiquark pair of a specific flavor. The upper limits on the branching fraction are calculated assuming the gluon-gluon fusion production cross section of a 125 GeV Higgs boson at 13 TeV [60]. When the long-lived scalar particle decays to a light-flavor quark-antiquark pair, branching fractions larger than 1% are excluded for $c\tau_0$ between 1 and 340 mm with

$m_S \geq 40$ GeV. When the long-lived scalar particle decays to a bottom quark-antiquark pair, branching fractions larger than 10% are excluded for $c\tau_0$ between 1 and 530 mm with $m_S \geq 40$ GeV. These are the most stringent limits to date on this model for $c\tau_0$ between 1 and 1000 mm. For $m_S = 15$ GeV, where the track multiplicity of the SV is small, and the tracks are collimated due to the boost of S, the limits become worse. The limits are also worse for the case where the scalar particle decays to a bottom quark-antiquark pair, because the decays of b hadrons can produce tertiary vertices, which can be missed by the SV reconstruction we deploy in this search.

The expected and observed upper limits on the pair production cross section of long-lived gluinos in the GMSB $\tilde{g} \to g\tilde{G}$ model are shown in Fig. 9, where a branching fraction of 100% for the gluino to decay into a gluon and a gravitino is assumed. Since we do not require the reconstructed SV to have associated tracks from both jets, the two separate displaced single jets produced by the decays of the two long-lived gluinos in the $\tilde{g} \to g\tilde{G}$ model can be paired together and pass the selections, therefore the search is sensitive to the models with similar signatures. When the gluino mass is 2400 GeV, signal efficiencies are around 21, 53, and 41% in the 2017 and 2018 analysis for $c\tau_0 = 3$, 30, and 300 mm, respectively. With the data samples collected in 2016–2018, gluino pair production cross sections larger than 0.1 fb are excluded for $c\tau_0$ between 7 and 600 mm at $m_{\tilde{g}} = 2400$ GeV. We then compute the upper limits on the gluino mass for different $c\tau_0$ according to the upper limits on the pair production cross section, and a calculation at next-to-next-to-leading logarithmic precision matched to the approximated next-to-next-to-leading order predictions ($\text{NNLO}_{\text{approx}} + \text{NNLL}$) of the gluino pair production cross section at $\sqrt{s} = 13$ TeV [98–103]. Gluino masses up to 2450 GeV are excluded for $c\tau_0$ between 6 and 550 mm. The largest gluino mass excluded is 2560 GeV with a $c\tau_0$ of 30 mm. These limits are the most restrictive to date on this model for $c\tau_0$ between 1 and 1000 mm.

Figure 10 shows the expected and observed upper limits on the pair production cross section of the long-lived gluinos in the minisplit $\tilde{g} \to q\bar{q}\tilde{\chi}_1^0$ model, assuming a branching fraction of 100% for the gluino to decay into a quark-antiquark pair and the lightest neutralino. The neutralino mass is assumed to be 100 GeV. When the gluino mass is 2400 GeV, signal efficiencies are around 31, 69, and 51% in the 2017 and 2018 analysis for $c\tau_0 = 3$, 30, and 300 mm, respectively. With the data samples collected in 2016–2018, gluino pair production cross sections larger than 0.1 fb are excluded for proper decay lengths between 3 and 900 mm. The upper limits on the pair production cross sections are then translated into upper limits on the gluino mass for different $c\tau_0$, based on the $\text{NNLO}_{\text{approx}} + \text{NNLL}$ gluino pair production cross sections. Gluino masses up to 2500 GeV are excluded for $c\tau_0$ between 7 and 360 mm. The largest gluino mass excluded is 2610 GeV with a $c\tau_0$ of

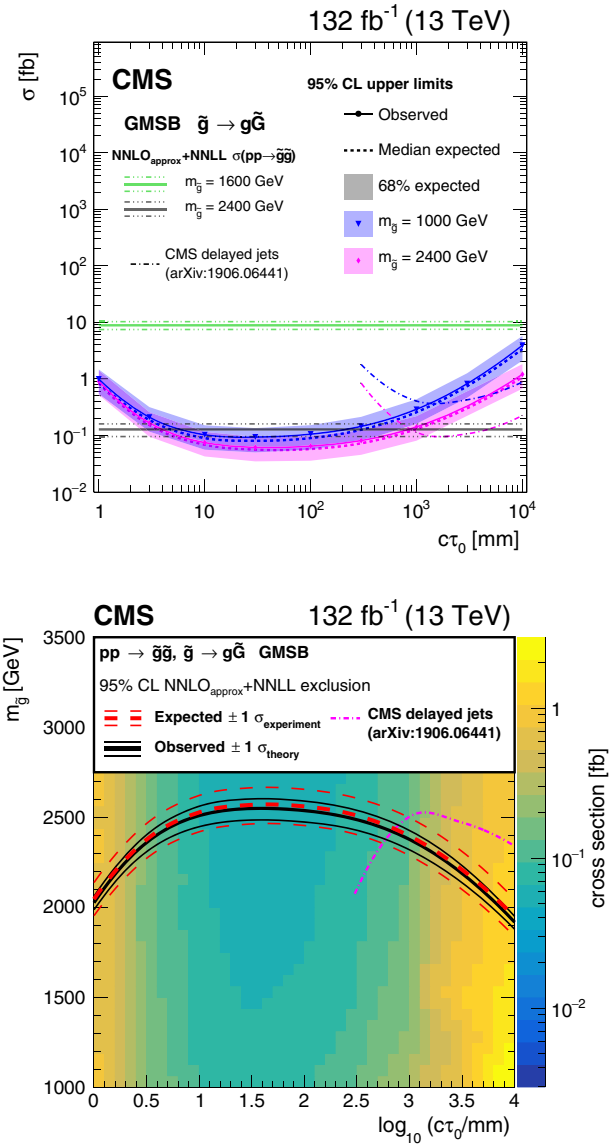


FIG. 9. Upper: the 95% C.L. upper limits on the pair production cross section for the long-lived gluinos with $m_{\tilde{g}} = 2400$ and 1600 GeV, where a 100% branching fraction for $\tilde{g} \to g\tilde{G}$ decays is assumed. The $\text{NNLO}_{\text{approx}} + \text{NNLL}$ gluino pair production cross sections for $m_{\tilde{g}} = 2400$ and 1600 GeV, as well as their variations due to the theoretical uncertainties, are shown as horizontal lines. The solid (dashed) curves show the observed (median expected) limits, and the shaded bands indicate the regions containing 68% of the distributions of the limits expected under the background-only hypothesis. The observed limits from the CMS search utilizing the timing capabilities of the ECAL system [48] are also shown for comparison. Lower: the 95% C.L. upper limits on the pair production cross section for the $\tilde{g} \to g\tilde{G}$ model as a function of the mean proper decay length $c\tau_0$ and the gluino mass $m_{\tilde{g}}$. The thick solid black (dashed red) curve shows the observed (median expected) 95% C.L. limit on the gluino mass as a function of $c\tau_0$, assuming the $\text{NNLO}_{\text{approx}} + \text{NNLL}$ cross sections. The thin dashed red curves indicate the region containing 68% of the distribution of the limits expected under the background-only hypothesis. The thin solid black curves represent the change in the observed limit when the signal cross sections are varied according to their theoretical uncertainties.

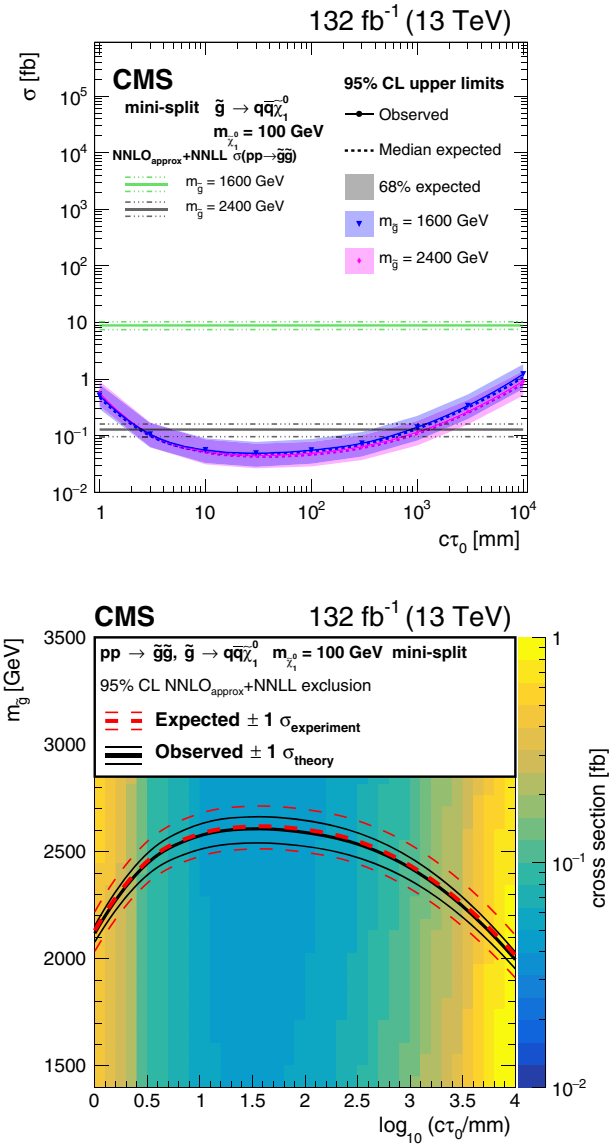


FIG. 10. Upper: the 95% C.L. upper limits on the pair production cross section for the long-lived gluinos with $m_{\tilde{g}} =$ 2400 GeV and 1600 GeV, where a 100% branching fraction for $\tilde{g} \to q\bar{q}\tilde{\chi}_1^0$ decays is assumed. The $\mathrm{NNLO_{approx}} + \mathrm{NNLL}$ gluino pair production cross sections for $m_{\tilde{g}} = 2400$ and 1600 GeV, as well as their variations due to the theoretical uncertainties, are shown as horizontal lines. The solid (dashed) curves show the observed (median expected) limits, and the shaded bands indicate the regions containing 68% of the distributions of the limits expected under the background-only hypothesis. Lower: the 95% C.L. limits on the pair production cross section for the $\tilde{g} \to q\bar{q}\tilde{\chi}_1^0$ model as a function of the mean proper decay length $c\tau_0$ and the gluino mass $m_{\tilde{g}}$. The thick solid black (dashed red) curve shows the observed (median expected) 95% C.L. limits on the gluino mass as a function of $c\tau_0$, assuming the $\mathrm{NNLO_{approx}} + \mathrm{NNLL}$ cross sections. The thin dashed red curves indicate the region containing 68% of the distribution of the limits expected under the background-only hypothesis. The thin solid black curves represent the change in the observed limit when the signal cross sections are varied according to their theoretical uncertainties.

30 mm. These bounds are the most stringent to date on this model for $c\tau_0$ between 10 and 1000 mm.

The expected and observed upper limits on the pair production cross section of the long-lived gluinos in the $\tilde{g} \to tbs$ model are shown in Fig. 11, where a branching fraction of 100% for the gluino to decay into top, bottom, and strange quarks is assumed. When the gluino mass is 2400 GeV, signal efficiencies are around 41, 81, and 66% in the 2017 and 2018 analysis for $c\tau_0 = 3$, 30, and 300 mm, respectively. With the data samples collected in 2016–2018, gluino pair production cross sections larger than 0.1 fb are excluded for $c\tau_0$ between 3 and 1490 mm at $m_{\tilde{g}} = 2400$ GeV. We then compute the upper limits on the gluino mass for different $c\tau_0$ according to the upper limits on the pair production cross section and the calculation of the $\mathrm{NNLO_{approx}} + \mathrm{NNLL}$ gluino pair production cross sections. Gluino masses up to 2500 GeV are excluded for $c\tau_0$ between 3 and 1000 mm. The largest gluino mass excluded is 2640 GeV with a $c\tau_0$ of 30 mm. These limits are the most stringent to date on this model for $c\tau_0$ between 30 and 10^4 mm.

The expected and observed upper limits on the pair production cross section of the long-lived top squarks in the RPV $\tilde{t} \to b\ell$ model are shown in Fig. 12, where a branching fraction of 100% for the top squark to decay into a bottom quark and a charged lepton is assumed, with equal branching fractions for e, μ, and τ. When the top squark mass is 1600 GeV, signal efficiencies are around 22, 43, and 26% in the 2017 and 2018 analysis for $c\tau_0 = 3$, 30, and 300 mm, respectively. With the data samples collected in 2016–2018, top squark pair production cross sections larger than 0.1 fb are excluded for $c\tau_0$ between 8 and 160 mm at $m_{\tilde{t}} = 1600$ GeV. We then compute the upper limits on the top squark mass for different $c\tau_0$ according to the upper limits on the pair production cross section and the calculation of the $\mathrm{NNLO_{approx}} + \mathrm{NNLL}$ top squark pair production cross sections. Top squark masses up to 1600 GeV are excluded for $c\tau_0$ between 5 and 240 mm. The largest top squark mass excluded is 1720 GeV with a $c\tau_0$ of 30 mm. These limits are the most stringent to date on this model in the tested $c\tau_0$ range.

The expected and observed upper limits on the pair production cross section of the long-lived top squarks in the RPV $\tilde{t} \to \bar{d}\bar{d}$ model are shown in Fig. 13, where a branching fraction of 100% for the top squark to decay into a down quark and a charged lepton, with equal branching fractions for e, μ, and τ. When the top squark mass is 1600 GeV, signal efficiencies are around 25, 48, and 29% in the 2017 and 2018 analysis for $c\tau_0 = 3$, 30, and 300 mm, respectively. With the data samples collected in 2016–2018, and top squark pair production cross sections larger than 0.1 fb are excluded for $c\tau_0$ between 7 and 220 mm. We then compute the upper limits on the top squark mass for different $c\tau_0$ according to the upper limits on the pair production cross section and the calculation of

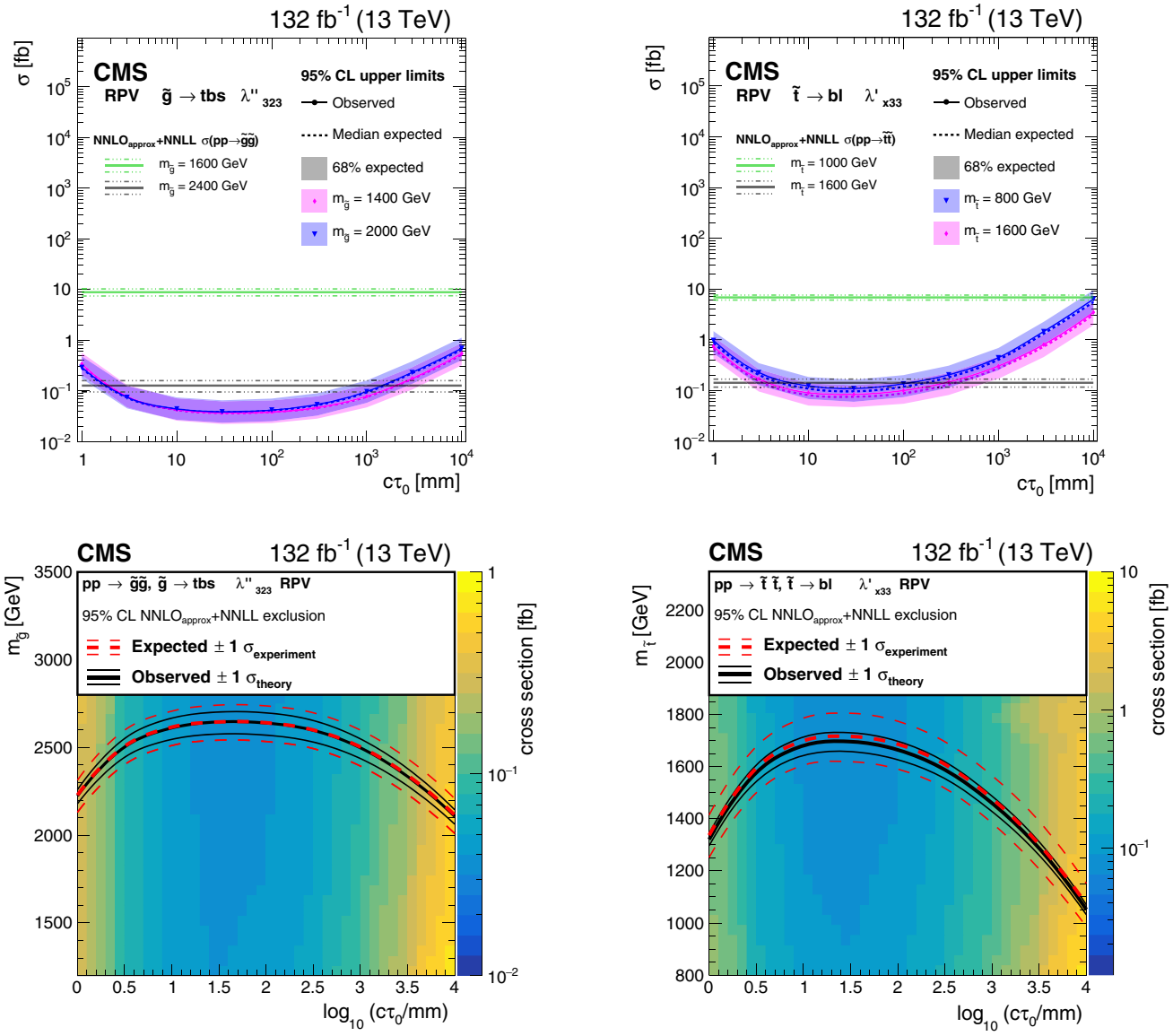


FIG. 11. Upper: the 95% C.L. upper limits on the pair production cross section for the long-lived gluinos with $m_{\tilde{g}} = 2000$ GeV and 1400 GeV, where a 100% branching fraction for $\tilde{g} \to tbs$ decays is assumed. The $\mathrm{NNLO_{approx}} + \mathrm{NNLL}$ gluino pair production cross sections for $m_{\tilde{g}} = 2400$ and 1600 GeV, as well as their variations due to the theoretical uncertainties, are shown as horizontal lines. The solid (dashed) curves show the observed (median expected) limits, and the shaded bands indicate the regions containing 68% of the distributions of the limits expected under the background-only hypothesis. Lower: the 95% C.L. limits on the pair production cross section for the $\tilde{g} \to tbs$ model as a function of the mean proper decay length $c\tau_0$ and the gluino mass $m_{\tilde{g}}$. The thick solid black (dashed red) curve shows the observed (median expected) 95% C.L. limits on the gluino mass as a function of $c\tau_0$, assuming the $\mathrm{NNLO_{approx}} + \mathrm{NNLL}$ cross sections. The thin dashed red curves indicate the region containing 68% of the distribution of the limits expected under the background-only hypothesis. The thin solid black curves represent the change in the observed limit when the signal cross sections are varied according to their theoretical uncertainties.

FIG. 12. Upper: the 95% C.L. upper limits on the pair production cross section for the long-lived top squarks with $m_{\tilde{t}} = 1600$ GeV and 800 GeV, where a 100% branching fraction for $\tilde{t} \to b\ell$ decays is assumed, with equal branching fractions for e, μ, and τ. The $\mathrm{NNLO_{approx}} + \mathrm{NNLL}$ top squark pair production cross sections for $m_{\tilde{t}} = 1600$ and 1000 GeV, as well as their variations due to the theoretical uncertainties, are shown as horizontal lines. The solid (dashed) curves show the observed (median expected) limits, and the shaded bands indicate the regions containing 68% of the distributions of the limits expected under the background-only hypothesis. Lower: the 95% C.L. limits on the pair production cross section for the $\tilde{t} \to b\ell$ model as a function of the mean proper decay length $c\tau_0$ and the top squark mass $m_{\tilde{t}}$. The thick solid black (dashed red) curve shows the observed (median expected) 95% C.L. limits on the top squark mass as a function of $c\tau_0$, assuming the $\mathrm{NNLO_{approx}} + \mathrm{NNLL}$ cross sections. The thin dashed red curves indicate the region containing 68% of the distribution of the limits expected under the background-only hypothesis. The thin solid black curves represent the change in the observed limit when the signal cross sections are varied according to their theoretical uncertainties.

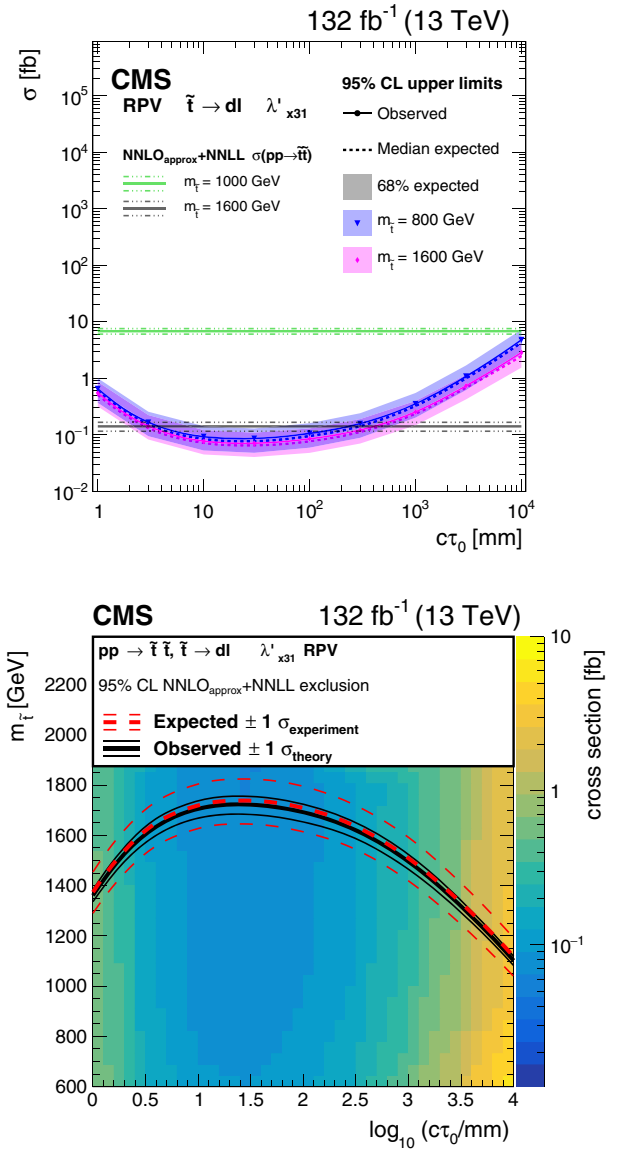


FIG. 13. Upper: the 95% C.L. upper limits on the pair production cross section for the long-lived top squarks with $m_{\tilde{t}} = 1600$ GeV and 800 GeV, where a 100% branching fraction for $\tilde{t} \to d\ell$ decays is assumed, with equal branching fractions for e, μ, and τ. The $\mathrm{NNLO_{approx}} + \mathrm{NNLL}$ top squark pair production cross sections for $m_{\tilde{t}} = 1600$ and 1000 GeV, as well as their variations due to the theoretical uncertainties, are shown as horizontal lines. The solid (dashed) curves show the observed (median expected) limits, and the shaded bands indicate the regions containing 68% of the distributions of the limits expected under the background-only hypothesis. Lower: the 95% C.L. limits on the pair production cross section for the $\tilde{t} \to d\ell$ model as a function of the mean proper decay length $c\tau_0$ and the top squark mass $m_{\tilde{t}}$. The thick solid black (dashed red) curve shows the observed (median expected) 95% C.L. limits on the top squark mass as a function of $c\tau_0$, assuming the $\mathrm{NNLO_{approx}} + \mathrm{NNLL}$ cross sections. The thin dashed red curves indicate the region containing 68% of the distribution of the limits expected under the background-only hypothesis. The thin solid black curves represent the change in the observed limit when the signal cross sections are varied according to their theoretical uncertainties.

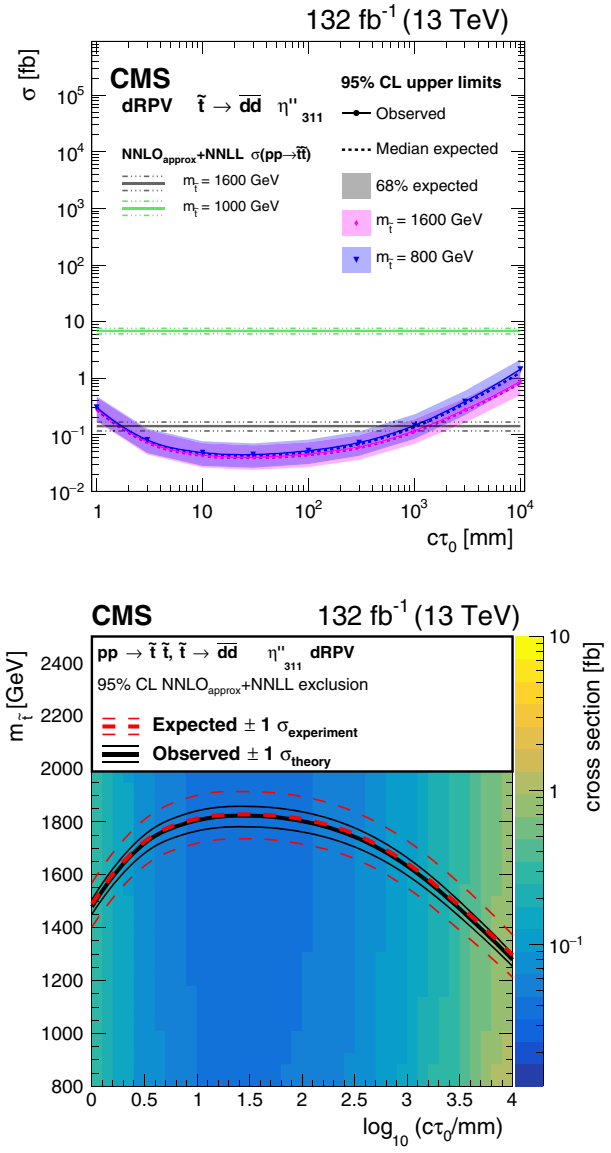


FIG. 14. Upper: the 95% C.L. upper limits on the pair production cross section for the long-lived top squarks with $m_{\tilde{t}} = 1600$ GeV and 800 GeV, where a 100% branching fraction for $\tilde{t} \to \bar{d}\bar{d}$ decays is assumed. The $\mathrm{NNLO_{approx}} + \mathrm{NNLL}$ top squark pair production cross sections for $m_{\tilde{t}} = 1600$ and 1000 GeV, as well as their variations due to the theoretical uncertainties, are shown as horizontal lines. The solid (dashed) curves show the observed (median expected) limits, and the shaded bands indicate the regions containing 68% of the distributions of the limits expected under the background-only hypothesis. Lower: the 95% C.L. limits on the pair production cross section for the $\tilde{t} \to \bar{d}\bar{d}$ model as a function of the mean proper decay length $c\tau_0$ and the top squark mass $m_{\tilde{t}}$. The thick solid black (dashed red) curve shows the observed (median expected) 95% C.L. limits on the top squark mass as a function of $c\tau_0$, assuming the $\mathrm{NNLO_{approx}} + \mathrm{NNLL}$ cross sections. The thin dashed red curves indicate the region containing 68% of the distribution of the limits expected under the background-only hypothesis. The thin solid black curves represent the change in the observed limit when the signal cross sections are varied according to their theoretical uncertainties.

the $\mathrm{NNLO_{approx}} + \mathrm{NNLL}$ top squark pair production cross sections. Top squark masses up to 1600 GeV are excluded for $c\tau_0$ between 3 and 360 mm. The largest top squark mass excluded is 1740 GeV with a $c\tau_0$ of 30 mm. These limits are the most restrictive to date on this model in the tested $c\tau_0$ range.

The expected and observed upper limits on the pair production cross section of the long-lived top squarks in the dRPV $\tilde{t} \to \bar{d}\bar{d}$ model are shown in Fig. 14, where a branching fraction of 100% for the top squark to decay into two down antiquarks is assumed. When the top squark mass is 1600 GeV, signal efficiencies are around 43, 76, and 53% in the 2017 and 2018 analysis for $c\tau_0 = 3$, 30, and 300 mm, respectively. With the data samples collected in 2016–2018, top squark pair production cross sections larger than 0.1 fb are excluded for $c\tau_0$ between 3 and 820 mm at $m_{\tilde{t}} = 1600$ GeV. We then compute the upper limits on the top squark mass for different $c\tau_0$ according to the upper limits on the pair production cross section and the calculation of the $\mathrm{NNLO_{approx}} + \mathrm{NNLL}$ top squark pair production cross sections. Top squark masses up to 1600 GeV are excluded for $c\tau_0$ between 2 and 1320 mm. The largest top squark mass excluded is 1820 GeV with a $c\tau_0$ of 30 mm. These bounds are the most stringent to date on this model for $c\tau_0$ between 10 and 10^4 mm.

VIII. SUMMARY

A search has been presented for long-lived particles decaying to jets, using proton-proton collision data collected with the CMS experiment at a center-of-mass energy of 13 TeV in 2017 and 2018. The results are combined with those of a previous CMS search for displaced jets using proton-proton collision data from 2016, accumulating to a total integrated luminosity of 132 fb^{-1}. After all selections, one event is observed in the data collected in 2017 and 2018, which is consistent with the predicted background yield. The search is designed to be model independent, and is sensitive to a large number of models predicting displaced-jets signatures with different final-state topologies.

The best current limits are set on a variety of models that have long-lived particles with mean proper decay lengths between 1 mm and 10 m. All limits are computed at the 95% confidence level. For a simplified model where pair-produced long-lived neutral particles decay to quark-antiquark pairs, pair production cross sections larger than 0.07 fb are excluded for mean proper decay lengths between 2 and 250 mm at high mass ($m_{\mathrm{X}} > 500$ GeV). For a model where the standard model-like Higgs boson decays to two long-lived scalar particles and each long-lived scalar particle decays to a down (bottom) quark-antiquark pair, branching fractions for the exotic Higgs boson decay larger than 1% (10%) are excluded for mean proper decay lengths between 1 and 340 mm (530 mm) when the scalar particle mass is larger than 40 GeV. For a supersymmetric (SUSY) model in the general gauge mediation scenario, where the long-lived gluino decays to a gluon and a lightest SUSY particle, gluino masses up to 2450 GeV are excluded for mean proper decay lengths between 6 and 550 mm. For another SUSY model in the mini-split scenario, where the long-lived gluino can decay to a quark-antiquark pair and the lightest neutralino, gluino masses up to 2500 GeV are excluded for mean proper decay lengths between 7 and 360 mm. An R-parity violating (RPV) SUSY model is also tested, where the long-lived gluino can decay to top, bottom, and strange antiquarks, and gluino masses up to 2500 GeV are excluded for mean proper decay lengths between 3 and 1000 mm. Another RPV SUSY model is studied, where the long-lived top squark can decay to a bottom quark and a charged lepton, and top squark masses up to 1600 GeV are excluded for mean proper decay lengths between 5 and 240 mm. For an RPV SUSY model, where the long-lived top squark can decay to a down quark and a charged lepton, top squark masses up to 1600 GeV are excluded for mean proper decay lengths between 3 and 360 mm. Finally, for a dynamical-RPV SUSY model, where the long-lived top squark can decay to two down antiquarks, top squark masses up to 1600 GeV are excluded for mean proper decay lengths between 2 and 1320 mm. These are the most stringent limits to date on these models.

ACKNOWLEDGMENTS

We congratulate our colleagues in the CERN accelerator departments for the excellent performance of the LHC and thank the technical and administrative staffs at CERN and at other CMS institutes for their contributions to the success of the CMS effort. In addition, we gratefully acknowledge the computing centers and personnel of the Worldwide LHC Computing Grid for delivering so effectively the computing infrastructure essential to our analyses. Finally, we acknowledge the enduring support for the construction and operation of the LHC and the CMS detector provided by the following funding agencies: BMBWF and FWF (Austria); FNRS and FWO (Belgium); CNPq, CAPES, FAPERJ, FAPERGS, and FAPESP (Brazil); MES (Bulgaria); CERN; CAS, MoST, and NSFC (China); COLCIENCIAS (Colombia); MSES and CSF (Croatia); RIF (Cyprus); SENESCYT (Ecuador); MoER, ERC PUT and ERDF (Estonia); Academy of Finland, MEC, and HIP (Finland); CEA and CNRS/IN2P3 (France); BMBF, DFG, and HGF (Germany); GSRT (Greece); NKFIA (Hungary); DAE and DST (India); IPM (Iran); SFI (Ireland); INFN (Italy); MSIP and NRF (Republic of Korea); MES (Latvia); LAS (Lithuania); MOE and UM (Malaysia); BUAP, CINVESTAV, CONACYT, LNS, SEP, and UASLP-FAI (Mexico); MOS (Montenegro); MBIE (New Zealand); PAEC (Pakistan); MSHE and NSC (Poland); FCT (Portugal); JINR (Dubna); MON, RosAtom, RAS, RFBR, and NRC KI (Russia); MESTD (Serbia); SEIDI, CPAN, PCTI, and FEDER (Spain); MOSTR (Sri Lanka);

Swiss Funding Agencies (Switzerland); MST (Taipei); ThEPCenter, IPST, STAR, and NSTDA (Thailand); TUBITAK and TAEK (Turkey); NASU (Ukraine); STFC (United Kingdom); DOE and NSF (USA). Individuals have received support from the Marie-Curie program and the European Research Council and Horizon 2020 Grant, contracts No. 675440, No. 724704, No. 752730, and No. 765710 (European Union); the Leventis Foundation; the A. P. Sloan Foundation; the Alexander von Humboldt Foundation; the Belgian Federal Science Policy Office; the Fonds pour la Formation *à la* Recherche dans l'Industrie et dans l'Agriculture (FRIA-Belgium); the Agentschap voor Innovatie door Wetenschap en Technologie (IWT-Belgium); the F. R. S.-FNRS and FWO (Belgium) under the "Excellence of Science—EOS"—be.h project n. 30820817; the Beijing Municipal Science & Technology Commission, No. Z191100007219010; the Ministry of Education, Youth and Sports (MEYS) of the Czech Republic; the Deutsche Forschungsgemeinschaft (DFG) under Germany's Excellence Strategy—EXC 2121 "Quantum Universe"—390833306; the Lendület ("Momentum") Program and the János Bolyai Research Scholarship of the Hungarian Academy of Sciences, the New National Excellence Program ÚNKP, the NKFIA research grants No. 123842, No. 123959, No. 124845, No. 124850, No. 125105, No. 128713, No. 128786, and No. 129058 (Hungary); the Council of Science and Industrial Research, India; the HOMING PLUS program of the Foundation for Polish Science, cofinanced from European Union, Regional Development Fund, the Mobility Plus program of the Ministry of Science and Higher Education, the National Science Center (Poland), contracts Harmonia 2014/14/M/ST2/00428, Opus 2014/13/B/ST2/02543, 2014/15/B/ST2/03998, and 2015/19/B/ST2/02861, Sonata-bis 2012/07/E/ST2/01406; the National Priorities Research Program by Qatar National Research Fund; the Ministry of Science and Higher Education, project no. 0723-2020-0041 (Russia); the Tomsk Polytechnic University Competitiveness Enhancement Program; the Programa Estatal de Fomento de la Investigación Científica y Técnica de Excelencia María de Maeztu, Grant No. MDM-2015-0509 and the Programa Severo Ochoa del Principado de Asturias; the Thalis and Aristeia programs cofinanced by EU-ESF and the Greek NSRF; the Rachadapisek Sompot Fund for Postdoctoral Fellowship, Chulalongkorn University and the Chulalongkorn Academic into Its 2nd Century Project Advancement Project (Thailand); the Kavli Foundation; the Nvidia Corporation; the SuperMicro Corporation; the Welch Foundation, Contract C-1845; and the Weston Havens Foundation (USA).

APPENDIX: SIGNAL EFFICIENCIES FOR REPRESENTATIVE SIGNAL POINTS IN DIFFERENT MODELS

TABLE V. Signal efficiencies for the jet-jet model in the 2017 and 2018 analysis at different mean proper decay lengths $c\tau_0$ and different masses m_X. Selection requirements are cumulative from the first row to the last for each value of m_X. Uncertainties are statistical only.

		$c\tau_0$				
Efficiency (%)	m_X (GeV)	1 mm	10 mm	30 mm	100 mm	1000 mm
Trigger	1000	29.47 ± 0.38	89.98 ± 0.67	91.16 ± 0.68	84.41 ± 0.65	71.72 ± 0.66
Preselection		22.56 ± 0.34	85.22 ± 0.65	84.92 ± 0.65	73.83 ± 0.61	27.47 ± 0.41
Final selection		16.27 ± 0.29	73.63 ± 0.61	73.51 ± 0.61	61.51 ± 0.55	20.13 ± 0.35
Trigger	300	25.05 ± 0.35	70.50 ± 0.59	68.19 ± 0.58	58.97 ± 0.54	30.22 ± 0.39
Preselection		17.42 ± 0.30	59.89 ± 0.55	55.40 ± 0.53	42.38 ± 0.46	9.11 ± 0.21
Final selection		12.06 ± 0.25	48.41 ± 0.49	45.13 ± 0.48	32.42 ± 0.40	5.87 ± 0.17
Trigger	100	2.65 ± 0.12	6.97 ± 0.19	6.47 ± 0.18	4.87 ± 0.16	0.95 ± 0.07
Preselection		1.81 ± 0.10	4.94 ± 0.16	4.41 ± 0.15	2.59 ± 0.11	0.28 ± 0.04
Final selection		1.03 ± 0.07	3.47 ± 0.13	3.00 ± 0.12	1.64 ± 0.09	0.17 ± 0.03

TABLE VI. Signal efficiencies for the model where the SM-like Higgs boson decays to two long-lived scalar particles S in the 2017 and 2018 analysis at different mean proper decay lengths $c\tau_0$ and with $m_S = 55$ GeV. The long-lived scalar particle is assumed to decay to a down quark-antiquark pair ($S \to d\bar{d}$). Selection requirements are cumulative from the first row to the last. Uncertainties are statistical only.

		$c\tau_0$				
Efficiency $\times 10^4$	m_S (GeV)	1 mm	10 mm	30 mm	100 mm	1000 mm
Trigger	55	6.63 ± 0.13	32.07 ± 0.29	33.44 ± 1.16	25.25 ± 0.26	5.71 ± 0.12
Preselection		3.11 ± 0.09	13.61 ± 0.19	13.72 ± 0.75	9.39 ± 0.16	1.36 ± 0.06
Final selection		0.95 ± 0.05	6.12 ± 0.13	6.34 ± 0.42	4.46 ± 0.11	0.64 ± 0.04

TABLE VII. Signal efficiencies for the model where the SM-like Higgs boson decays to two long-lived scalar particles S in the 2017 and 2018 analysis at different mean proper decay lengths $c\tau_0$ and with $m_S = 55$ GeV . The long-lived scalar particle is assumed to decay to a bottom quark-antiquark pair ($S \to b\bar{b}$). Selection requirements are cumulative from the first row to the last. Uncertainties are statistical only.

		$c\tau_0$				
Efficiency $\times 10^4$	m_S (GeV)	1 mm	10 mm	30 mm	100 mm	1000 mm
Trigger	55	4.30 ± 0.11	22.56 ± 0.24	24.45 ± 0.48	17.78 ± 0.21	4.05 ± 0.10
Preselection		0.66 ± 0.04	3.30 ± 0.09	3.97 ± 0.19	3.37 ± 0.09	0.57 ± 0.04
Final selection		0.08 ± 0.01	0.96 ± 0.05	1.17 ± 0.10	1.09 ± 0.05	0.19 ± 0.02

TABLE VIII. Signal efficiencies for the $\tilde{g} \to g\tilde{G}$ model in the 2017 and 2018 analysis at different mean proper decay lengths $c\tau_0$ and different masses $m_{\tilde{g}}$. Selection requirements are cumulative from the first row to the last for each value of $m_{\tilde{g}}$. Uncertainties are statistical only.

		$c\tau_0$				
Efficiency (%)	$m_{\tilde{g}}$ (GeV)	1 mm	10 mm	30 mm	100 mm	1000 mm
Trigger	2400	10.69 ± 0.24	69.70 ± 0.60	81.86 ± 0.65	82.86 ± 0.66	73.07 ± 0.38
Preselection		7.03 ± 0.19	63.62 ± 0.57	72.80 ± 0.61	69.67 ± 0.60	35.54 ± 0.27
Final selection		3.84 ± 0.14	44.20 ± 0.48	52.69 ± 0.52	50.84 ± 0.52	24.19 ± 0.22
Trigger	1600	12.04 ± 0.25	68.36 ± 0.59	79.64 ± 0.64	79.96 ± 0.64	67.49 ± 0.38
Preselection		7.52 ± 0.20	60.55 ± 0.56	68.74 ± 0.59	63.47 ± 0.57	29.57 ± 0.25
Final selection		4.02 ± 0.15	41.33 ± 0.46	47.67 ± 0.49	43.16 ± 0.47	19.53 ± 0.20
Trigger	1000	12.14 ± 0.25	62.77 ± 0.56	72.44 ± 0.60	71.90 ± 0.60	52.77 ± 0.51
Preselection		7.29 ± 0.19	53.19 ± 0.52	57.56 ± 0.54	52.25 ± 0.51	21.10 ± 0.32
Final selection		3.75 ± 0.14	34.57 ± 0.42	37.55 ± 0.43	33.84 ± 0.41	12.88 ± 0.25

TABLE IX. Signal efficiencies for the $\tilde{g} \to q\bar{q}\tilde{\chi}_1^0$ model ($m_{\tilde{\chi}_1^0} = 100$ GeV) in the 2017 and 2018 analysis at different mean proper decay lengths $c\tau_0$ and different masses $m_{\tilde{g}}$. Selection requirements are cumulative from the first row to the last for each value of $m_{\tilde{g}}$. Uncertainties are statistical only.

		$c\tau_0$				
Efficiency (%)	$m_{\tilde{g}}$ (GeV)	1 mm	10 mm	30 mm	100 mm	1000 mm
Trigger	2600	15.08 ± 0.28	82.32 ± 0.66	90.46 ± 0.69	87.65 ± 0.68	78.78 ± 0.65
Preselection		9.91 ± 0.23	77.60 ± 0.64	85.82 ± 0.67	80.22 ± 0.65	43.24 ± 0.48
Final selection		5.75 ± 0.17	59.12 ± 0.56	68.44 ± 0.60	63.26 ± 0.58	30.84 ± 0.41
Trigger	2000	17.70 ± 0.31	83.21 ± 0.67	90.46 ± 0.69	87.66 ± 0.68	79.04 ± 0.65
Preselection		11.20 ± 0.24	77.74 ± 0.65	85.04 ± 0.67	79.45 ± 0.65	39.69 ± 0.46
Final selection		6.57 ± 0.19	58.36 ± 0.56	66.29 ± 0.59	60.96 ± 0.57	27.12 ± 0.38
Trigger	1600	19.39 ± 0.32	82.56 ± 0.66	90.27 ± 0.69	87.70 ± 0.68	78.31 ± 0.64
Preselection		12.16 ± 0.26	76.59 ± 0.64	84.13 ± 0.59	77.71 ± 0.64	37.41 ± 0.44
Final selection		6.76 ± 0.19	57.19 ± 0.55	64.37 ± 0.58	57.98 ± 0.55	25.02 ± 0.36

TABLE X. Signal efficiencies for the $\tilde{g} \to tbs$ model in the 2017 and 2018 analysis at different mean proper decay lengths $c\tau_0$ and different masses $m_{\tilde{g}}$. Selection requirements are cumulative from the first row to the last for each value of $m_{\tilde{g}}$. Uncertainties are statistical only.

		$c\tau_0$				
Efficiency (%)	$m_{\tilde{g}}$ (GeV)	1 mm	10 mm	30 mm	100 mm	1000 mm
Trigger	2600	25.14 ± 0.39	90.65 ± 0.70	95.78 ± 0.73	91.42 ± 0.73	83.61 ± 0.67
Preselection		16.26 ± 0.31	87.43 ± 0.69	94.08 ± 0.73	89.30 ± 0.72	56.49 ± 0.55
Final selection		9.60 ± 0.24	71.09 ± 0.62	81.12 ± 0.67	77.55 ± 0.67	42.62 ± 0.48
Trigger	2000	29.89 ± 0.42	91.95 ± 0.71	95.53 ± 0.73	91.58 ± 0.72	83.38 ± 0.68
Preselection		18.93 ± 0.34	88.27 ± 0.70	93.55 ± 0.72	89.17 ± 0.71	52.54 ± 0.54
Final selection		11.29 ± 0.26	72.14 ± 0.63	79.58 ± 0.67	75.52 ± 0.65	38.12 ± 0.46
Trigger	1600	31.61 ± 0.43	92.16 ± 0.71	95.58 ± 0.76	92.03 ± 0.72	84.50 ± 0.67
Preselection		20.06 ± 0.34	88.40 ± 0.70	93.46 ± 0.75	89.04 ± 0.71	50.46 ± 0.52
Final selection		11.71 ± 0.26	70.85 ± 0.63	78.52 ± 0.69	73.77 ± 0.65	35.91 ± 0.44

TABLE XI. Signal efficiencies for the $\tilde{t} \to b\ell$ model in the 2017 and 2018 analysis at different mean proper decay lengths $c\tau_0$ and different masses $m_{\tilde{t}}$. Selection requirements are cumulative from the first row to the last for each value of $m_{\tilde{t}}$. Uncertainties are statistical only.

		$c\tau_0$				
Efficiency (%)	$m_{\tilde{t}}$ (GeV)	1 mm	10 mm	30 mm	100 mm	1000 mm
Trigger	1600	18.00 ± 0.30	66.30 ± 0.58	74.36 ± 0.62	74.48 ± 0.62	66.67 ± 0.59
Preselection		8.45 ± 0.21	54.41 ± 0.53	59.13 ± 0.56	52.63 ± 0.52	21.00 ± 0.33
Final selection		5.03 ± 0.16	39.77 ± 0.45	42.85 ± 0.48	37.02 ± 0.44	12.58 ± 0.25
Trigger	1000	20.13 ± 0.32	65.37 ± 0.58	73.13 ± 0.61	73.74 ± 0.61	61.20 ± 0.56
Preselection		8.32 ± 0.21	48.92 ± 0.49	53.45 ± 0.53	47.68 ± 0.49	16.99 ± 0.30
Final selection		4.65 ± 0.16	33.46 ± 0.41	37.56 ± 0.44	31.81 ± 0.40	10.12 ± 0.23
Trigger	600	19.96 ± 0.32	58.90 ± 0.54	64.58 ± 0.58	64.93 ± 0.58	48.32 ± 0.50
Preselection		6.85 ± 0.19	39.15 ± 0.44	42.25 ± 0.47	36.80 ± 0.44	11.59 ± 0.25
Final selection		3.33 ± 0.13	24.44 ± 0.35	27.69 ± 0.38	23.12 ± 0.35	6.47 ± 0.18

TABLE XII. Signal efficiencies for the $\tilde{t} \to d\ell$ model in the 2017 and 2018 analysis at different mean proper decay lengths $c\tau_0$ and different masses $m_{\tilde{t}}$. Selection requirements are cumulative from the first row to the last for each value of $m_{\tilde{t}}$. Uncertainties are statistical only.

		$c\tau_0$				
Efficiency (%)	$m_{\tilde{t}}$ (GeV)	1 mm	10 mm	30 mm	100 mm	1000 mm
Trigger	1600	18.58 ± 0.31	66.73 ± 0.59	74.69 ± 0.63	74.59 ± 0.64	67.27 ± 0.60
Preselection		10.72 ± 0.24	57.96 ± 0.55	63.08 ± 0.58	56.77 ± 0.56	22.79 ± 0.35
Final selection		6.62 ± 0.19	43.88 ± 0.48	47.92 ± 0.51	41.09 ± 0.47	14.33 ± 0.28
Trigger	1000	19.95 ± 0.33	66.23 ± 0.59	73.87 ± 0.63	73.99 ± 0.64	62.66 ± 0.57
Preselection		9.71 ± 0.23	55.31 ± 0.54	59.93 ± 0.57	53.79 ± 0.54	19.80 ± 0.32
Final selection		5.60 ± 0.17	41.22 ± 0.47	44.38 ± 0.49	38.07 ± 0.46	12.34 ± 0.25
Trigger	600	20.27 ± 0.33	60.49 ± 0.58	66.86 ± 0.61	66.85 ± 0.61	49.73 ± 0.52
Preselection		8.83 ± 0.22	47.48 ± 0.51	50.55 ± 0.53	44.37 ± 0.50	13.46 ± 0.27
Final selection		5.14 ± 0.17	33.96 ± 0.43	36.03 ± 0.45	30.16 ± 0.41	8.19 ± 0.21

TABLE XIII. Signal efficiencies for the $\tilde{t} \to \bar{d}\,\bar{d}$ model in the 2017 and 2018 analysis at different mean proper decay lengths $c\tau_0$ and different masses $m_{\tilde{t}}$. Selection requirements are cumulative from the first row to the last for each value of $m_{\tilde{t}}$. Uncertainties are statistical only.

		$c\tau_0$				
Efficiency (%)	$m_{\tilde{t}}$ (GeV)	1 mm	10 mm	30 mm	100 mm	1000 mm
Trigger	1600	22.10 ± 0.35	87.15 ± 0.71	92.19 ± 0.72	87.73 ± 0.71	79.12 ± 0.67
Preselection		17.06 ± 0.31	84.06 ± 0.70	88.49 ± 0.71	81.10 ± 0.68	39.89 ± 0.48
Final selection		11.78 ± 0.26	71.44 ± 0.65	76.02 ± 0.66	67.02 ± 0.62	28.52 ± 0.40
Trigger	1000	23.86 ± 0.36	86.99 ± 0.72	91.58 ± 0.77	88.19 ± 0.70	78.31 ± 0.66
Preselection		16.96 ± 0.30	82.33 ± 0.70	86.73 ± 0.75	79.72 ± 0.67	35.91 ± 0.45
Final selection		11.91 ± 0.26	69.01 ± 0.64	73.52 ± 0.69	64.23 ± 0.60	25.52 ± 0.38
Trigger	600	24.51 ± 0.37	84.75 ± 0.68	89.27 ± 0.70	85.55 ± 0.68	69.66 ± 0.61
Preselection		15.80 ± 0.29	78.05 ± 0.66	81.84 ± 0.67	74.51 ± 0.64	29.37 ± 0.39
Final selection		11.15 ± 0.25	64.32 ± 0.60	67.68 ± 0.61	58.85 ± 0.57	20.66 ± 0.33

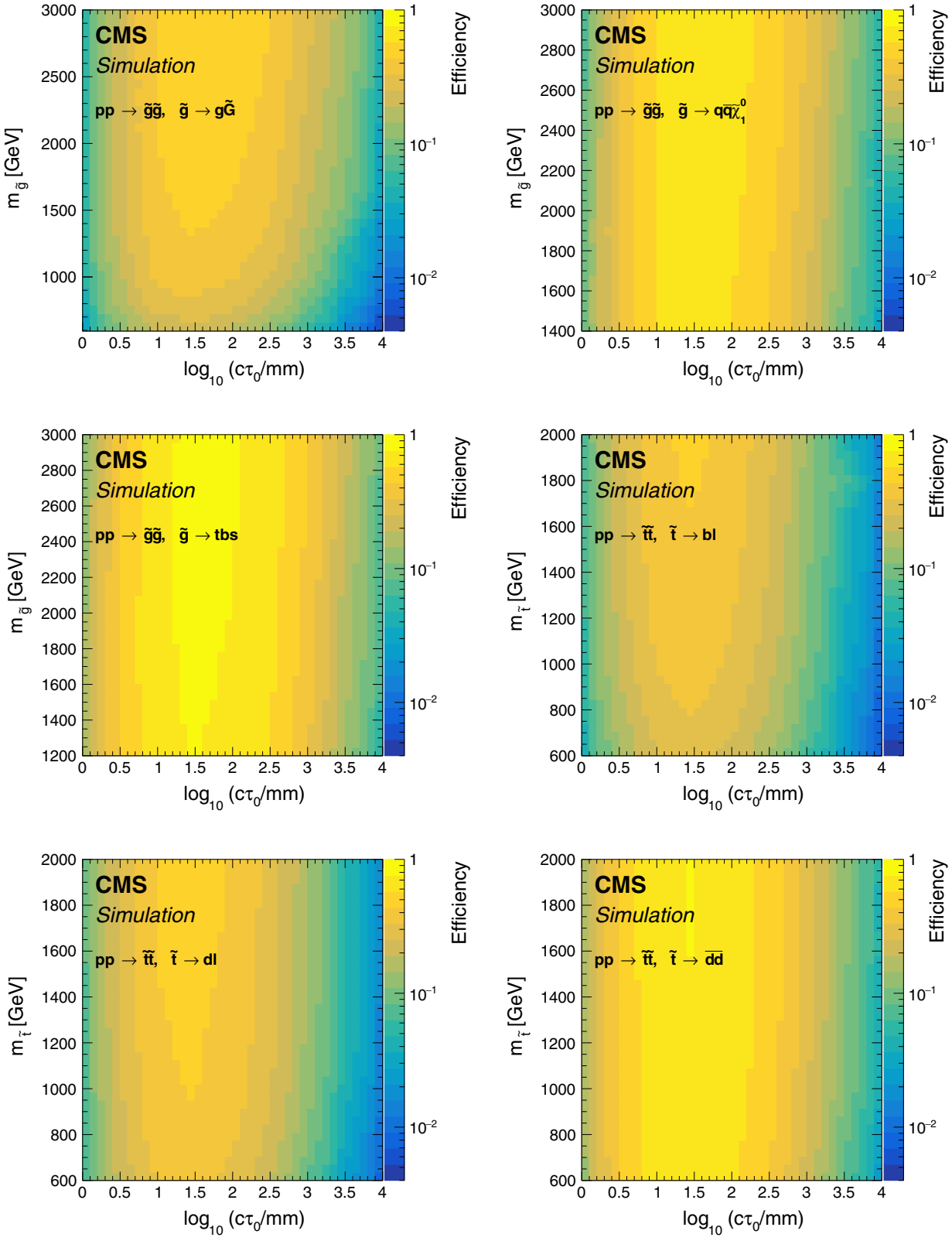


FIG. 15. The signal efficiencies as functions of the long-lived particle mass and mean proper decay length in the 2017 and 2018 analysis, for the $\tilde{g} \to g\tilde{G}$ model (upper left), the $\tilde{g} \to q\bar{q}\tilde{\chi}_1^0$ model (upper right), the $\tilde{g} \to tbs$ model (middle left), the $\tilde{t} \to b\ell$ model (middle right), the $\tilde{t} \to d\ell$ model (lower left), and the $\tilde{t} \to \bar{d}\,\bar{d}$ model (lower right).

[1] N. Arkani-Hamed and S. Dimopoulos, Supersymmetric unification without low energy supersymmetry and signatures for fine-tuning at the LHC, J. High Energy Phys. 06 (2005) 073.

[2] G. F. Giudice and A. Romanino, Split supersymmetry, Nucl. Phys. **B699**, 65 (2004); Erratum, Nucl. Phys. **B706**, 487 (2005).

[3] J. L. Hewett, B. Lillie, M. Masip, and T. G. Rizzo, Signatures of long-lived gluinos in split supersymmetry, J. High Energy Phys. 09 (2004) 070.

[4] N. Arkani-Hamed, S. Dimopoulos, G. F. Giudice, and A. Romanino, Aspects of split supersymmetry, Nucl. Phys. **B709**, 3 (2005).

[5] P. Gambino, G. F. Giudice, and P. Slavich, Gluino decays in split supersymmetry, Nucl. Phys. **B726**, 35 (2005).

[6] A. Arvanitaki, N. Craig, S. Dimopoulos, and G. Villadoro, Mini-Split, J. High Energy Phys. 02 (2013) 126.

[7] N. Arkani-Hamed, A. Gupta, D. E. Kaplan, N. Weiner, and T. Zorawski, Simply unnatural supersymmetry, arXiv: 1212.6971.

[8] P. Fayet, Supergauge invariant extension of the Higgs mechanism and a model for the electron and its neutrino, Nucl. Phys. **B90**, 104 (1975).

[9] G. R. Farrar and P. Fayet, Phenomenology of the production, decay, and detection of new hadronic states associated with supersymmetry, Phys. Lett. **76B**, 575 (1978).

[10] S. Weinberg, Supersymmetry at ordinary energies. 1. Masses and conservation laws, Phys. Rev. D **26**, 287 (1982).

[11] L. J. Hall and M. Suzuki, Explicit *R*-parity breaking in supersymmetric models, Nucl. Phys. **B231**, 419 (1984).

[12] R. Barbier, C. Bérat, M. Besançon, M. Chemtob, A. Deandrea, E. Dudas, P. Fayet, S. Lavignac, G. Moreau, E. Perez, and Y. Sirois, *R*-parity violating supersymmetry, Phys. Rep. **420**, 1 (2005).

[13] G. F. Giudice and R. Rattazzi, Theories with gauge mediated supersymmetry breaking, Phys. Rep. **322**, 419 (1999).

[14] P. Meade, N. Seiberg, and D. Shih, General gauge mediation, Prog. Theor. Phys. Suppl. **177**, 143 (2009).

[15] M. Buican, P. Meade, N. Seiberg, and D. Shih, Exploring general gauge mediation, J. High Energy Phys. 03 (2009) 016.

[16] J. Fan, M. Reece, and J. T. Ruderman, Stealth supersymmetry, J. High Energy Phys. 11 (2011) 012.

[17] J. Fan, M. Reece, and J. T. Ruderman, A stealth supersymmetry sampler, J. High Energy Phys. 07 (2012) 196.

[18] M. J. Strassler and K. M. Zurek, Echoes of a hidden valley at hadron colliders, Phys. Lett. B **651**, 374 (2007).

[19] M. J. Strassler and K. M. Zurek, Discovering the Higgs through highly-displaced vertices, Phys. Lett. B **661**, 263 (2008).

[20] T. Han, Z. Si, K. M. Zurek, and M. J. Strassler, Phenomenology of hidden valleys at hadron colliders, J. High Energy Phys. 07 (2008) 008.

[21] D. E. Kaplan, M. A. Luty, and K. M. Zurek, Asymmetric dark matter, Phys. Rev. D **79**, 115016 (2009).

[22] L. J. Hall, K. Jedamzik, J. March-Russell, and S. M. West, Freeze-in production of FIMP dark matter, J. High Energy Phys. 03 (2010) 080.

[23] I.-W. Kim and K. M. Zurek, Flavor and collider signatures of asymmetric dark matter, Phys. Rev. D **89**, 035008 (2014).

[24] Y. Cui and B. Shuve, Probing baryogenesis with displaced vertices at the LHC, J. High Energy Phys. 02 (2015) 049.

[25] R. T. Co, F. D'Eramo, L. J. Hall, and D. Pappadopulo, Freeze-In dark matter with displaced signatures at colliders, J. Cosmol. Astropart. Phys. 12 (2015) 024.

[26] L. Calibbi, L. Lopez-Honorez, S. Lowette, and A. Mariotti, Singlet-doublet dark matter freeze-in: LHC displaced signatures versus cosmology, J. High Energy Phys. 09 (2018) 037.

[27] Y. Cui, L. Randall, and B. Shuve, A WIMPy baryogenesis miracle, J. High Energy Phys. 04 (2012) 075.

[28] Y. Cui and R. Sundrum, Baryogenesis for weakly interacting massive particles, Phys. Rev. D **87**, 116013 (2013).

[29] A. Atre, T. Han, S. Pascoli, and B. Zhang, The search for heavy Majorana neutrinos, J. High Energy Phys. 05 (2009) 030.

[30] M. Drewes, The phenomenology of right handed neutrinos, Int. J. Mod. Phys. E **22**, 1330019 (2013).

[31] F. F. Deppisch, P. S. Bhupal Dev, and A. Pilaftsis, Neutrinos and collider physics, New J. Phys. **17**, 075019 (2015).

[32] Y. Cai, T. Han, T. Li, and R. Ruiz, Lepton number violation: Seesaw models and their collider tests, Front. Phys. **6**, 40 (2018).

[33] Z. Chacko, H.-S. Goh, and R. Harnik, Natural Electroweak Breaking from a Mirror Symmetry, Phys. Rev. Lett. **96**, 231802 (2006).

[34] H. Cai, H.-C. Cheng, and J. Terning, A quirky little Higgs model, J. High Energy Phys. 05 (2009) 045.

[35] N. Craig, S. Knapen, and P. Longhi, Neutral Naturalness from Orbifold Higgs Models, Phys. Rev. Lett. **114**, 061803 (2015).

[36] N. Craig, A. Katz, M. Strassler, and R. Sundrum, Naturalness in the dark at the LHC, J. High Energy Phys. 07 (2015) 105.

[37] D. Curtin and C. B. Verhaaren, Discovering uncolored naturalness in exotic Higgs decays, J. High Energy Phys. 12 (2015) 072.

[38] S. Alipour-Fard, N. Craig, S. Gori, S. Koren, and D. Redigolo, The second Higgs at the lifetime frontier, J. High Energy Phys. 07 (2020) 029.

[39] CMS Collaboration, The CMS experiment at the CERN LHC, J. Instrum. **3**, S08004 (2008).

[40] CMS Collaboration, Search for long-lived particles decaying into displaced jets in proton-proton collisions at $\sqrt{s} = 13$ TeV, Phys. Rev. D **99**, 032011 (2019).

[41] ATLAS Collaboration, Search for long-lived, massive particles in events with displaced vertices and missing transverse momentum in $\sqrt{s} = 13$ TeV pp collisions with the ATLAS detector, Phys. Rev. D **97**, 052012 (2018).

[42] ATLAS Collaboration, Search for long-lived particles produced in pp collisions at $\sqrt{s} = 13$ TeV that decay into displaced hadronic jets in the ATLAS muon spectrometer, Phys. Rev. D **99**, 052005 (2019).

[43] ATLAS Collaboration, Search for long-lived neutral particles in pp collisions at $\sqrt{s} = 13$ TeV that decay into

displaced hadronic jets in the ATLAS calorimeter, Eur. Phys. J. C **79**, 481 (2019).
[44] ATLAS Collaboration, Search for long-lived, massive particles in events with a displaced vertex and a muon with large impact parameter in pp collisions at $\sqrt{s} =$ 13 TeV with the ATLAS detector, Phys. Rev. D **102**, 032006 (2020).
[45] ATLAS Collaboration, Search for long-lived neutral particles produced in pp collisions at $\sqrt{s} = 13$ TeV decaying into displaced hadronic jets in the ATLAS inner detector and muon spectrometer, Phys. Rev. D **101**, 052013 (2020).
[46] CMS Collaboration, Search for new long-lived particles at $\sqrt{s} = 13$ TeV, Phys. Lett. B **780**, 432 (2018).
[47] CMS Collaboration, Search for long-lived particles with displaced vertices in multijet events in proton-proton collisions at $\sqrt{s} = 13$ TeV, Phys. Rev. D **98**, 092011 (2018).
[48] CMS Collaboration, Search for long-lived particles using nonprompt jets and missing transverse momentum with proton-proton collisions at $\sqrt{s} = 13$ TeV, Phys. Lett. B **797**, 134876 (2019).
[49] CMS Collaboration, Description and performance of track and primary-vertex reconstruction with the CMS tracker, J. Instrum. **9**, P10009 (2014).
[50] CMS Collaboration, The CMS trigger system, J. Instrum. **12**, P01020 (2017).
[51] M. Cacciari, G. P. Salam, and G. Soyez, The anti-k_T jet clustering algorithm, J. High Energy Phys. 04 (2008) 063.
[52] M. Cacciari, G. P. Salam, and G. Soyez, FastJet user manual, Eur. Phys. J. C **72**, 1896 (2012).
[53] CMS Collaboration, Jet energy scale and resolution in the CMS experiment in pp collisions at 8 TeV, J. Instrum. **12**, P02014 (2017).
[54] CMS Collaboration, Technical proposal for the Phase-II upgrade of the CMS detector, CMS Technical proposal CERN-LHCC-2015-010, CMS-TDR-15-02, 2015.
[55] J. Alwall, R. Frederix, S. Frixione, V. Hirschi, F. Maltoni, O. Mattelaer, H. S. Shao, T. Stelzer, P. Torrielli, and M. Zaro, The automated computation of tree-level and next-to-leading order differential cross sections, and their matching to parton shower simulations, J. High Energy Phys. 07 (2014) 079.
[56] T. Sjöstrand, S. Ask, J. R. Christiansen, R. Corke, N. Desai, P. Ilten, S. Mrenna, S. Prestel, C. O. Rasmussen, and P. Z. Skands, An introduction to PYTHIA8.2, Comput. Phys. Commun. **191**, 159 (2015).
[57] J. Alwall *et al.*, Comparative study of various algorithms for the merging of parton showers and matrix elements in hadronic collisions, Eur. Phys. J. C **53**, 473 (2008).
[58] CMS Collaboration, Extraction and validation of a new set of CMS PYTHIA8 tunes from underlying-event measurements, Eur. Phys. J. C **80**, 4 (2020).
[59] R. D. Ball *et al.* (NNPDF Collaboration), Parton distributions from high-precision collider data, Eur. Phys. J. C **77**, 663 (2017).
[60] LHC Higgs Cross Section Working Group, Handbook of LHC Higgs cross sections: 4. Deciphering the nature of the Higgs sector, CERN Report CERN-2017-002-M, 2016.
[61] G. Burdman, Z. Chacko, H.-S. Goh, and R. Harnik, Folded supersymmetry and the LEP paradox, J. High Energy Phys. 02 (2007) 009.
[62] P. Nason, A new method for combining NLO QCD with shower Monte Carlo algorithms, J. High Energy Phys. 11 (2004) 040.
[63] S. Frixione, P. Nason, and C. Oleari, Matching NLO QCD computations with parton shower simulations: The POWHEG method, J. High Energy Phys. 11 (2007) 070.
[64] S. Alioli, P. Nason, C. Oleari, and E. Re, A general framework for implementing NLO calculations in shower Monte Carlo programs: The POWHEG BOX, J. High Energy Phys. 06 (2010) 043.
[65] E. Bagnaschi, G. Degrassi, P. Slavich, and A. Vicini, Higgs production via gluon fusion in the POWHEG approach in the SM and in the MSSM, J. High Energy Phys. 02 (2012) 088.
[66] Z. Liu and B. Tweedie, The fate of long-lived superparticles with hadronic decays after LHC Run 1, J. High Energy Phys. 06 (2015) 042.
[67] C. Csaki, Y. Grossman, and B. Heidenreich, Minimal flavor violation supersymmetry: A natural theory for R-parity violation, Phys. Rev. D **85**, 095009 (2012).
[68] P. W. Graham, D. E. Kaplan, S. Rajendran, and P. Saraswat, Displaced supersymmetry, J. High Energy Phys. 07 (2012) 149.
[69] C. Csaki, E. Kuflik, and T. Volansky, Dynamical R-Parity Violation, Phys. Rev. Lett. **112**, 131801 (2014).
[70] C. Csaki, E. Kuflik, O. Slone, and T. Volansky, Models of dynamical R-parity violation, J. High Energy Phys. 06 (2015) 045.
[71] C. Csaki, E. Kuflik, S. Lombardo, O. Slone, and T. Volansky, Phenomenology of a long-lived LSP with R-parity violation, J. High Energy Phys. 08 (2015) 016.
[72] G. R. Farrar and P. Fayet, Bounds on R-hadron production from calorimetry experiments, Phys. Lett. **79B**, 442 (1978).
[73] M. Fairbairn, A. C. Kraan, D. A. Milstead, T. Sjostrand, P. Z. Skands, and T. Sloan, Stable massive particles at colliders, Phys. Rep. **438**, 1 (2007).
[74] R. Mackeprang and A. Rizzi, Interactions of coloured heavy stable particles in matter, Eur. Phys. J. C **50**, 353 (2007).
[75] R. Mackeprang and D. Milstead, An updated description of heavy-hadron interactions in GEANT-4, Eur. Phys. J. C **66**, 493 (2010).
[76] S. Agostinelli *et al.* (GEANT4 Collaboration), GEANT4—A simulation toolkit, Nucl. Instrum. Methods Phys. Res., Sect. A **506**, 250 (2003).
[77] R. Frühwirth, W. Waltenberger, and P. Vanlaer, Adaptive vertex fitting, J. Phys. G **34**, N343 (2007).
[78] CMS Collaboration, Precision measurement of the structure of the CMS inner tracking system using nuclear interactions, J. Instrum. **13**, P10034 (2018).
[79] CMS Collaboration, CMS technical design report for the pixel detector upgrade, Technical Report No. CERN-LHCC-2012-016, CMS-TDR-011, 2012.
[80] S. C. Johnson, Hierarchical clustering schemes, Psychometrika **32**, 241 (1967).

[81] Y. Freund and R. E. Schapire, Experiments with a new boosting algorithm, in *Proceedings of the Thirteenth International Conference on International Conference on Machine Learning*, ICML'96 (Morgan Kaufmann Publishers Inc., San Francisco, CA, USA, 1996), p. 148.
[82] J. Friedman, T. Hastie, and R. Tibshirani, Additive logistic regression: A statistical view of boosting (with discussion and a rejoinder by the authors), Ann. Stat. **28**, 337 (2000).
[83] J. H. Friedman, Greedy function approximation: A gradient boosting machine, Ann. Stat. **29**, 1189 (2001).
[84] H. Voss, A. Höcker, J. Stelzer, and F. Tegenfeldt, TMVA, the toolkit for multivariate data analysis with ROOT, in *XIth International Workshop on Advanced Computing and Analysis Techniques in Physics Research (ACAT)* (2007), p. 40.
[85] F. Pedregosa *et al.*, Scikit-learn: Machine learning in PYTHON, J. Mach. Learn. Res. **12**, 2825 (2011), https://www.jmlr.org/papers/volume12/pedregosa11a/pedregosa11a.pdf.
[86] G. Punzi, Sensitivity of searches for new signals and its optimization, in *Statistical Problems in Particle Physics, Astrophysics and Cosmology. Proceedings, Conference, PHYSTAT 2003, Stanford, USA, 2003* (2003), p. MODT002, [eConf C030908/MOTD002], arXiv:physics/0308063.
[87] CMS Collaboration, CMS luminosity measurement for the 2017 data-taking period at $\sqrt{s} = 13$ TeV, CMS Physics Analysis Summary CMS-PAS-LUM-17-004, 2018.
[88] CMS Collaboration, CMS luminosity measurement for the 2018 data-taking period at $\sqrt{s} = 13$ TeV, CMS Physics Analysis Summary CMS-PAS-LUM-18-002, 2019.
[89] CMS Collaboration, Measurement of the inelastic proton-proton cross section at $\sqrt{s} = 13$ TeV, J. High Energy Phys. 07 (2018) 161.
[90] S. Dulat, T.-J. Hou, J. Gao, M. Guzzi, J. Huston, P. Nadolsky, J. Pumplin, C. Schmidt, D. Stump, and C. P. Yuan, New parton distribution functions from a global analysis of quantum chromodynamics, Phys. Rev. D **93**, 033006 (2016).
[91] L. A. Harland-Lang, A. D. Martin, P. Motylinski, and R. S. Thorne, Parton distributions in the LHC era: MMHT 2014 PDFs, Eur. Phys. J. C **75**, 204 (2015).
[92] J. Butterworth *et al.*, PDF4LHC recommendations for LHC Run II, J. Phys. G **43**, 023001 (2016).
[93] A. Buckley, J. Ferrando, S. Lloyd, K. Nordström, B. Page, M. Rüfenacht, M. Schönherr, and G. Watt, LHAPDF6: Parton density access in the LHC precision era, Eur. Phys. J. C **75**, 132 (2015).
[94] T. Junk, Confidence level computation for combining searches with small statistics, Nucl. Instrum. Methods Phys. Res., Sect. A **434**, 435 (1999).
[95] A. L. Read, Presentation of search results: The CL_s technique, J. Phys. G **28**, 2693 (2002).
[96] G. Cowan, K. Cranmer, E. Gross, and O. Vitells, Asymptotic formulae for likelihood-based tests of new physics, Eur. Phys. J. C **71**, 1554 (2011).
[97] ATLAS and CMS Collaborations, The LHC Higgs Combination group, Procedure for the LHC Higgs boson search combination in Summer 2011, Technical Report No. CMS-NOTE-2011-005, ATL-PHYS-PUB-2011-11, 2011.
[98] W. Beenakker, R. Hopker, M. Spira, and P. M. Zerwas, Squark and gluino production at hadron colliders, Nucl. Phys. **B492**, 51 (1997).
[99] A. Kulesza and L. Motyka, Threshold Resummation for Squark-Antisquark and Gluino-Pair Production at the LHC, Phys. Rev. Lett. **102**, 111802 (2009).
[100] A. Kulesza and L. Motyka, Soft gluon resummation for the production of gluino-gluino and squark-antisquark pairs at the LHC, Phys. Rev. D **80**, 095004 (2009).
[101] W. Beenakker, S. Brensing, M. n. Kramer, A. Kulesza, E. Laenen, L. Motyka, and I. Niessen, Squark and gluino hadroproduction, Int. J. Mod. Phys. A **26**, 2637 (2011).
[102] C. Borschensky, M. Krämer, A. Kulesza, M. Mangano, S. Padhi, T. Plehn, and X. Portell, Squark and gluino production cross sections in pp collisions at $\sqrt{s} = 13$, 14, 33 and 100 TeV, Eur. Phys. J. C **74**, 3174 (2014).
[103] W. Beenakker, C. Borschensky, M. Krämer, A. Kulesza, and E. Laenen, NNLL-fast: Predictions for coloured supersymmetric particle production at the LHC with threshold and Coulomb resummation, J. High Energy Phys. 12 (2016) 133.

A. M. Sirunyan,[1,a] A. Tumasyan,[1] W. Adam,[2] F. Ambrogi,[2] T. Bergauer,[2] M. Dragicevic,[2] J. Erö,[2] A. Escalante Del Valle,[2] R. Frühwirth,[2,b] M. Jeitler,[2,b] N. Krammer,[2] L. Lechner,[2] D. Liko,[2] T. Madlener,[2] I. Mikulec,[2] F. M. Pitters,[2] N. Rad,[2] J. Schieck,[2,b] R. Schöfbeck,[2] M. Spanring,[2] S. Templ,[2] W. Waltenberger,[2] C.-E. Wulz,[2,b] M. Zarucki,[2] V. Chekhovsky,[3] A. Litomin,[3] V. Makarenko,[3] J. Suarez Gonzalez,[3] M. R. Darwish,[4,c] E. A. De Wolf,[4] D. Di Croce,[4] X. Janssen,[4] T. Kello,[4,d] A. Lelek,[4] M. Pieters,[4] H. Rejeb Sfar,[4] H. Van Haevermaet,[4] P. Van Mechelen,[4] S. Van Putte,[4] N. Van Remortel,[4] F. Blekman,[5] E. S. Bols,[5] S. S. Chhibra,[5] J. D'Hondt,[5] J. De Clercq,[5] D. Lontkovskyi,[5] S. Lowette,[5] I. Marchesini,[5] S. Moortgat,[5] A. Morton,[5] Q. Python,[5] S. Tavernier,[5] W. Van Doninck,[5] P. Van Mulders,[5] D. Beghin,[6] B. Bilin,[6] B. Clerbaux,[6] G. De Lentdecker,[6] B. Dorney,[6] L. Favart,[6] A. Grebenyuk,[6] A. K. Kalsi,[6] I. Makarenko,[6] L. Moureaux,[6] L. Pétré,[6] A. Popov,[6] N. Postiau,[6] E. Starling,[6] L. Thomas,[6] C. Vander Velde,[6] P. Vanlaer,[6] D. Vannerom,[6] L. Wezenbeek,[6] T. Cornelis,[7] D. Dobur,[7] M. Gruchala,[7] I. Khvastunov,[7,e] M. Niedziela,[7] C. Roskas,[7] K. Skovpen,[7] M. Tytgat,[7] W. Verbeke,[7] B. Vermassen,[7] M. Vit,[7] G. Bruno,[8] F. Bury,[8] C. Caputo,[8] P. David,[8] C. Delaere,[8] M. Delcourt,[8] I. S. Donertas,[8]

A. Giammanco,[8] V. Lemaitre,[8] K. Mondal,[8] J. Prisciandaro,[8] A. Taliercio,[8] M. Teklishyn,[8] P. Vischia,[8] S. Wuyckens,[8] J. Zobec,[8] G. A. Alves,[9] G. Correia Silva,[9] C. Hensel,[9] A. Moraes,[9] W. L. Aldá Júnior,[10] E. Belchior Batista Das Chagas,[10] H. Brandao Malbouisson,[10] W. Carvalho,[10] J. Chinellato,[10,f] E. Coelho,[10] E. M. Da Costa,[10] G. G. Da Silveira,[10,g] D. De Jesus Damiao,[10] S. Fonseca De Souza,[10] J. Martins,[10,h] D. Matos Figueiredo,[10] M. Medina Jaime,[10,i] M. Melo De Almeida,[10] C. Mora Herrera,[10] L. Mundim,[10] H. Nogima,[10] P. Rebello Teles,[10] L. J. Sanchez Rosas,[10] A. Santoro,[10] S. M. Silva Do Amaral,[10] A. Sznajder,[10] M. Thiel,[10] E. J. Tonelli Manganote,[10,f] F. Torres Da Silva De Araujo,[10] A. Vilela Pereira,[10] C. A. Bernardes,[11a] L. Calligaris,[11a] T. R. Fernandez Perez Tomei,[11a] E. M. Gregores,[11a,11b] D. S. Lemos,[11a] P. G. Mercadante,[11a,11b] S. F. Novaes,[11a] Sandra S. Padula,[11a] A. Aleksandrov,[12] G. Antchev,[12] I. Atanasov,[12] R. Hadjiiska,[12] P. Iaydjiev,[12] M. Misheva,[12] M. Rodozov,[12] M. Shopova,[12] G. Sultanov,[12] M. Bonchev,[13] A. Dimitrov,[13] T. Ivanov,[13] L. Litov,[13] B. Pavlov,[13] P. Petkov,[13] A. Petrov,[13] W. Fang,[14,d] Q. Guo,[14] H. Wang,[14] L. Yuan,[14] M. Ahmad,[15] Z. Hu,[15] Y. Wang,[15] E. Chapon,[16] G. M. Chen,[16,j] H. S. Chen,[16,j] M. Chen,[16] D. Leggat,[16] H. Liao,[16] Z. Liu,[16] R. Sharma,[16] A. Spiezia,[16] J. Tao,[16] J. Thomas-Wilsker,[16] J. Wang,[16] H. Zhang,[16] S. Zhang,[16,j] J. Zhao,[16] A. Agapitos,[17] Y. Ban,[17] C. Chen,[17] A. Levin,[17] Q. Li,[17] M. Lu,[17] X. Lyu,[17] Y. Mao,[17] S. J. Qian,[17] D. Wang,[17] Q. Wang,[17] J. Xiao,[17] Z. You,[18] X. Gao,[19,d] M. Xiao,[20] C. Avila,[21] A. Cabrera,[21] C. Florez,[21] J. Fraga,[21] A. Sarkar,[21] M. A. Segura Delgado,[21] J. Jaramillo,[22] J. Mejia Guisao,[22] F. Ramirez,[22] J. D. Ruiz Alvarez,[22] C. A. Salazar González,[22] N. Vanegas Arbelaez,[22] D. Giljanovic,[23] N. Godinovic,[23] D. Lelas,[23] I. Puljak,[23] T. Sculac,[23] Z. Antunovic,[24] M. Kovac,[24] V. Brigljevic,[25] D. Ferencek,[25] D. Majumder,[25] M. Roguljic,[25] A. Starodumov,[25,k] T. Susa,[25] M. W. Ather,[26] A. Attikis,[26] E. Erodotou,[26] A. Ioannou,[26] G. Kole,[26] M. Kolosova,[26] S. Konstantinou,[26] G. Mavromanolakis,[26] J. Mousa,[26] C. Nicolaou,[26] F. Ptochos,[26] P. A. Razis,[26] H. Rykaczewski,[26] H. Saka,[26] D. Tsiakkouri,[26] M. Finger,[27,l] M. Finger Jr.,[27,l] A. Kveton,[27] J. Tomsa,[27] E. Ayala,[28] E. Carrera Jarrin,[29] S. Abu Zeid,[30,m] S. Elgammal,[30,n] A. Ellithi Kamel,[30,o] M. A. Mahmoud,[31] Y. Mohammed,[31,p] S. Bhowmik,[32] A. Carvalho Antunes De Oliveira,[32] R. K. Dewanjee,[32] K. Ehataht,[32] M. Kadastik,[32] M. Raidal,[32] C. Veelken,[32] P. Eerola,[33] L. Forthomme,[33] H. Kirschenmann,[33] K. Osterberg,[33] M. Voutilainen,[33] E. Brücken,[34] F. Garcia,[34] J. Havukainen,[34] V. Karimäki,[34] M. S. Kim,[34] R. Kinnunen,[34] T. Lampén,[34] K. Lassila-Perini,[34] S. Laurila,[34] S. Lehti,[34] T. Lindén,[34] H. Siikonen,[34] E. Tuominen,[34] J. Tuominiemi,[34] P. Luukka,[35] T. Tuuva,[35] C. Amendola,[36] M. Besancon,[36] F. Couderc,[36] M. Dejardin,[36] D. Denegri,[36] J. L. Faure,[36] F. Ferri,[36] S. Ganjour,[36] A. Givernaud,[36] P. Gras,[36] G. Hamel de Monchenault,[36] P. Jarry,[36] B. Lenzi,[36] E. Locci,[36] J. Malcles,[36] J. Rander,[36] A. Rosowsky,[36] M. Ö. Sahin,[36] A. Savoy-Navarro,[36,q] M. Titov,[36] G. B. Yu,[36] S. Ahuja,[37] F. Beaudette,[37] M. Bonanomi,[37] A. Buchot Perraguin,[37] P. Busson,[37] C. Charlot,[37] O. Davignon,[37] B. Diab,[37] G. Falmagne,[37] R. Granier de Cassagnac,[37] A. Hakimi,[37] I. Kucher,[37] A. Lobanov,[37] C. Martin Perez,[37] M. Nguyen,[37] C. Ochando,[37] P. Paganini,[37] J. Rembser,[37] R. Salerno,[37] J. B. Sauvan,[37] Y. Sirois,[37] A. Zabi,[37] A. Zghiche,[37] J.-L. Agram,[38,r] J. Andrea,[38] D. Bloch,[38] G. Bourgatte,[38] J.-M. Brom,[38] E. C. Chabert,[38] C. Collard,[38] J.-C. Fontaine,[38,r] D. Gelé,[38] U. Goerlach,[38] C. Grimault,[38] A.-C. Le Bihan,[38] P. Van Hove,[38] E. Asilar,[39] S. Beauceron,[39] C. Bernet,[39] G. Boudoul,[39] C. Camen,[39] A. Carle,[39] N. Chanon,[39] D. Contardo,[39] P. Depasse,[39] H. El Mamouni,[39] J. Fay,[39] S. Gascon,[39] M. Gouzevitch,[39] B. Ille,[39] Sa. Jain,[39] I. B. Laktineh,[39] H. Lattaud,[39] A. Lesauvage,[39] M. Lethuillier,[39] L. Mirabito,[39] L. Torterotot,[39] G. Touquet,[39] M. Vander Donckt,[39] S. Viret,[39] I. Bagaturia,[40,s] Z. Tsamalaidze,[40,l] L. Feld,[41] K. Klein,[41] M. Lipinski,[41] D. Meuser,[41] A. Pauls,[41] M. Preuten,[41] M. P. Rauch,[41] J. Schulz,[41] M. Teroerde,[41] D. Eliseev,[42] M. Erdmann,[42] P. Fackeldey,[42] B. Fischer,[42] S. Ghosh,[42] T. Hebbeker,[42] K. Hoepfner,[42] H. Keller,[42] L. Mastrolorenzo,[42] M. Merschmeyer,[42] A. Meyer,[42] P. Millet,[42] G. Mocellin,[42] S. Mondal,[42] S. Mukherjee,[42] D. Noll,[42] A. Novak,[42] T. Pook,[42] A. Pozdnyakov,[42] T. Quast,[42] M. Radziej,[42] Y. Rath,[42] H. Reithler,[42] J. Roemer,[42] A. Schmidt,[42] S. C. Schuler,[42] A. Sharma,[42] S. Wiedenbeck,[42] S. Zaleski,[42] C. Dziwok,[43] G. Flügge,[43] W. Haj Ahmad,[43,t] O. Hlushchenko,[43] T. Kress,[43] A. Nowack,[43] C. Pistone,[43] O. Pooth,[43] D. Roy,[43] H. Sert,[43] A. Stahl,[43,u] T. Ziemons,[43] H. Aarup Petersen,[44] M. Aldaya Martin,[44] P. Asmuss,[44] I. Babounikau,[44] S. Baxter,[44] O. Behnke,[44] A. Bermúdez Martínez,[44] A. A. Bin Anuar,[44] K. Borras,[44,v] V. Botta,[44] D. Brunner,[44] A. Campbell,[44] A. Cardini,[44] P. Connor,[44] S. Consuegra Rodríguez,[44] V. Danilov,[44] A. De Wit,[44] M. M. Defranchis,[44] L. Didukh,[44] D. Domínguez Damiani,[44] G. Eckerlin,[44] D. Eckstein,[44] T. Eichhorn,[44] L. I. Estevez Banos,[44] E. Gallo,[44,w] A. Geiser,[44] A. Giraldi,[44] A. Grohsjean,[44] M. Guthoff,[44] A. Harb,[44] A. Jafari,[44,x] N. Z. Jomhari,[44] H. Jung,[44] A. Kasem,[44,v] M. Kasemann,[44] H. Kaveh,[44] C. Kleinwort,[44] J. Knolle,[44] D. Krücker,[44] W. Lange,[44] T. Lenz,[44] J. Lidrych,[44] K. Lipka,[44] W. Lohmann,[44,y] R. Mankel,[44] I.-A. Melzer-Pellmann,[44] J. Metwally,[44] A. B. Meyer,[44] M. Meyer,[44] M. Missiroli,[44] J. Mnich,[44] A. Mussgiller,[44] V. Myronenko,[44] Y. Otarid,[44] D. Pérez Adán,[44] S. K. Pflitsch,[44] D. Pitzl,[44] A. Raspereza,[44] A. Saggio,[44] A. Saibel,[44] M. Savitskyi,[44] V. Scheurer,[44] P. Schütze,[44]

C. Schwanenberger,[44] A. Singh,[44] R. E. Sosa Ricardo,[44] N. Tonon,[44] O. Turkot,[44] A. Vagnerini,[44] M. Van De Klundert,[44] R. Walsh,[44] D. Walter,[44] Y. Wen,[44] K. Wichmann,[44] C. Wissing,[44] S. Wuchterl,[44] O. Zenaiev,[44] R. Zlebcik,[44] R. Aggleton,[45] S. Bein,[45] L. Benato,[45] A. Benecke,[45] K. De Leo,[45] T. Dreyer,[45] A. Ebrahimi,[45] M. Eich,[45] F. Feindt,[45] A. Fröhlich,[45] C. Garbers,[45] E. Garutti,[45] P. Gunnellini,[45] J. Haller,[45] A. Hinzmann,[45] A. Karavdina,[45] G. Kasieczka,[45] R. Klanner,[45] R. Kogler,[45] V. Kutzner,[45] J. Lange,[45] T. Lange,[45] A. Malara,[45] C. E. N. Niemeyer,[45] A. Nigamova,[45] K. J. Pena Rodriguez,[45] O. Rieger,[45] P. Schleper,[45] S. Schumann,[45] J. Schwandt,[45] D. Schwarz,[45] J. Sonneveld,[45] H. Stadie,[45] G. Steinbrück,[45] B. Vormwald,[45] I. Zoi,[45] M. Baselga,[46] S. Baur,[46] J. Bechtel,[46] T. Berger,[46] E. Butz,[46] R. Caspart,[46] T. Chwalek,[46] W. De Boer,[46] A. Dierlamm,[46] A. Droll,[46] K. El Morabit,[46] N. Faltermann,[46] K. Flöh,[46] M. Giffels,[46] A. Gottmann,[46] F. Hartmann,[46,u] C. Heidecker,[46] U. Husemann,[46] M. A. Iqbal,[46] I. Katkov,[46,z] P. Keicher,[46] R. Koppenhöfer,[46] S. Maier,[46] M. Metzler,[46] S. Mitra,[46] D. Müller,[46] Th. Müller,[46] M. Musich,[46] G. Quast,[46] K. Rabbertz,[46] J. Rauser,[46] D. Savoiu,[46] D. Schäfer,[46] M. Schnepf,[46] M. Schröder,[46] D. Seith,[46] I. Shvetsov,[46] H. J. Simonis,[46] R. Ulrich,[46] M. Wassmer,[46] M. Weber,[46] R. Wolf,[46] S. Wozniewski,[46] G. Anagnostou,[47] P. Asenov,[47] G. Daskalakis,[47] T. Geralis,[47] A. Kyriakis,[47] D. Loukas,[47] G. Paspalaki,[47] A. Stakia,[47] M. Diamantopoulou,[48] D. Karasavvas,[48] G. Karathanasis,[48] P. Kontaxakis,[48] C. K. Koraka,[48] A. Manousakis-Katsikakis,[48] A. Panagiotou,[48] I. Papavergou,[48] N. Saoulidou,[48] K. Theofilatos,[48] K. Vellidis,[48] E. Vourliotis,[48] G. Bakas,[49] K. Kousouris,[49] I. Papakrivopoulos,[49] G. Tsipolitis,[49] A. Zacharopoulou,[49] I. Evangelou,[50] C. Foudas,[50] P. Gianneios,[50] P. Katsoulis,[50] P. Kokkas,[50] S. Mallios,[50] K. Manitara,[50] N. Manthos,[50] I. Papadopoulos,[50] J. Strologas,[50] M. Bartók,[51,aa] R. Chudasama,[51] M. Csanad,[51] M. M. A. Gadallah,[51,bb] S. Lökös,[51,cc] P. Major,[51] K. Mandal,[51] A. Mehta,[51] G. Pasztor,[51] O. Surányi,[51] G. I. Veres,[51] G. Bencze,[52] C. Hajdu,[52] D. Horvath,[52,dd] F. Sikler,[52] V. Veszpremi,[52] G. Vesztergombi,[52,a,cc] S. Czellar,[53] J. Karancsi,[53,aa] J. Molnar,[53] Z. Szillasi,[53] D. Teyssier,[53] P. Raics,[54] Z. L. Trocsanyi,[54] B. Ujvari,[54] T. Csorgo,[55] F. Nemes,[55] T. Novak,[55] S. Choudhury,[56] J. R. Komaragiri,[56] D. Kumar,[56] L. Panwar,[56] P. C. Tiwari,[56] S. Bahinipati,[57,ee] D. Dash,[57] C. Kar,[57] P. Mal,[57] T. Mishra,[57] V. K. Muraleedharan Nair Bindhu,[57] A. Nayak,[57,ff] D. K. Sahoo,[57,ee] N. Sur,[57] S. K. Swain,[57] S. Bansal,[58] S. B. Beri,[58] V. Bhatnagar,[58] S. Chauhan,[58] N. Dhingra,[58,gg] R. Gupta,[58] A. Kaur,[58] S. Kaur,[58] P. Kumari,[58] M. Lohan,[58] M. Meena,[58] K. Sandeep,[58] S. Sharma,[58] J. B. Singh,[58] A. K. Virdi,[58] A. Ahmed,[59] A. Bhardwaj,[59] B. C. Choudhary,[59] R. B. Garg,[59] M. Gola,[59] S. Keshri,[59] A. Kumar,[59] M. Naimuddin,[59] P. Priyanka,[59] K. Ranjan,[59] A. Shah,[59] M. Bharti,[60,hh] R. Bhattacharya,[60] S. Bhattacharya,[60] D. Bhowmik,[60] S. Dutta,[60] S. Ghosh,[60] B. Gomber,[60,ii] M. Maity,[60,jj] S. Nandan,[60] P. Palit,[60] A. Purohit,[60] P. K. Rout,[60] G. Saha,[60] S. Sarkar,[60] M. Sharan,[60] B. Singh,[60,hh] S. Thakur,[60,hh] P. K. Behera,[61] S. C. Behera,[61] P. Kalbhor,[61] A. Muhammad,[61] R. Pradhan,[61] P. R. Pujahari,[61] A. Sharma,[61] A. K. Sikdar,[61] D. Dutta,[62] V. Kumar,[62] K. Naskar,[62,kk] P. K. Netrakanti,[62] L. M. Pant,[62] P. Shukla,[62] T. Aziz,[63] M. A. Bhat,[63] S. Dugad,[63] R. Kumar Verma,[63] U. Sarkar,[63] S. Banerjee,[64] S. Bhattacharya,[64] S. Chatterjee,[64] P. Das,[64] M. Guchait,[64] S. Karmakar,[64] S. Kumar,[64] G. Majumder,[64] K. Mazumdar,[64] S. Mukherjee,[64] D. Roy,[64] N. Sahoo,[64] S. Dube,[65] B. Kansal,[65] A. Kapoor,[65] K. Kothekar,[65] S. Pandey,[65] A. Rane,[65] A. Rastogi,[65] S. Sharma,[65] H. Bakhshiansohi,[66,ll] S. Chenarani,[67,mm] S. M. Etesami,[67] M. Khakzad,[67] M. Mohammadi Najafabadi,[67] M. Felcini,[68] M. Grunewald,[68] M. Abbrescia,[69a,69b] R. Aly,[69a,69b,nn] C. Aruta,[69a,69b] A. Colaleo,[69a] D. Creanza,[69a,69c] N. De Filippis,[69a,69c] M. De Palma,[69a,69b] A. Di Florio,[69a,69b] A. Di Pilato,[69a,69b] W. Elmetenawee,[69a,69b] L. Fiore,[69a] A. Gelmi,[69a,69b] M. Gul,[69a] G. Iaselli,[69a,69c] M. Ince,[69a,69b] S. Lezki,[69a,69b] G. Maggi,[69a,69c] M. Maggi,[69a] I. Margjeka,[69a,69b] J. A. Merlin,[69a] S. My,[69a,69b] S. Nuzzo,[69a,69b] A. Pompili,[69a,69b] G. Pugliese,[69a,69c] A. Ranieri,[69a] G. Selvaggi,[69a,69b] L. Silvestris,[69a] F. M. Simone,[69a,69b] R. Venditti,[69a] P. Verwilligen,[69a] G. Abbiendi,[70a] C. Battilana,[70a,70b] D. Bonacorsi,[70a,70b] L. Borgonovi,[70a,70b] S. Braibant-Giacomelli,[70a,70b] R. Campanini,[70a,70b] P. Capiluppi,[70a,70b] A. Castro,[70a,70b] F. R. Cavallo,[70a] M. Cuffiani,[70a,70b] G. M. Dallavalle,[70a] T. Diotalevi,[70a,70b] F. Fabbri,[70a] A. Fanfani,[70a,70b] E. Fontanesi,[70a,70b] P. Giacomelli,[70a] L. Giommi,[70a,70b] C. Grandi,[70a] L. Guiducci,[70a,70b] F. Iemmi,[70a,70b] S. Lo Meo,[70a,oo] S. Marcellini,[70a] G. Masetti,[70a] F. L. Navarria,[70a,70b] A. Perrotta,[70a] F. Primavera,[70a,70b] A. M. Rossi,[70a,70b] T. Rovelli,[70a,70b] G. P. Siroli,[70a,70b] N. Tosi,[70a] S. Albergo,[71a,71b,pp] S. Costa,[71a,71b] A. Di Mattia,[71a] R. Potenza,[71a,71b] A. Tricomi,[71a,71b,pp] C. Tuve,[71a,71b] G. Barbagli,[72a] A. Cassese,[72a] R. Ceccarelli,[72a,72b] V. Ciulli,[72a,72b] C. Civinini,[72a] R. D'Alessandro,[72a,72b] F. Fiori,[72a] E. Focardi,[72a,72b] G. Latino,[72a,72b] P. Lenzi,[72a,72b] M. Lizzo,[72a,72b] M. Meschini,[72a] S. Paoletti,[72a] R. Seidita,[72a,72b] G. Sguazzoni,[72a] L. Viliani,[72a] L. Benussi,[73] S. Bianco,[73] D. Piccolo,[73] M. Bozzo,[74a,74b] F. Ferro,[74a] R. Mulargia,[74a,74b] E. Robutti,[74a] S. Tosi,[74a,74b] A. Benaglia,[75a] A. Beschi,[75a,75b] F. Brivio,[75a,75b] F. Cetorelli,[75a,75b] V. Ciriolo,[75a,75b,u] F. De Guio,[75a,75b] M. E. Dinardo,[75a,75b] P. Dini,[75a] S. Gennai,[75a] A. Ghezzi,[75a,75b] P. Govoni,[75a,75b] L. Guzzi,[75a,75b] M. Malberti,[75a] S. Malvezzi,[75a] D. Menasce,[75a] F. Monti,[75a,75b] L. Moroni,[75a] M. Paganoni,[75a,75b] D. Pedrini,[75a] S. Ragazzi,[75a,75b] T. Tabarelli de Fatis,[75a,75b] D. Valsecchi,[75a,75b,u]

D. Zuolo,[75a,75b] S. Buontempo,[76a] N. Cavallo,[76a,76c] A. De Iorio,[76a,76b] F. Fabozzi,[76a,76c] F. Fienga,[76a] A. O. M. Iorio,[76a,76b] L. Layer,[76a,76b] L. Lista,[76a,76b] S. Meola,[76a,76d,u] P. Paolucci,[76a,u] B. Rossi,[76a] C. Sciacca,[76a,76b] E. Voevodina,[76a,76b] P. Azzi,[77a] N. Bacchetta,[77a] A. Boletti,[77a,77b] A. Bragagnolo,[77a,77b] R. Carlin,[77a,77b] P. Checchia,[77a] P. De Castro Manzano,[77a] T. Dorigo,[77a] F. Gasparini,[77a,77b] U. Gasparini,[77a,77b] S. Y. Hoh,[77a,77b] M. Margoni,[77a,77b] A. T. Meneguzzo,[77a,77b] M. Presilla,[77a,77b] P. Ronchese,[77a,77b] R. Rossin,[77a,77b] F. Simonetto,[77a,77b] G. Strong,[77a] A. Tiko,[77a] M. Tosi,[77a,77b] H. YARAR,[77a,77b] M. Zanetti,[77a,77b] P. Zotto,[77a,77b] A. Zucchetta,[77a,77b] G. Zumerle,[77a,77b] A. Braghieri,[78a] S. Calzaferri,[78a,78b] D. Fiorina,[78a,78b] P. Montagna,[78a,78b] S. P. Ratti,[78a,78b] V. Re,[78a] M. Ressegotti,[78a,78b] C. Riccardi,[78a,78b] P. Salvini,[78a] I. Vai,[78a] P. Vitulo,[78a,78b] M. Biasini,[79a,79b] G. M. Bilei,[79a] D. Ciangottini,[79a,79b] L. Fanò,[79a,79b] P. Lariccia,[79a,79b] G. Mantovani,[79a,79b] V. Mariani,[79a,79b] M. Menichelli,[79a] F. Moscatelli,[79a] A. Rossi,[79a,79b] A. Santocchia,[79a,79b] D. Spiga,[79a] T. Tedeschi,[79a,79b] K. Androsov,[80a] P. Azzurri,[80a] G. Bagliesi,[80a] V. Bertacchi,[80a,80c] L. Bianchini,[80a] T. Boccali,[80a] R. Castaldi,[80a] M. A. Ciocci,[80a,80b] R. Dell'Orso,[80a] M. R. Di Domenico,[80a,80b] S. Donato,[80a] L. Giannini,[80a,80c] A. Giassi,[80a] M. T. Grippo,[80a] F. Ligabue,[80a,80c] E. Manca,[80a,80c] G. Mandorli,[80a,80c] A. Messineo,[80a,80b] F. Palla,[80a] G. Ramirez-Sanchez,[80a,80c] A. Rizzi,[80a,80b] G. Rolandi,[80a,80c] S. Roy Chowdhury,[80a,80c] A. Scribano,[80a] N. Shafiei,[80a,80b] P. Spagnolo,[80a] R. Tenchini,[80a] G. Tonelli,[80a,80b] N. Turini,[80a] A. Venturi,[80a] P. G. Verdini,[80a] F. Cavallari,[81a] M. Cipriani,[81a,81b] D. Del Re,[81a,81b] E. Di Marco,[81a] M. Diemoz,[81a] E. Longo,[81a,81b] P. Meridiani,[81a] G. Organtini,[81a,81b] F. Pandolfi,[81a] R. Paramatti,[81a,81b] C. Quaranta,[81a,81b] S. Rahatlou,[81a,81b] C. Rovelli,[81a] F. Santanastasio,[81a,81b] L. Soffi,[81a,81b] R. Tramontano,[81a,81b] N. Amapane,[82a,82b] R. Arcidiacono,[82a,82c] S. Argiro,[82a,82b] M. Arneodo,[82a,82c] N. Bartosik,[82a] R. Bellan,[82a,82b] A. Bellora,[82a,82b] C. Biino,[82a] A. Cappati,[82a,82b] N. Cartiglia,[82a] S. Cometti,[82a] M. Costa,[82a,82b] R. Covarelli,[82a,82b] N. Demaria,[82a] B. Kiani,[82a,82b] F. Legger,[82a] C. Mariotti,[82a] S. Maselli,[82a] E. Migliore,[82a,82b] V. Monaco,[82a,82b] E. Monteil,[82a,82b] M. Monteno,[82a] M. M. Obertino,[82a,82b] G. Ortona,[82a] L. Pacher,[82a,82b] N. Pastrone,[82a] M. Pelliccioni,[82a] G. L. Pinna Angioni,[82a,82b] M. Ruspa,[82a,82c] R. Salvatico,[82a,82b] F. Siviero,[82a,82b] V. Sola,[82a] A. Solano,[82a,82b] D. Soldi,[82a,82b] A. Staiano,[82a] D. Trocino,[82a,82b] S. Belforte,[83a] V. Candelise,[83a,83b] M. Casarsa,[83a] F. Cossutti,[83a] A. Da Rold,[83a,83b] G. Della Ricca,[83a,83b] F. Vazzoler,[83a,83b] S. Dogra,[84] C. Huh,[84] B. Kim,[84] D. H. Kim,[84] G. N. Kim,[84] J. Lee,[84] S. W. Lee,[84] C. S. Moon,[84] Y. D. Oh,[84] S. I. Pak,[84] B. C. Radburn-Smith,[84] S. Sekmen,[84] Y. C. Yang,[84] H. Kim,[85] D. H. Moon,[85] B. Francois,[86] T. J. Kim,[86] J. Park,[86] S. Cho,[87] S. Choi,[87] Y. Go,[87] S. Ha,[87] B. Hong,[87] K. Lee,[87] K. S. Lee,[87] J. Lim,[87] J. Park,[87] S. K. Park,[87] J. Yoo,[87] J. Goh,[88] A. Gurtu,[88] H. S. Kim,[89] Y. Kim,[89] J. Almond,[90] J. H. Bhyun,[90] J. Choi,[90] S. Jeon,[90] J. Kim,[90] J. S. Kim,[90] S. Ko,[90] H. Kwon,[90] H. Lee,[90] K. Lee,[90] S. Lee,[90] K. Nam,[90] B. H. Oh,[90] M. Oh,[90] S. B. Oh,[90] H. Seo,[90] U. K. Yang,[90] I. Yoon,[90] D. Jeon,[91] J. H. Kim,[91] B. Ko,[91] J. S. H. Lee,[91] I. C. Park,[91] Y. Roh,[91] D. Song,[91] I. J. Watson,[91] H. D. Yoo,[92] Y. Choi,[93] C. Hwang,[93] Y. Jeong,[93] H. Lee,[93] Y. Lee,[93] I. Yu,[93] Y. Maghrbi,[94] V. Veckalns,[95,qq] A. Juodagalvis,[96] A. Rinkevicius,[96] G. Tamulaitis,[96] W. A. T. Wan Abdullah,[97] M. N. Yusli,[97] Z. Zolkapli,[97] J. F. Benitez,[98] A. Castaneda Hernandez,[98] J. A. Murillo Quijada,[98] L. Valencia Palomo,[98] H. Castilla-Valdez,[99] E. De La Cruz-Burelo,[99] I. Heredia-De La Cruz,[99,rr] R. Lopez-Fernandez,[99] A. Sanchez-Hernandez,[99] S. Carrillo Moreno,[100] C. Oropeza Barrera,[100] M. Ramirez-Garcia,[100] F. Vazquez Valencia,[100] J. Eysermans,[101] I. Pedraza,[101] H. A. Salazar Ibarguen,[101] C. Uribe Estrada,[101] A. Morelos Pineda,[102] J. Mijuskovic,[103,e] N. Raicevic,[103] D. Krofcheck,[104] S. Bheesette,[105] P. H. Butler,[105] A. Ahmad,[106] M. I. Asghar,[106] M. I. M. Awan,[106] H. R. Hoorani,[106] W. A. Khan,[106] M. A. Shah,[106] M. Shoaib,[106] M. Waqas,[106] V. Avati,[107] L. Grzanka,[107] M. Malawski,[107] H. Bialkowska,[108] M. Bluj,[108] B. Boimska,[108] T. Frueboes,[108] M. Górski,[108] M. Kazana,[108] M. Szleper,[108] P. Traczyk,[108] P. Zalewski,[108] K. Bunkowski,[109] A. Byszuk,[109,ss] K. Doroba,[109] A. Kalinowski,[109] M. Konecki,[109] J. Krolikowski,[109] M. Olszewski,[109] M. Walczak,[109] M. Araujo,[110] P. Bargassa,[110] D. Bastos,[110] P. Faccioli,[110] M. Gallinaro,[110] J. Hollar,[110] N. Leonardo,[110] T. Niknejad,[110] J. Seixas,[110] K. Shchelina,[110] O. Toldaiev,[110] J. Varela,[110] S. Afanasiev,[111] P. Bunin,[111] Y. Ershov,[111] M. Gavrilenko,[111] A. Golunov,[111] I. Golutvin,[111] N. Gorbounov,[111] I. Gorbunov,[111] V. Karjavine,[111] A. Lanev,[111] A. Malakhov,[111] V. Matveev,[111,tt,uu] P. Moisenz,[111] V. Palichik,[111] V. Perelygin,[111] M. Savina,[111] S. Shmatov,[111] S. Shulha,[111] V. Smirnov,[111] O. Teryaev,[111] N. Voytishin,[111] B. S. Yuldashev,[111,vv] A. Zarubin,[111] G. Gavrilov,[112] V. Golovtcov,[112] Y. Ivanov,[112] V. Kim,[112,ww] E. Kuznetsova,[112,xx] V. Murzin,[112] V. Oreshkin,[112] I. Smirnov,[112] D. Sosnov,[112] V. Sulimov,[112] L. Uvarov,[112] S. Volkov,[112] A. Vorobyev,[112] Yu. Andreev,[113] A. Dermenev,[113] S. Gninenko,[113] N. Golubev,[113] A. Karneyeu,[113] M. Kirsanov,[113] N. Krasnikov,[113] A. Pashenkov,[113] G. Pivovarov,[113] D. Tlisov,[113,a] A. Toropin,[113] V. Epshteyn,[114] V. Gavrilov,[114] N. Lychkovskaya,[114] A. Nikitenko,[114,yy] V. Popov,[114] G. Safronov,[114] A. Spiridonov,[114] A. Stepennov,[114] M. Toms,[114] E. Vlasov,[114] A. Zhokin,[114] T. Aushev,[115] O. Bychkova,[116] M. Chadeeva,[116,zz] D. Philippov,[116] E. Popova,[116] V. Rusinov,[116] V. Andreev,[117] M. Azarkin,[117] I. Dremin,[117] M. Kirakosyan,[117] A. Terkulov,[117] A. Baskakov,[118] A. Belyaev,[118] E. Boos,[118]

V. Bunichev,[118] M. Dubinin,[118,aaa] L. Dudko,[118] A. Ershov,[118] A. Gribushin,[118] V. Klyukhin,[118] O. Kodolova,[118] I. Lokhtin,[118] S. Obraztsov,[118] V. Savrin,[118] V. Blinov,[119,bbb] T. Dimova,[119,bbb] L. Kardapoltsev,[119,bbb] I. Ovtin,[119,bbb] Y. Skovpen,[119,bbb] I. Azhgirey,[120] I. Bayshev,[120] V. Kachanov,[120] A. Kalinin,[120] D. Konstantinov,[120] V. Petrov,[120] R. Ryutin,[120] A. Sobol,[120] S. Troshin,[120] N. Tyurin,[120] A. Uzunian,[120] A. Volkov,[120] A. Babaev,[121] A. Iuzhakov,[121] V. Okhotnikov,[121] L. Sukhikh,[121] V. Borchsh,[122] V. Ivanchenko,[122] E. Tcherniaev,[122] P. Adzic,[123,ccc] P. Cirkovic,[123] M. Dordevic,[123] P. Milenovic,[123] J. Milosevic,[123] M. Aguilar-Benitez,[124] J. Alcaraz Maestre,[124] A. Álvarez Fernández,[124] I. Bachiller,[124] M. Barrio Luna,[124] Cristina F. Bedoya,[124] J. A. Brochero Cifuentes,[124] C. A. Carrillo Montoya,[124] M. Cepeda,[124] M. Cerrada,[124] N. Colino,[124] B. De La Cruz,[124] A. Delgado Peris,[124] J. P. Fernández Ramos,[124] J. Flix,[124] M. C. Fouz,[124] A. García Alonso,[124] O. Gonzalez Lopez,[124] S. Goy Lopez,[124] J. M. Hernandez,[124] M. I. Josa,[124] J. León Holgado,[124] D. Moran,[124] Á. Navarro Tobar,[124] A. Pérez-Calero Yzquierdo,[124] J. Puerta Pelayo,[124] I. Redondo,[124] L. Romero,[124] S. Sánchez Navas,[124] M. S. Soares,[124] A. Triossi,[124] L. Urda Gómez,[124] C. Willmott,[124] C. Albajar,[125] J. F. de Trocóniz,[125] R. Reyes-Almanza,[125] B. Alvarez Gonzalez,[126] J. Cuevas,[126] C. Erice,[126] J. Fernandez Menendez,[126] S. Folgueras,[126] I. Gonzalez Caballero,[126] E. Palencia Cortezon,[126] C. Ramón Álvarez,[126] J. Ripoll Sau,[126] V. Rodríguez Bouza,[126] S. Sanchez Cruz,[126] A. Trapote,[126] I. J. Cabrillo,[127] A. Calderon,[127] B. Chazin Quero,[127] J. Duarte Campderros,[127] M. Fernandez,[127] P. J. Fernández Manteca,[127] G. Gomez,[127] C. Martinez Rivero,[127] P. Martinez Ruiz del Arbol,[127] F. Matorras,[127] J. Piedra Gomez,[127] C. Prieels,[127] F. Ricci-Tam,[127] T. Rodrigo,[127] A. Ruiz-Jimeno,[127] L. Scodellaro,[127] I. Vila,[127] J. M. Vizan Garcia,[127] MK Jayananda,[128] B. Kailasapathy,[128,ddd] D. U. J. Sonnadara,[128] DDC Wickramarathna,[128] W. G. D. Dharmaratna,[129] K. Liyanage,[129] N. Perera,[129] N. Wickramage,[129] T. K. Aarrestad,[130] D. Abbaneo,[130] B. Akgun,[130] E. Auffray,[130] G. Auzinger,[130] J. Baechler,[130] P. Baillon,[130] A. H. Ball,[130] D. Barney,[130] J. Bendavid,[130] N. Beni,[130] M. Bianco,[130] A. Bocci,[130] P. Bortignon,[130] E. Bossini,[130] E. Brondolin,[130] T. Camporesi,[130] G. Cerminara,[130] L. Cristella,[130] D. d'Enterria,[130] A. Dabrowski,[130] N. Daci,[130] V. Daponte,[130] A. David,[130] A. De Roeck,[130] M. Deile,[130] R. Di Maria,[130] M. Dobson,[130] M. Dünser,[130] N. Dupont,[130] A. Elliott-Peisert,[130] N. Emriskova,[130] F. Fallavollita,[130,eee] D. Fasanella,[130] S. Fiorendi,[130] G. Franzoni,[130] J. Fulcher,[130] W. Funk,[130] S. Giani,[130] D. Gigi,[130] K. Gill,[130] F. Glege,[130] L. Gouskos,[130] M. Guilbaud,[130] D. Gulhan,[130] M. Haranko,[130] J. Hegeman,[130] Y. Iiyama,[130] V. Innocente,[130] T. James,[130] P. Janot,[130] J. Kaspar,[130] J. Kieseler,[130] M. Komm,[130] N. Kratochwil,[130] C. Lange,[130] P. Lecoq,[130] K. Long,[130] C. Lourenço,[130] L. Malgeri,[130] M. Mannelli,[130] A. Massironi,[130] F. Meijers,[130] S. Mersi,[130] E. Meschi,[130] F. Moortgat,[130] M. Mulders,[130] J. Ngadiuba,[130] J. Niedziela,[130] S. Orfanelli,[130] L. Orsini,[130] F. Pantaleo,[130,u] L. Pape,[130] E. Perez,[130] M. Peruzzi,[130] A. Petrilli,[130] G. Petrucciani,[130] A. Pfeiffer,[130] M. Pierini,[130] D. Rabady,[130] A. Racz,[130] M. Rieger,[130] M. Rovere,[130] H. Sakulin,[130] J. Salfeld-Nebgen,[130] S. Scarfi,[130] C. Schäfer,[130] C. Schwick,[130] M. Selvaggi,[130] A. Sharma,[130] P. Silva,[130] W. Snoeys,[130] P. Sphicas,[130,fff] J. Steggemann,[130] S. Summers,[130] V. R. Tavolaro,[130] D. Treille,[130] A. Tsirou,[130] G. P. Van Onsem,[130] A. Vartak,[130] M. Verzetti,[130] K. A. Wozniak,[130] W. D. Zeuner,[130] L. Caminada,[131,ggg] W. Erdmann,[131] R. Horisberger,[131] Q. Ingram,[131] H. C. Kaestli,[131] D. Kotlinski,[131] U. Langenegger,[131] T. Rohe,[131] M. Backhaus,[132] P. Berger,[132] A. Calandri,[132] N. Chernyavskaya,[132] G. Dissertori,[132] M. Dittmar,[132] M. Donegà,[132] C. Dorfer,[132] T. Gadek,[132] T. A. Gómez Espinosa,[132] C. Grab,[132] D. Hits,[132] W. Lustermann,[132] A.-M. Lyon,[132] R. A. Manzoni,[132] M. T. Meinhard,[132] F. Micheli,[132] F. Nessi-Tedaldi,[132] F. Pauss,[132] V. Perovic,[132] G. Perrin,[132] L. Perrozzi,[132] S. Pigazzini,[132] M. G. Ratti,[132] M. Reichmann,[132] C. Reissel,[132] T. Reitenspiess,[132] B. Ristic,[132] D. Ruini,[132] D. A. Sanz Becerra,[132] M. Schönenberger,[132] V. Stampf,[132] M. L. Vesterbacka Olsson,[132] R. Wallny,[132] D. H. Zhu,[132] C. Amsler,[133,hhh] C. Botta,[133] D. Brzhechko,[133] M. F. Canelli,[133] A. De Cosa,[133] R. Del Burgo,[133] J. K. Heikkilä,[133] M. Huwiler,[133] A. Jofrehei,[133] B. Kilminster,[133] S. Leontsinis,[133] A. Macchiolo,[133] P. Meiring,[133] V. M. Mikuni,[133] U. Molinatti,[133] I. Neutelings,[133] G. Rauco,[133] A. Reimers,[133] P. Robmann,[133] K. Schweiger,[133] Y. Takahashi,[133] S. Wertz,[133] C. Adloff,[134,iii] C. M. Kuo,[134] W. Lin,[134] A. Roy,[134] T. Sarkar,[134,jj] S. S. Yu,[134] L. Ceard,[135] P. Chang,[135] Y. Chao,[135] K. F. Chen,[135] P. H. Chen,[135] W.-S. Hou,[135] Y. y. Li,[135] R.-S. Lu,[135] E. Paganis,[135] A. Psallidas,[135] A. Steen,[135] E. Yazgan,[135] B. Asavapibhop,[136] C. Asawatangtrakuldee,[136] N. Srimanobhas,[136] F. Boran,[137] S. Damarseckin,[137,jjj] Z. S. Demiroglu,[137] F. Dolek,[137] C. Dozen,[137,kkk] I. Dumanoglu,[137,lll] E. Eskut,[137] G. Gokbulut,[137] Y. Guler,[137] E. Gurpinar Guler,[137,mmm] I. Hos,[137,nnn] C. Isik,[137] E. E. Kangal,[137,ooo] O. Kara,[137] A. Kayis Topaksu,[137] U. Kiminsu,[137] G. Onengut,[137] K. Ozdemir,[137,ppp] A. Polatoz,[137] A. E. Simsek,[137] B. Tali,[137,qqq] U. G. Tok,[137] S. Turkcapar,[137] I. S. Zorbakir,[137] C. Zorbilmez,[137] B. Isildak,[138,rrr] G. Karapinar,[138,sss] K. Ocalan,[138,ttt] M. Yalvac,[138,uuu] I. O. Atakisi,[139] E. Gülmez,[139] M. Kaya,[139,vvv] O. Kaya,[139,www] Ö. Özçelik,[139] S. Tekten,[139,xxx] E. A. Yetkin,[139,yyy] A. Cakir,[140] K. Cankocak,[140,lll] Y. Komurcu,[140] S. Sen,[140,zzz] F. Aydogmus Sen,[141] S. Cerci,[141,qqq] B. Kaynak,[141]

S. Ozkorucuklu,[141] D. Sunar Cerci,[141,qqq] B. Grynyov,[142] L. Levchuk,[143] E. Bhal,[144] S. Bologna,[144] J. J. Brooke,[144] E. Clement,[144] D. Cussans,[144] H. Flacher,[144] J. Goldstein,[144] G. P. Heath,[144] H. F. Heath,[144] L. Kreczko,[144] B. Krikler,[144] S. Paramesvaran,[144] T. Sakuma,[144] S. Seif El Nasr-Storey,[144] V. J. Smith,[144] J. Taylor,[144] A. Titterton,[144] K. W. Bell,[145] A. Belyaev,[145,aaaa] C. Brew,[145] R. M. Brown,[145] D. J. A. Cockerill,[145] K. V. Ellis,[145] K. Harder,[145] S. Harper,[145] J. Linacre,[145] K. Manolopoulos,[145] D. M. Newbold,[145] E. Olaiya,[145] D. Petyt,[145] T. Reis,[145] T. Schuh,[145] C. H. Shepherd-Themistocleous,[145] A. Thea,[145] I. R. Tomalin,[145] T. Williams,[145] R. Bainbridge,[146] P. Bloch,[146] S. Bonomally,[146] J. Borg,[146] S. Breeze,[146] O. Buchmuller,[146] A. Bundock,[146] V. Cepaitis,[146] G. S. Chahal,[146,bbbb] D. Colling,[146] P. Dauncey,[146] G. Davies,[146] M. Della Negra,[146] P. Everaerts,[146] G. Fedi,[146] G. Hall,[146] G. Iles,[146] J. Langford,[146] L. Lyons,[146] A.-M. Magnan,[146] S. Malik,[146] A. Martelli,[146] V. Milosevic,[146] J. Nash,[146,cccc] V. Palladino,[146] M. Pesaresi,[146] D. M. Raymond,[146] A. Richards,[146] A. Rose,[146] E. Scott,[146] C. Seez,[146] A. Shtipliyski,[146] M. Stoye,[146] A. Tapper,[146] K. Uchida,[146] T. Virdee,[146,u] N. Wardle,[146] S. N. Webb,[146] D. Winterbottom,[146] A. G. Zecchinelli,[146] J. E. Cole,[147] P. R. Hobson,[147] A. Khan,[147] P. Kyberd,[147] C. K. Mackay,[147] I. D. Reid,[147] L. Teodorescu,[147] S. Zahid,[147] A. Brinkerhoff,[148] K. Call,[148] B. Caraway,[148] J. Dittmann,[148] K. Hatakeyama,[148] A. R. Kanuganti,[148] C. Madrid,[148] B. McMaster,[148] N. Pastika,[148] S. Sawant,[148] C. Smith,[148] R. Bartek,[149] A. Dominguez,[149] R. Uniyal,[149] A. M. Vargas Hernandez,[149] A. Buccilli,[150] O. Charaf,[150] S. I. Cooper,[150] S. V. Gleyzer,[150] C. Henderson,[150] P. Rumerio,[150] C. West,[150] A. Akpinar,[151] A. Albert,[151] D. Arcaro,[151] C. Cosby,[151] Z. Demiragli,[151] D. Gastler,[151] C. Richardson,[151] J. Rohlf,[151] K. Salyer,[151] D. Sperka,[151] D. Spitzbart,[151] I. Suarez,[151] S. Yuan,[151] D. Zou,[151] G. Benelli,[152] B. Burkle,[152] X. Coubez,[152,v] D. Cutts,[152] Y. t. Duh,[152] M. Hadley,[152] U. Heintz,[152] J. M. Hogan,[152,dddd] K. H. M. Kwok,[152] E. Laird,[152] G. Landsberg,[152] K. T. Lau,[152] J. Lee,[152] M. Narain,[152] S. Sagir,[152,eeee] R. Syarif,[152] E. Usai,[152] W. Y. Wong,[152] D. Yu,[152] W. Zhang,[152] R. Band,[153] C. Brainerd,[153] R. Breedon,[153] M. Calderon De La Barca Sanchez,[153] M. Chertok,[153] J. Conway,[153] R. Conway,[153] P. T. Cox,[153] R. Erbacher,[153] C. Flores,[153] G. Funk,[153] F. Jensen,[153] W. Ko,[153,a] O. Kukral,[153] R. Lander,[153] M. Mulhearn,[153] D. Pellett,[153] J. Pilot,[153] M. Shi,[153] D. Taylor,[153] K. Tos,[153] M. Tripathi,[153] Y. Yao,[153] F. Zhang,[153] M. Bachtis,[154] R. Cousins,[154] A. Dasgupta,[154] A. Florent,[154] D. Hamilton,[154] J. Hauser,[154] M. Ignatenko,[154] T. Lam,[154] N. Mccoll,[154] W. A. Nash,[154] S. Regnard,[154] D. Saltzberg,[154] C. Schnaible,[154] B. Stone,[154] V. Valuev,[154] K. Burt,[155] Y. Chen,[155] R. Clare,[155] J. W. Gary,[155] S. M. A. Ghiasi Shirazi,[155] G. Hanson,[155] G. Karapostoli,[155] O. R. Long,[155] N. Manganelli,[155] M. Olmedo Negrete,[155] M. I. Paneva,[155] W. Si,[155] S. Wimpenny,[155] Y. Zhang,[155] J. G. Branson,[156] P. Chang,[156] S. Cittolin,[156] S. Cooperstein,[156] N. Deelen,[156] M. Derdzinski,[156] J. Duarte,[156] R. Gerosa,[156] D. Gilbert,[156] B. Hashemi,[156] V. Krutelyov,[156] J. Letts,[156] M. Masciovecchio,[156] S. May,[156] S. Padhi,[156] M. Pieri,[156] V. Sharma,[156] M. Tadel,[156] F. Würthwein,[156] A. Yagil,[156] N. Amin,[157] C. Campagnari,[157] M. Citron,[157] A. Dorsett,[157] V. Dutta,[157] J. Incandela,[157] B. Marsh,[157] H. Mei,[157] A. Ovcharova,[157] H. Qu,[157] M. Quinnan,[157] J. Richman,[157] U. Sarica,[157] D. Stuart,[157] S. Wang,[157] D. Anderson,[158] A. Bornheim,[158] O. Cerri,[158] I. Dutta,[158] J. M. Lawhorn,[158] N. Lu,[158] J. Mao,[158] H. B. Newman,[158] T. Q. Nguyen,[158] J. Pata,[158] M. Spiropulu,[158] J. R. Vlimant,[158] S. Xie,[158] Z. Zhang,[158] R. Y. Zhu,[158] J. Alison,[159] M. B. Andrews,[159] T. Ferguson,[159] T. Mudholkar,[159] M. Paulini,[159] M. Sun,[159] I. Vorobiev,[159] J. P. Cumalat,[160] W. T. Ford,[160] E. MacDonald,[160] T. Mulholland,[160] R. Patel,[160] A. Perloff,[160] K. Stenson,[160] K. A. Ulmer,[160] S. R. Wagner,[160] J. Alexander,[161] Y. Cheng,[161] J. Chu,[161] D. J. Cranshaw,[161] A. Datta,[161] A. Frankenthal,[161] K. Mcdermott,[161] J. Monroy,[161] J. R. Patterson,[161] D. Quach,[161] A. Ryd,[161] W. Sun,[161] S. M. Tan,[161] Z. Tao,[161] J. Thom,[161] P. Wittich,[161] M. Zientek,[161] S. Abdullin,[162] M. Albrow,[162] M. Alyari,[162] G. Apollinari,[162] A. Apresyan,[162] A. Apyan,[162] S. Banerjee,[162] L. A. T. Bauerdick,[162] A. Beretvas,[162] D. Berry,[162] J. Berryhill,[162] P. C. Bhat,[162] K. Burkett,[162] J. N. Butler,[162] A. Canepa,[162] G. B. Cerati,[162] H. W. K. Cheung,[162] F. Chlebana,[162] M. Cremonesi,[162] V. D. Elvira,[162] J. Freeman,[162] Z. Gecse,[162] E. Gottschalk,[162] L. Gray,[162] D. Green,[162] S. Grünendahl,[162] O. Gutsche,[162] R. M. Harris,[162] S. Hasegawa,[162] R. Heller,[162] T. C. Herwig,[162] J. Hirschauer,[162] B. Jayatilaka,[162] S. Jindariani,[162] M. Johnson,[162] U. Joshi,[162] P. Klabbers,[162] T. Klijnsma,[162] B. Klima,[162] M. J. Kortelainen,[162] S. Lammel,[162] D. Lincoln,[162] R. Lipton,[162] M. Liu,[162] T. Liu,[162] J. Lykken,[162] K. Maeshima,[162] D. Mason,[162] P. McBride,[162] P. Merkel,[162] S. Mrenna,[162] S. Nahn,[162] V. O'Dell,[162] V. Papadimitriou,[162] K. Pedro,[162] C. Pena,[162,aaa] O. Prokofyev,[162] F. Ravera,[162] A. Reinsvold Hall,[162] L. Ristori,[162] B. Schneider,[162] E. Sexton-Kennedy,[162] N. Smith,[162] A. Soha,[162] W. J. Spalding,[162] L. Spiegel,[162] S. Stoynev,[162] J. Strait,[162] L. Taylor,[162] S. Tkaczyk,[162] N. V. Tran,[162] L. Uplegger,[162] E. W. Vaandering,[162] H. A. Weber,[162] A. Woodard,[162] D. Acosta,[163] P. Avery,[163] D. Bourilkov,[163] L. Cadamuro,[163] V. Cherepanov,[163] F. Errico,[163] R. D. Field,[163] D. Guerrero,[163] B. M. Joshi,[163] M. Kim,[163] J. Konigsberg,[163] A. Korytov,[163] K. H. Lo,[163] K. Matchev,[163] N. Menendez,[163] G. Mitselmakher,[163] D. Rosenzweig,[163] K. Shi,[163] J. Wang,[163] S. Wang,[163] X. Zuo,[163] T. Adams,[164] A. Askew,[164] D. Diaz,[164]

R. Habibullah,[164] S. Hagopian,[164] V. Hagopian,[164] K. F. Johnson,[164] R. Khurana,[164] T. Kolberg,[164] G. Martinez,[164] H. Prosper,[164] C. Schiber,[164] R. Yohay,[164] J. Zhang,[164] M. M. Baarmand,[165] S. Butalla,[165] T. Elkafrawy,[165,m] M. Hohlmann,[165] D. Noonan,[165] M. Rahmani,[165] M. Saunders,[165] F. Yumiceva,[165] M. R. Adams,[166] L. Apanasevich,[166] H. Becerril Gonzalez,[166] R. Cavanaugh,[166] X. Chen,[166] S. Dittmer,[166] O. Evdokimov,[166] C. E. Gerber,[166] D. A. Hangal,[166] D. J. Hofman,[166] C. Mills,[166] G. Oh,[166] T. Roy,[166] M. B. Tonjes,[166] N. Varelas,[166] J. Viinikainen,[166] X. Wang,[166] Z. Wu,[166] M. Alhusseini,[167] K. Dilsiz,[167,ffff] S. Durgut,[167] R. P. Gandrajula,[167] M. Haytmyradov,[167] V. Khristenko,[167] O. K. Köseyan,[167] J.-P. Merlo,[167] A. Mestvirishvili,[167,gggg] A. Moeller,[167] J. Nachtman,[167] H. Ogul,[167,hhhh] Y. Onel,[167] F. Ozok,[167,iiii] A. Penzo,[167] C. Snyder,[167] E. Tiras,[167] J. Wetzel,[167] K. Yi,[167,jjjj] O. Amram,[168] B. Blumenfeld,[168] L. Corcodilos,[168] M. Eminizer,[168] A. V. Gritsan,[168] S. Kyriacou,[168] P. Maksimovic,[168] C. Mantilla,[168] J. Roskes,[168] M. Swartz,[168] T. Á. Vámi,[168] C. Baldenegro Barrera,[169] P. Baringer,[169] A. Bean,[169] A. Bylinkin,[169] T. Isidori,[169] S. Khalil,[169] J. King,[169] G. Krintiras,[169] A. Kropivnitskaya,[169] C. Lindsey,[169] N. Minafra,[169] M. Murray,[169] C. Rogan,[169] C. Royon,[169] S. Sanders,[169] E. Schmitz,[169] J. D. Tapia Takaki,[169] Q. Wang,[169] J. Williams,[169] G. Wilson,[169] S. Duric,[170] A. Ivanov,[170] K. Kaadze,[170] D. Kim,[170] Y. Maravin,[170] T. Mitchell,[170] A. Modak,[170] A. Mohammadi,[170] F. Rebassoo,[171] D. Wright,[171] E. Adams,[172] A. Baden,[172] O. Baron,[172] A. Belloni,[172] S. C. Eno,[172] Y. Feng,[172] N. J. Hadley,[172] S. Jabeen,[172] G. Y. Jeng,[172] R. G. Kellogg,[172] T. Koeth,[172] A. C. Mignerey,[172] S. Nabili,[172] M. Seidel,[172] A. Skuja,[172] S. C. Tonwar,[172] L. Wang,[172] K. Wong,[172] D. Abercrombie,[173] B. Allen,[173] R. Bi,[173] S. Brandt,[173] W. Busza,[173] I. A. Cali,[173] Y. Chen,[173] M. D'Alfonso,[173] G. Gomez Ceballos,[173] M. Goncharov,[173] P. Harris,[173] D. Hsu,[173] M. Hu,[173] M. Klute,[173] D. Kovalskyi,[173] J. Krupa,[173] Y.-J. Lee,[173] P. D. Luckey,[173] B. Maier,[173] A. C. Marini,[173] C. Mcginn,[173] C. Mironov,[173] S. Narayanan,[173] X. Niu,[173] C. Paus,[173] D. Rankin,[173] C. Roland,[173] G. Roland,[173] Z. Shi,[173] G. S. F. Stephans,[173] K. Sumorok,[173] K. Tatar,[173] D. Velicanu,[173] J. Wang,[173] T. W. Wang,[173] Z. Wang,[173] B. Wyslouch,[173] R. M. Chatterjee,[174] A. Evans,[174] S. Guts,[174,a] P. Hansen,[174] J. Hiltbrand,[174] Sh. Jain,[174] M. Krohn,[174] Y. Kubota,[174] Z. Lesko,[174] J. Mans,[174] M. Revering,[174] R. Rusack,[174] R. Saradhy,[174] N. Schroeder,[174] N. Strobbe,[174] M. A. Wadud,[174] J. G. Acosta,[175] S. Oliveros,[175] K. Bloom,[176] S. Chauhan,[176] D. R. Claes,[176] C. Fangmeier,[176] L. Finco,[176] F. Golf,[176] J. R. González Fernández,[176] I. Kravchenko,[176] J. E. Siado,[176] G. R. Snow,[176,a] B. Stieger,[176] W. Tabb,[176] F. Yan,[176] G. Agarwal,[177] C. Harrington,[177] L. Hay,[177] I. Iashvili,[177] A. Kharchilava,[177] C. McLean,[177] D. Nguyen,[177] A. Parker,[177] J. Pekkanen,[177] S. Rappoccio,[177] B. Roozbahani,[177] G. Alverson,[178] E. Barberis,[178] C. Freer,[178] Y. Haddad,[178] A. Hortiangtham,[178] G. Madigan,[178] B. Marzocchi,[178] D. M. Morse,[178] V. Nguyen,[178] T. Orimoto,[178] L. Skinnari,[178] A. Tishelman-Charny,[178] T. Wamorkar,[178] B. Wang,[178] A. Wisecarver,[178] D. Wood,[178] S. Bhattacharya,[179] J. Bueghly,[179] Z. Chen,[179] A. Gilbert,[179] T. Gunter,[179] K. A. Hahn,[179] N. Odell,[179] M. H. Schmitt,[179] K. Sung,[179] M. Velasco,[179] R. Bucci,[180] N. Dev,[180] R. Goldouzian,[180] M. Hildreth,[180] K. Hurtado Anampa,[180] C. Jessop,[180] D. J. Karmgard,[180] K. Lannon,[180] W. Li,[180] N. Loukas,[180] N. Marinelli,[180] I. Mcalister,[180] F. Meng,[180] K. Mohrman,[180] Y. Musienko,[180,tt] R. Ruchti,[180] P. Siddireddy,[180] S. Taroni,[180] M. Wayne,[180] A. Wightman,[180] M. Wolf,[180] L. Zygala,[180] J. Alimena,[181] B. Bylsma,[181] B. Cardwell,[181] L. S. Durkin,[181] B. Francis,[181] C. Hill,[181] A. Lefeld,[181] B. L. Winer,[181] B. R. Yates,[181] G. Dezoort,[182] P. Elmer,[182] B. Greenberg,[182] N. Haubrich,[182] S. Higginbotham,[182] A. Kalogeropoulos,[182] G. Kopp,[182] S. Kwan,[182] D. Lange,[182] M. T. Lucchini,[182] J. Luo,[182] D. Marlow,[182] K. Mei,[182] I. Ojalvo,[182] J. Olsen,[182] C. Palmer,[182] P. Piroué,[182] D. Stickland,[182] C. Tully,[182] S. Malik,[183] S. Norberg,[183] V. E. Barnes,[184] R. Chawla,[184] S. Das,[184] L. Gutay,[184] M. Jones,[184] A. W. Jung,[184] B. Mahakud,[184] G. Negro,[184] N. Neumeister,[184] C. C. Peng,[184] S. Piperov,[184] H. Qiu,[184] J. F. Schulte,[184] N. Trevisani,[184] F. Wang,[184] R. Xiao,[184] W. Xie,[184] T. Cheng,[185] J. Dolen,[185] N. Parashar,[185] M. Stojanovic,[185] A. Baty,[186] S. Dildick,[186] K. M. Ecklund,[186] S. Freed,[186] F. J. M. Geurts,[186] M. Kilpatrick,[186] A. Kumar,[186] W. Li,[186] B. P. Padley,[186] R. Redjimi,[186] J. Roberts,[186,a] J. Rorie,[186] W. Shi,[186] A. G. Stahl Leiton,[186] A. Bodek,[187] P. de Barbaro,[187] R. Demina,[187] J. L. Dulemba,[187] C. Fallon,[187] T. Ferbel,[187] M. Galanti,[187] A. Garcia-Bellido,[187] O. Hindrichs,[187] A. Khukhunaishvili,[187] E. Ranken,[187] R. Taus,[187] B. Chiarito,[188] J. P. Chou,[188] A. Gandrakota,[188] Y. Gershtein,[188] E. Halkiadakis,[188] A. Hart,[188] M. Heindl,[188] E. Hughes,[188] S. Kaplan,[188] O. Karacheban,[188,y] I. Laflotte,[188] A. Lath,[188] R. Montalvo,[188] K. Nash,[188] M. Osherson,[188] S. Salur,[188] S. Schnetzer,[188] S. Somalwar,[188] R. Stone,[188] S. A. Thayil,[188] S. Thomas,[188] H. Wang,[188] H. Acharya,[189] A. G. Delannoy,[189] S. Spanier,[189] O. Bouhali,[190,kkkk] M. Dalchenko,[190] A. Delgado,[190] R. Eusebi,[190] J. Gilmore,[190] T. Huang,[190] T. Kamon,[190,llll] H. Kim,[190] S. Luo,[190] S. Malhotra,[190] R. Mueller,[190] D. Overton,[190] L. Perniè,[190] D. Rathjens,[190] A. Safonov,[190] J. Sturdy,[190] N. Akchurin,[191] J. Damgov,[191] V. Hegde,[191] S. Kunori,[191] K. Lamichhane,[191] S. W. Lee,[191] T. Mengke,[191] S. Muthumuni,[191] T. Peltola,[191] S. Undleeb,[191] I. Volobouev,[191] Z. Wang,[191] A. Whitbeck,[191] E. Appelt,[192] S. Greene,[192] A. Gurrola,[192] R. Janjam,[192] W. Johns,[192] C. Maguire,[192] A. Melo,[192] H. Ni,[192] K. Padeken,[192] F. Romeo,[192] P. Sheldon,[192] S. Tuo,[192]

J. Velkovska,[192] M. Verweij,[192] L. Ang,[193] M. W. Arenton,[193] B. Cox,[193] G. Cummings,[193] J. Hakala,[193] R. Hirosky,[193] M. Joyce,[193] A. Ledovskoy,[193] C. Neu,[193] B. Tannenwald,[193] Y. Wang,[193] E. Wolfe,[193] F. Xia,[193] P. E. Karchin,[194] N. Poudyal,[194] P. Thapa,[194] K. Black,[195] T. Bose,[195] J. Buchanan,[195] C. Caillol,[195] S. Dasu,[195] I. De Bruyn,[195] C. Galloni,[195] H. He,[195] M. Herndon,[195] A. Hervé,[195] U. Hussain,[195] A. Lanaro,[195] A. Loeliger,[195] R. Loveless,[195] J. Madhusudanan Sreekala,[195] A. Mallampalli,[195] D. Pinna,[195] T. Ruggles,[195] A. Savin,[195] V. Shang,[195] V. Sharma,[195] W. H. Smith,[195] D. Teague,[195] S. Trembath-Reichert,[195] and W. Vetens[195]

CMS Collaboration

[1]*Yerevan Physics Institute, Yerevan, Armenia*
[2]*Institut für Hochenergiephysik, Wien, Austria*
[3]*Institute for Nuclear Problems, Minsk, Belarus*
[4]*Universiteit Antwerpen, Antwerpen, Belgium*
[5]*Vrije Universiteit Brussel, Brussel, Belgium*
[6]*Université Libre de Bruxelles, Bruxelles, Belgium*
[7]*Ghent University, Ghent, Belgium*
[8]*Université Catholique de Louvain, Louvain-la-Neuve, Belgium*
[9]*Centro Brasileiro de Pesquisas Fisicas, Rio de Janeiro, Brazil*
[10]*Universidade do Estado do Rio de Janeiro, Rio de Janeiro, Brazil*
[11a]*Universidade Estadual Paulista, São Paulo, Brazil*
[11b]*Universidade Federal do ABC, São Paulo, Brazil*
[12]*Institute for Nuclear Research and Nuclear Energy, Bulgarian Academy of Sciences, Sofia, Bulgaria*
[13]*University of Sofia, Sofia, Bulgaria*
[14]*Beihang University, Beijing, China*
[15]*Department of Physics, Tsinghua University, Beijing, China*
[16]*Institute of High Energy Physics, Beijing, China*
[17]*State Key Laboratory of Nuclear Physics and Technology, Peking University, Beijing, China*
[18]*Sun Yat-Sen University, Guangzhou, China*
[19]*Institute of Modern Physics and Key Laboratory of Nuclear Physics and Ion-beam Application (MOE)—Fudan University, Shanghai, China*
[20]*Zhejiang University, Hangzhou, China*
[21]*Universidad de Los Andes, Bogota, Colombia*
[22]*Universidad de Antioquia, Medellin, Colombia*
[23]*University of Split, Faculty of Electrical Engineering, Mechanical Engineering and Naval Architecture, Split, Croatia*
[24]*University of Split, Faculty of Science, Split, Croatia*
[25]*Institute Rudjer Boskovic, Zagreb, Croatia*
[26]*University of Cyprus, Nicosia, Cyprus*
[27]*Charles University, Prague, Czech Republic*
[28]*Escuela Politecnica Nacional, Quito, Ecuador*
[29]*Universidad San Francisco de Quito, Quito, Ecuador*
[30]*Academy of Scientific Research and Technology of the Arab Republic of Egypt, Egyptian Network of High Energy Physics, Cairo, Egypt*
[31]*Center for High Energy Physics (CHEP-FU), Fayoum University, El-Fayoum, Egypt*
[32]*National Institute of Chemical Physics and Biophysics, Tallinn, Estonia*
[33]*Department of Physics, University of Helsinki, Helsinki, Finland*
[34]*Helsinki Institute of Physics, Helsinki, Finland*
[35]*Lappeenranta University of Technology, Lappeenranta, Finland*
[36]*IRFU, CEA, Université Paris-Saclay, Gif-sur-Yvette, France*
[37]*Laboratoire Leprince-Ringuet, CNRS/IN2P3, Ecole Polytechnique, Institut Polytechnique de Paris, Palaiseau, France*
[38]*Université de Strasbourg, CNRS, IPHC UMR 7178, Strasbourg, France*
[39]*Université de Lyon, Université Claude Bernard Lyon 1, CNRS-IN2P3, Institut de Physique Nucléaire de Lyon, Villeurbanne, France*
[40]*Georgian Technical University, Tbilisi, Georgia*
[41]*RWTH Aachen University, I. Physikalisches Institut, Aachen, Germany*
[42]*RWTH Aachen University, III. Physikalisches Institut A, Aachen, Germany*
[43]*RWTH Aachen University, III. Physikalisches Institut B, Aachen, Germany*

[44]*Deutsches Elektronen-Synchrotron, Hamburg, Germany*
[45]*University of Hamburg, Hamburg, Germany*
[46]*Karlsruher Institut fuer Technologie, Karlsruhe, Germany*
[47]*Institute of Nuclear and Particle Physics (INPP), NCSR Demokritos, Aghia Paraskevi, Greece*
[48]*National and Kapodistrian University of Athens, Athens, Greece*
[49]*National Technical University of Athens, Athens, Greece*
[50]*University of Ioánnina, Ioánnina, Greece*
[51]*MTA-ELTE Lendület CMS Particle and Nuclear Physics Group, Eötvös Loránd University, Budapest, Hungary*
[52]*Wigner Research Centre for Physics, Budapest, Hungary*
[53]*Institute of Nuclear Research ATOMKI, Debrecen, Hungary*
[54]*Institute of Physics, University of Debrecen, Debrecen, Hungary*
[55]*Eszterhazy Karoly University, Karoly Robert Campus, Gyongyos, Hungary*
[56]*Indian Institute of Science (IISc), Bangalore, India*
[57]*National Institute of Science Education and Research, HBNI, Bhubaneswar, India*
[58]*Panjab University, Chandigarh, India*
[59]*University of Delhi, Delhi, India*
[60]*Saha Institute of Nuclear Physics, HBNI, Kolkata, India*
[61]*Indian Institute of Technology Madras, Madras, India*
[62]*Bhabha Atomic Research Centre, Mumbai, India*
[63]*Tata Institute of Fundamental Research-A, Mumbai, India*
[64]*Tata Institute of Fundamental Research-B, Mumbai, India*
[65]*Indian Institute of Science Education and Research (IISER), Pune, India*
[66]*Department of Physics, Isfahan University of Technology, Isfahan, Iran*
[67]*Institute for Research in Fundamental Sciences (IPM), Tehran, Iran*
[68]*University College Dublin, Dublin, Ireland*
[69a]*INFN Sezione di Bari, Bari, Italy*
[69b]*Università di Bari, Bari, Italy*
[69c]*Politecnico di Bari, Bari, Italy*
[70a]*INFN Sezione di Bologna, Bologna, Italy*
[70b]*Università di Bologna, Bologna, Italy*
[71a]*INFN Sezione di Catania, Catania, Italy*
[71b]*Università di Catania, Catania, Italy*
[72a]*INFN Sezione di Firenze, Firenze, Italy*
[72b]*Università di Firenze, Firenze, Italy*
[73]*INFN Laboratori Nazionali di Frascati, Frascati, Italy*
[74a]*INFN Sezione di Genova, Genova, Italy*
[74b]*Università di Genova, Genova, Italy*
[75a]*INFN Sezione di Milano-Bicocca, Milano, Italy*
[75b]*Università di Milano-Bicocca, Milano, Italy*
[76a]*INFN Sezione di Napoli, Napoli, Italy*
[76b]*Università di Napoli 'Federico II', Napoli, Italy*
[76c]*Università della Basilicata, Potenza, Italy*
[76d]*Università G. Marconi, Roma, Italy*
[77a]*INFN Sezione di Padova, Padova, Italy*
[77b]*Università di Padova, Padova, Italy*
[77c]*Università di Trento, Trento, Italy*
[78a]*INFN Sezione di Pavia, Pavia, Italy*
[78b]*Università di Pavia, Pavia, Italy*
[79a]*INFN Sezione di Perugia, Perugia, Italy*
[79b]*Università di Perugia, Perugia, Italy*
[80a]*INFN Sezione di Pisa, Pisa Italy*
[80b]*Università di Pisa, Pisa Italy*
[80c]*Scuola Normale Superiore di Pisa, Pisa Italy*
[80d]*Università di Siena, Siena, Italy*
[81a]*INFN Sezione di Roma, Rome, Italy*
[81b]*Sapienza Università di Roma, Rome, Italy*
[82a]*INFN Sezione di Torino, Torino, Italy*
[82b]*Università di Torino, Torino, Italy*
[82c]*Università del Piemonte Orientale, Novara, Italy*

[83a]INFN Sezione di Trieste, Trieste, Italy
[83b]Università di Trieste, Trieste, Italy
[84]Kyungpook National University, Daegu, Korea
[85]Chonnam National University, Institute for Universe and Elementary Particles, Kwangju, Korea
[86]Hanyang University, Seoul, Korea
[87]Korea University, Seoul, Korea
[88]Kyung Hee University, Department of Physics, Seoul, Republic of Korea
[89]Sejong University, Seoul, Korea
[90]Seoul National University, Seoul, Korea
[91]University of Seoul, Seoul, Korea
[92]Yonsei University, Department of Physics, Seoul, Korea
[93]Sungkyunkwan University, Suwon, Korea
[94]College of Engineering and Technology, American University of the Middle East (AUM), Kuwait
[95]Riga Technical University, Riga, Latvia
[96]Vilnius University, Vilnius, Lithuania
[97]National Centre for Particle Physics, Universiti Malaya, Kuala Lumpur, Malaysia
[98]Universidad de Sonora (UNISON), Hermosillo, Mexico
[99]Centro de Investigacion y de Estudios Avanzados del IPN, Mexico City, Mexico
[100]Universidad Iberoamericana, Mexico City, Mexico
[101]Benemerita Universidad Autonoma de Puebla, Puebla, Mexico
[102]Universidad Autónoma de San Luis Potosí, San Luis Potosí, Mexico
[103]University of Montenegro, Podgorica, Montenegro
[104]University of Auckland, Auckland, New Zealand
[105]University of Canterbury, Christchurch, New Zealand
[106]National Centre for Physics, Quaid-I-Azam University, Islamabad, Pakistan
[107]AGH University of Science and Technology Faculty of Computer Science, Electronics and Telecommunications, Krakow, Poland
[108]National Centre for Nuclear Research, Swierk, Poland
[109]Institute of Experimental Physics, Faculty of Physics, University of Warsaw, Warsaw, Poland
[110]Laboratório de Instrumentação e Física Experimental de Partículas, Lisboa, Portugal
[111]Joint Institute for Nuclear Research, Dubna, Russia
[112]Petersburg Nuclear Physics Institute, Gatchina (St. Petersburg), Russia
[113]Institute for Nuclear Research, Moscow, Russia
[114]Institute for Theoretical and Experimental Physics named by A.I. Alikhanov of NRC 'Kurchatov Institute', Moscow, Russia
[115]Moscow Institute of Physics and Technology, Moscow, Russia
[116]National Research Nuclear University 'Moscow Engineering Physics Institute' (MEPhI), Moscow, Russia
[117]P.N. Lebedev Physical Institute, Moscow, Russia
[118]Skobeltsyn Institute of Nuclear Physics, Lomonosov Moscow State University, Moscow, Russia
[119]Novosibirsk State University (NSU), Novosibirsk, Russia
[120]Institute for High Energy Physics of National Research Centre 'Kurchatov Institute', Protvino, Russia
[121]National Research Tomsk Polytechnic University, Tomsk, Russia
[122]Tomsk State University, Tomsk, Russia
[123]University of Belgrade: Faculty of Physics and VINCA Institute of Nuclear Sciences, Belgrade, Serbia
[124]Centro de Investigaciones Energéticas Medioambientales y Tecnológicas (CIEMAT), Madrid, Spain
[125]Universidad Autónoma de Madrid, Madrid, Spain
[126]Universidad de Oviedo, Instituto Universitario de Ciencias y Tecnologías Espaciales de Asturias (ICTEA), Oviedo, Spain
[127]Instituto de Física de Cantabria (IFCA), CSIC-Universidad de Cantabria, Santander, Spain
[128]University of Colombo, Colombo, Sri Lanka
[129]University of Ruhuna, Department of Physics, Matara, Sri Lanka
[130]CERN, European Organization for Nuclear Research, Geneva, Switzerland
[131]Paul Scherrer Institut, Villigen, Switzerland
[132]ETH Zurich—Institute for Particle Physics and Astrophysics (IPA), Zurich, Switzerland
[133]Universität Zürich, Zurich, Switzerland
[134]National Central University, Chung-Li, Taiwan
[135]National Taiwan University (NTU), Taipei, Taiwan
[136]Chulalongkorn University, Faculty of Science, Department of Physics, Bangkok, Thailand
[137]Çukurova University, Physics Department, Science and Art Faculty, Adana, Turkey

[138]*Middle East Technical University, Physics Department, Ankara, Turkey*
[139]*Bogazici University, Istanbul, Turkey*
[140]*Istanbul Technical University, Istanbul, Turkey*
[141]*Istanbul University, Istanbul, Turkey*
[142]*Institute for Scintillation Materials of National Academy of Science of Ukraine, Kharkov, Ukraine*
[143]*National Scientific Center, Kharkov Institute of Physics and Technology, Kharkov, Ukraine*
[144]*University of Bristol, Bristol, United Kingdom*
[145]*Rutherford Appleton Laboratory, Didcot, United Kingdom*
[146]*Imperial College, London, United Kingdom*
[147]*Brunel University, Uxbridge, United Kingdom*
[148]*Baylor University, Waco, Texas, USA*
[149]*Catholic University of America, Washington, DC, USA*
[150]*The University of Alabama, Tuscaloosa, Alabama, USA*
[151]*Boston University, Boston, Massachusetts, USA*
[152]*Brown University, Providence, Rhode Island, USA*
[153]*University of California, Davis, Davis, California, USA*
[154]*University of California, Los Angeles, California, USA*
[155]*University of California, Riverside, Riverside, California, USA*
[156]*University of California, San Diego, La Jolla, California, USA*
[157]*University of California, Santa Barbara—Department of Physics, Santa Barbara, California, USA*
[158]*California Institute of Technology, Pasadena, California, USA*
[159]*Carnegie Mellon University, Pittsburgh, Pennsylvania, USA*
[160]*University of Colorado Boulder, Boulder, Colorado, USA*
[161]*Cornell University, Ithaca, New York, USA*
[162]*Fermi National Accelerator Laboratory, Batavia, Illinois, USA*
[163]*University of Florida, Gainesville, Florida, USA*
[164]*Florida State University, Tallahassee, Florida, USA*
[165]*Florida Institute of Technology, Melbourne, Florida, USA*
[166]*University of Illinois at Chicago (UIC), Chicago, Illinois, USA*
[167]*The University of Iowa, Iowa City, Iowa, USA*
[168]*Johns Hopkins University, Baltimore, Maryland, USA*
[169]*The University of Kansas, Lawrence, Kansas, USA*
[170]*Kansas State University, Manhattan, Kansas, USA*
[171]*Lawrence Livermore National Laboratory, Livermore, California, USA*
[172]*University of Maryland, College Park, Maryland, USA*
[173]*Massachusetts Institute of Technology, Cambridge, Massachusetts, USA*
[174]*University of Minnesota, Minneapolis, Minnesota, USA*
[175]*University of Mississippi, Oxford, Mississippi, USA*
[176]*University of Nebraska-Lincoln, Lincoln, Nebraska, USA*
[177]*State University of New York at Buffalo, Buffalo, New York, USA*
[178]*Northeastern University, Boston, Massachusetts, USA*
[179]*Northwestern University, Evanston, Illinois, USA*
[180]*University of Notre Dame, Notre Dame, Indiana, USA*
[181]*The Ohio State University, Columbus, Ohio, USA*
[182]*Princeton University, Princeton, New Jersey, USA*
[183]*University of Puerto Rico, Mayaguez, Puerto Rico, USA*
[184]*Purdue University, West Lafayette, Indiana, USA*
[185]*Purdue University Northwest, Hammond, Indiana, USA*
[186]*Rice University, Houston, Texas, USA*
[187]*University of Rochester, Rochester, New York, USA*
[188]*Rutgers, The State University of New Jersey, Piscataway, New Jersey, USA*
[189]*University of Tennessee, Knoxville, Tennessee, USA*
[190]*Texas A&M University, College Station, Texas, USA*
[191]*Texas Tech University, Lubbock, Texas, USA*
[192]*Vanderbilt University, Nashville, Tennessee, USA*
[193]*University of Virginia, Charlottesville, Virginia, USA*
[194]*Wayne State University, Detroit, Michigan, USA*
[195]*University of Wisconsin—Madison, Madison, Wisconsin, USA*

[a]Deceased.

[b]Also at Vienna University of Technology, Vienna, Austria
[c]Also at Institute of Basic and Applied Sciences, Faculty of Engineering, Arab Academy for Science, Technology and Maritime Transport, Alexandria, Egypt
[d]Also at Université Libre de Bruxelles, Bruxelles, Belgium
[e]Also at IRFU, CEA, Université Paris-Saclay, Gif-sur-Yvette, France
[f]Also at Universidade Estadual de Campinas, Campinas, Brazil
[g]Also at Federal University of Rio Grande do Sul, Porto Alegre, Brazil
[h]Also at Universidade Federal de Mato Grosso do Sul, Nova Andradina, Brazil
[i]Also at Universidade Federal de Pelotas, Pelotas, Brazil
[j]Also at University of Chinese Academy of Sciences, Bejing, China
[k]Also at Institute for Theoretical and Experimental Physics named by A.I. Alikhanov of NRC 'Kurchatov Institute', Moscow, Russia
[l]Also at Joint Institute for Nuclear Research, Dubna, Russia
[m]Also at Ain Shams University, Cairo, Egypt
[n]Also at British University in Egypt, Cairo, Egypt
[o]Also at Cairo University, Cairo, Egypt
[p]Also at Fayoum University, El-Fayoum, Egypt
[q]Also at Purdue University, West Lafayette, Indiana, USA
[r]Also at Université de Haute Alsace, Mulhouse, France
[s]Also at Ilia State University, Tbilisi, Georgia
[t]Also at Erzincan Binali Yildirim University, Erzincan, Turkey
[u]Also at CERN, European Organization for Nuclear Research, Geneva, Switzerland
[v]Also at RWTH Aachen University, III. Physikalisches Institut A, Aachen, Germany
[w]Also at University of Hamburg, Hamburg, Germany
[x]Also at Department of Physics, Isfahan University of Technology, Isfahan, Iran
[y]Also at Brandenburg University of Technology, Cottbus, Germany
[z]Also at Skobeltsyn Institute of Nuclear Physics, Lomonosov Moscow State University, Moscow, Russia
[aa]Also at Institute of Physics, University of Debrecen, Debrecen, Hungary
[bb]Also at Physics Department, Faculty of Science, Assiut University
[cc]Also at MTA-ELTE Lendület CMS Particle and Nuclear Physics Group, Eötvös Loránd University, Budapest, Hungary
[dd]Also at Institute of Nuclear Research ATOMKI, Debrecen, Hungary
[ee]Also at IIT Bhubaneswar, Bhubaneswar, India
[ff]Also at Institute of Physics, Bhubaneswar, India
[gg]Also at G.H.G. Khalsa College, Punjab, India
[hh]Also at Shoolini University, Solan, India
[ii]Also at University of Hyderabad, Hyderabad, India
[jj]Also at University of Visva-Bharati, Santiniketan, India
[kk]Also at Indian Institute of Technology (IIT), Mumbai, India
[ll]Also at Deutsches Elektronen-Synchrotron, Hamburg, Germany
[mm]Also at Department of Physics, University of Science and Technology of Mazandaran, Behshahr, Iran
[nn]Also at INFN Sezione di Bari, Università di Bari, Politecnico di Bari, Bari, Italy
[oo]Also at Italian National Agency for New Technologies, Energy and Sustainable Economic Development
[pp]Also at Centro Siciliano di Fisica Nucleare e di Struttura Della Materia
[qq]Also at Riga Technical University, Riga, Latvia
[rr]Also at Consejo Nacional de Ciencia y Tecnología, Mexico City, Mexico
[ss]Also at Warsaw University of Technology, Institute of Electronic Systems, Warsaw, Poland
[tt]Also at Institute for Nuclear Research, Moscow, Russia
[uu]Also at National Research Nuclear University 'Moscow Engineering Physics Institute' (MEPhI), Moscow, Russia
[vv]Also at Institute of Nuclear Physics of the Uzbekistan Academy of Sciences, Tashkent, Uzbekistan
[ww]Also at St. Petersburg State Polytechnical University, St. Petersburg, Russia
[xx]Also at University of Florida, Gainesville, Florida, USA
[yy]Also at Imperial College, London, United Kingdom
[zz]Also at P.N. Lebedev Physical Institute, Moscow, Russia
[aaa]Also at California Institute of Technology, Pasadena, California, USA
[bbb]Also at Budker Institute of Nuclear Physics, Novosibirsk, Russia
[ccc]Also at Faculty of Physics, University of Belgrade, Belgrade, Serbia
[ddd]Also at Trincomalee Campus, Eastern University, Sri Lanka
[eee]Also at INFN Sezione di Pavia, Università di Pavia, Pavia, Italy
[fff]Also at National and Kapodistrian University of Athens, Athens, Greece
[ggg]Also at Universität Zürich, Zurich, Switzerland

[hhh]Also at Stefan Meyer Institute for Subatomic Physics, Vienna, Austria
[iii]Also at Laboratoire d'Annecy-le-Vieux de Physique des Particules, IN2P3-CNRS, Annecy-le-Vieux, France
[jjj]Also at Şırnak University, Şırnak, Turkey
[kkk]Also at Department of Physics, Tsinghua University, Beijing, China
[lll]Also at Near East University, Research Center of Experimental Health Science, Nicosia, Turkey
[mmm]Also at Beykent University, Istanbul, Turkey
[nnn]Also at Istanbul Aydin University, Application and Research Center for Advanced Studies (App. & Res. Cent. for Advanced Studies)
[ooo]Also at Mersin University, Mersin, Turkey
[ppp]Also at Piri Reis University, Istanbul, Turkey
[qqq]Also at Adiyaman University, Adiyaman, Turkey
[rrr]Also at Ozyegin University, Istanbul, Turkey
[sss]Also at Izmir Institute of Technology, Izmir, Turkey
[ttt]Also at Necmettin Erbakan University, Konya, Turkey
[uuu]Also at Bozok Universitetesi Rektörlügü, Yozgat, Turkey
[vvv]Also at Marmara University, Istanbul, Turkey
[www]Also at Milli Savunma University
[xxx]Also at Kafkas University, Kars, Turkey
[yyy]Also at Istanbul Bilgi University, Istanbul, Turkey
[zzz]Also at Hacettepe University, Ankara, Turkey
[aaaa]Also at School of Physics and Astronomy, University of Southampton, Southampton, United Kingdom
[bbbb]Also at IPPP Durham University, Durham, England
[cccc]Also at Monash University, Faculty of Science, Clayton, Australia
[dddd]Also at Bethel University, St. Paul, Minneapolis, USA
[eeee]Also at Karamanoğlu Mehmetbey University, Karaman, Turkey
[ffff]Also at Bingol University, Bingol, Turkey
[gggg]Also at Georgian Technical University, Tbilisi, Georgia
[hhhh]Also at Sinop University, Sinop, Turkey
[iiii]Also at Mimar Sinan University, Istanbul, Istanbul, Turkey
[jjjj]Also at Nanjing Normal University Department of Physics
[kkkk]Also at Texas A&M University at Qatar, Doha, Qatar
[llll]Also at Kyungpook National University, Daegu, Korea